ENABLING AN IMPLANTABLE PERIPHERAL MAGNETIC STIMULATOR BY REDUCING ENERGY REQUIREMENTS AND HEAT PRODUCTION

by

Zachary Benjamin Kagan

A dissertation submitted to the faculty of
The University of Utah
in partial fulfillment of the requirements for the degree of

Doctor of Philosophy

Department of Bioengineering

The University of Utah

May 2017

Copyright © Zachary Benjamin Kagan 2017
All Rights Reserved

The University of Utah Graduate School

STATEMENT OF DISSERTATION APPROVAL

The dissertation of **Zachary Benjamin Kagan**

has been approved by the following supervisory committee members:

David J. Warren	, Chair	**December 9, 2016** Date Approved
Richard A. Normann	, Member	**December 9, 2016** Date Approved
Gianluca Lazzi	, Member	**December 9, 2016** Date Approved
Alan D. Dorval	, Member	**December 9, 2016** Date Approved
Christopher R. Butson	, Member	**December 9, 2016** Date Approved

and by **David W. Grainger** , Chair of

the Department of **Bioengineering**

and by David B. Kieda, Dean of The Graduate School.

ABSTRACT

Interfacing with the peripheral nervous system via stimulating neurotechnologies has allowed for therapies which can restore sensorimotor and autonomic function previously lost to injury or disease. Magnetic stimulation (MS) is one such technology that may provide a path to developing new neuroprosthetic devices which advance the state of the art of rehabilitation. Recently, micro-scale copper solenoid coils have been used to effectively stimulate tissue in the central nervous system using mJ energies, addressing the two most pressing issues with MS: stimulating coil size, which were previously in the cm-scale range, and heat development in the coil due to the large energy requirements, which were in the 50 J range.

The primary motivations for using MS rather than functional electrical stimulation (FES) are that MS does not require direct electrical contact to neural tissue and that biological tissue is uniformly permeable to magnetic fields. These advantages imply there will be no accumulation of potentially damaging byproducts at the electrode-electrolyte interface, and there is less need to develop complex multisite, current-steering stimulation protocols to evoke localized neural activity, respectively. With the stimulator size and energy requirements addressed in the central nervous system, there is a clear path forward to develop new neuroprosthetic devices. In this work, we propose to translate these MS results observed in the central nervous system to the peripheral nervous system to provide an effective neurostimulation modality as a viable alternative to FES.

We propose the following approaches to achieve this goal: First, we will develop and validate a multiresolution, heterogeneous simulation model of peripheral magnetic neurostimulation allowing optimization of stimulator and coil designs. Next, we will reduce energy requirements for peripheral magnetic stimulation by using cm- and mm-scale stimulating coils abutted against the nerve. Finally, we will further reduce energy requirements for peripheral magnetic stimulation by controlling the flow of

stimulating current. Such a small, low energy magnetic stimulator, developed as a result of achieving these aims, would allow clinical providers to better treat those with sensorimotor or autonomic deficits.

To everyone who has brought me joy.

Your mountain is waiting,

So... get on your way!

CONTENTS

LIST OF FIGURES

LIST OF TABLES

ACKNOWLEDGMENTS

First and foremost to my parents, Juli and David, my most ardent supporters, thank you for everything.

I would like to thank my Ph.D. committee, including Dr. Gianluca Lazzi, Dr. Alan "Chuck" Dorval, and Dr. Chris Butson, for their guidance throughout this process. In particular, Dr. Richard Normann and Dr. David Warren have been exceptional mentors in honing my critical thinking, communication, and work ethic. I would also like to thank some of the people who have helped me during this research: Dr. Anil RamRakhyani, Dr. Heather Wark, Dr. Mitchell Frankel, Kiran Mathews, Dr. David Page, David Kluger, and David Hilgart.

Finally, thanks to my friends, who have encouraged me and kept me laughing throughout this process: Katie, Sidh, Joe, Matt, Derrick, and so many more.

This research was made possible by funding provided by American taxpayers through federal grant-making agencies.

CHAPTER 1

INTRODUCTION

Background and Motivation

The nervous system of vertebrate animals is divided into the central nervous system (CNS) and peripheral nervous systems (PNS), which are primarily responsible for the processing and transmission of information, respectively, throughout the organism via electrochemical pathways and connections. More generally, the nervous system is responsible for perceiving and interacting with the world, as well as regulating normal bodily functions. This is largely done automatically with little conscious effort towards controlling any of these processes. These pathways may be influenced by external factors, such as chemicals or applied energy sources, so that they may be affected in any number of helpful ways, such as to treat pathologies, disorders, injuries, or symptoms resulting from them. Traditionally, one of the most common external factors has been the application of electricity to the nervous system so as to evoke, suppress, or modulate the natural activity of the nervous system, referred to as electrical stimulation. While devices that apply electricity to neural tissue have been effective in achieving the desired goal of altering nervous system activity, they typically need direct electrical contact to neural tissue [1]. More problematically, this connection has been shown to degrade over time in many of these types of devices due to issues of electrode material longevity and the foreign body response to implanted devices. As an alternative, the principles of electromagnetism can be exploited to stimulate neural tissue without direct contact, which is referred to as magnetic stimulation. Unfortunately, the benefit of magnetic stimulation comes at the cost of higher energies needed to evoke useful changes to neural activity compared to electrical stimulation. This difference in energies is enough to reduce the types of use cases available to magnetic stimulation due to the substantial heat produced in the coil. Furthermore, there are very few use cases unique to magnetic stimulation

as a consequence of it not requiring direct electrical contact. Recently, micro-scale copper solenoid coils have been used to successfully stimulate rabbit retinal neurons *in vitro* [2] and hamster dorsal cochlear nucleus neurons *in vivo* [3] with energy levels in the mJ range. These studies demonstrated that even very small stimulating coils can develop magnetic fields sufficient to excite neural tissue, and moreover that these devices do so with energies comparable to those used by electrically stimulating devices. This achievement overcomes the two biggest obstacles to developing magnetic stimulation systems for chronic implantation: heat production in the stimulating coil and stimulating coil size. Thus, translating these results of using mJ energy magnetic stimulation with micro-scale coils into the peripheral nervous system may allow for many of the use cases currently limited to electrical stimulation to be viable for magnetic stimulation, as well as opening new use cases unique to magnetic stimulation.

Physical and Biophysical Mechanisms of Magnetic Stimulation

Physical Mechanism

Most modern magnetic stimulation systems use a capacitive discharge system to develop the current in the stimulating coil necessary to evoke neural activity [4]. This current in the coil develops magnetic fields according to the Biot-Savart law, which describes the magnetic field ($\mathbf{B}$) at a position ($\mathbf{r}'$) generated by an constant electric current (I) along a closed curve ($d\mathbf{l}$, e.g., the wire in the coil) as shown in Equation 1.1.

$$\mathbf{B}(\mathbf{r}) = \frac{\mu_0}{4\pi} \int_C \frac{I d\mathbf{l} \times \mathbf{r}'}{|\mathbf{r}'|^3} \tag{1.1}$$

As an illustration, the time course of the current in a coil and the resulting magnetic field strength on the surface of the same coil are shown in Figure 1.1A. The current (left axis) and resulting magnetic field strength (right axis) are directly proportional to each other when measured at a fixed location, as indicated by Equation 1.1.

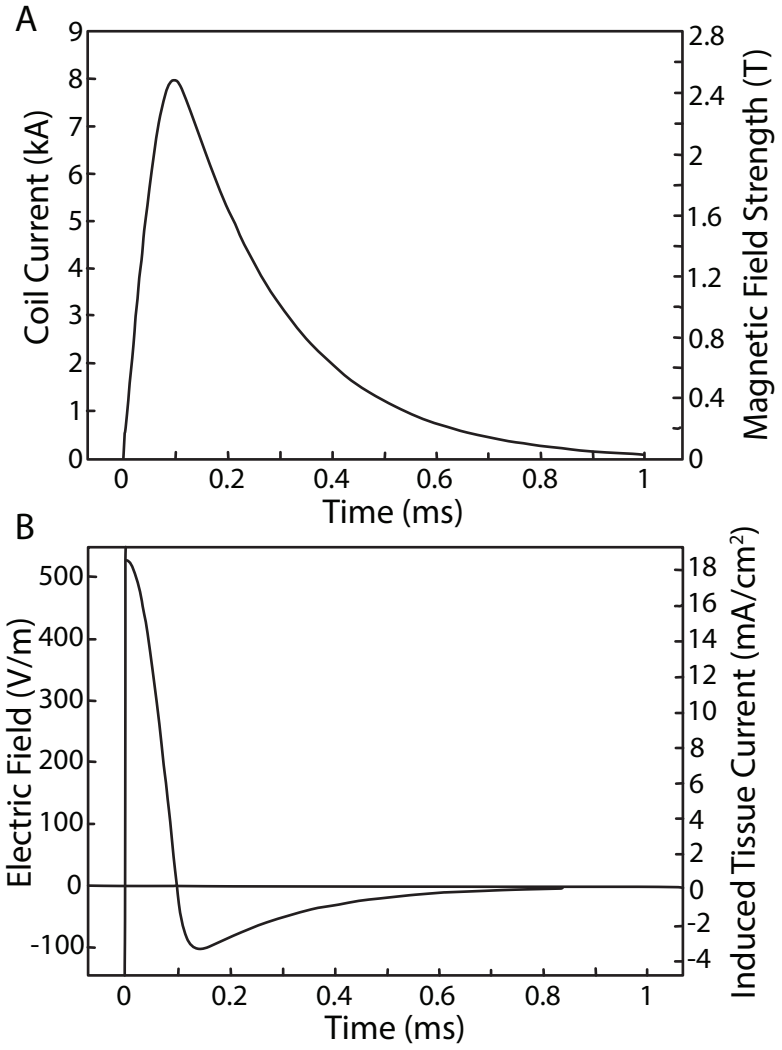

Figure 1.1: Coil Current and Electromagnetic Time-Varying Waveforms
(A) Coil current in (left axis) and peak magnetic field strength around (right axis) a 94 mm OD coil. Coil current is developed by capacitive discharge which results in an overdamped second-order response. The magnetic field strength is proportional to coil current, as a function of Equation 1.1. (B) Peak electric field (left axis) and induced tissue current (right axis) assuming homogeneous conductivity of 0.35 S/m. Each of these is proportional to the time derivative of coil current. Figure adapted from Jalinous [5] ©1991 American Electroencephalographic Society.

The coil was a 94 mm outer diameter coil for use with the MagStim Model 200 stimulator [5]. Magnetic stimulation of neural tissue operates by exploiting Faraday's law of induction, which describes the relationship between time-varying magnetic fields and the electromotive forces they induce. Namely, the magnetic flux through a surface is described by a surface integral as shown in Equation 1.2. This equation states that the magnetic flux (Φ_B) through an infinitesimally small wire loop bounding the surface S is proportional to the quantity of magnetic flux lines normal to the surface.

$$\Phi_B = \iint_S \mathbf{B} \cdot d\mathbf{S} \tag{1.2}$$

When the magnetic flux changes as a result of the magnetic field (B) changing, Faraday's law of induction states that the wire loop develops an electromotive force ($\mathcal{E}$) as per Equation 1.3.

$$\mathcal{E} = -\frac{d\Phi_B}{dt} \tag{1.3}$$

The direction of the induced electromotive force is given by Lenz's law, which states that the direction of current induced by Faraday's law of induction will create a field that opposes the change that produced it. This is represented by the negative sign in Faraday's law of induction. The induced electric field, which is proportional to the time derivative of the magnetic flux as per Equation 1.3, is shown in Figure 1.1B (left axis) for the same 94 mm outer diameter coil discussed previously [5]. In conductive media (e.g., biological tissue), the electric field develops currents according to Equation 1.4, the continuum form of Ohm's law.

$$\mathbf{J} = \sigma\mathbf{E} \tag{1.4}$$

In Equation 1.4, $\mathbf{J}$ is the current density, σ is conductivity, and $\mathbf{E}$ is the electric field. Continuing with this illustration, the induced current density in tissue is

shown in Figure 1.1B (right axis), assuming a uniform tissue conductivity of 0.35 S/m [5]. The physical mechanisms may be concisely summarized in the following way: **Electric currents are induced in conductive media with strength proportional to the time derivative of the current flowing through the stimulating coil, and with direction opposite to the flow of current in the stimulating coil.** However, it is important to note that charge accumulation as a result of these induced currents, which are ultimately responsible for neural activation, may be subject to environmental boundary effects (e.g., stimulation across a boundary layer of air) and conductivity inhomogeneities within the conductive medium (e.g., through different types of tissue).

In addition to the temporal aspect of current in the coil and the resulting electromagnetic fields, there are spatial relationships between coil geometry and electromagnetic fields. To illustrate this, magnetic and electric field strength are shown as a function of position below the surface of a 62 mm outer diameter coil and radially displaced from the central axis of the coil, as shown in Figure 1.2 [5]. The magnetic field strength has a peak with a radial displacement of 0 mm (i.e., in the center of the coil) for all depths except 0 mm (Figure 1.2A). The electric field strength, however, is 0 V/m at a radial displacement of 0, with maxima at a radial displacement of about 30 mm regardless of depth below the coil surface (Figure 1.2B).

Biophysical Mechanism

Once the electric field and associated currents have been induced within biological tissue, the mechanisms of neural activation are the same as with extracellular electrical stimulation [6, 7, 8, 9, 10, 11]. In particular, Rattay [7] describes how electric fields influence discretized neuronal compartments, covering exctracellular stimulation of unmyelinated and myelinated axons. While this approach does not work for all extracellular stimuli, and it does not provide explicit stimulation intensities required to evoke axonal responses [12], it does estimate the axonal response to an electric field adequate for magnetic stimulation with simple solenoid coils. The sum of the currents into an individual compartment must be equal to the sum of the currents leaving that compartment, as shown in Equation 1.5

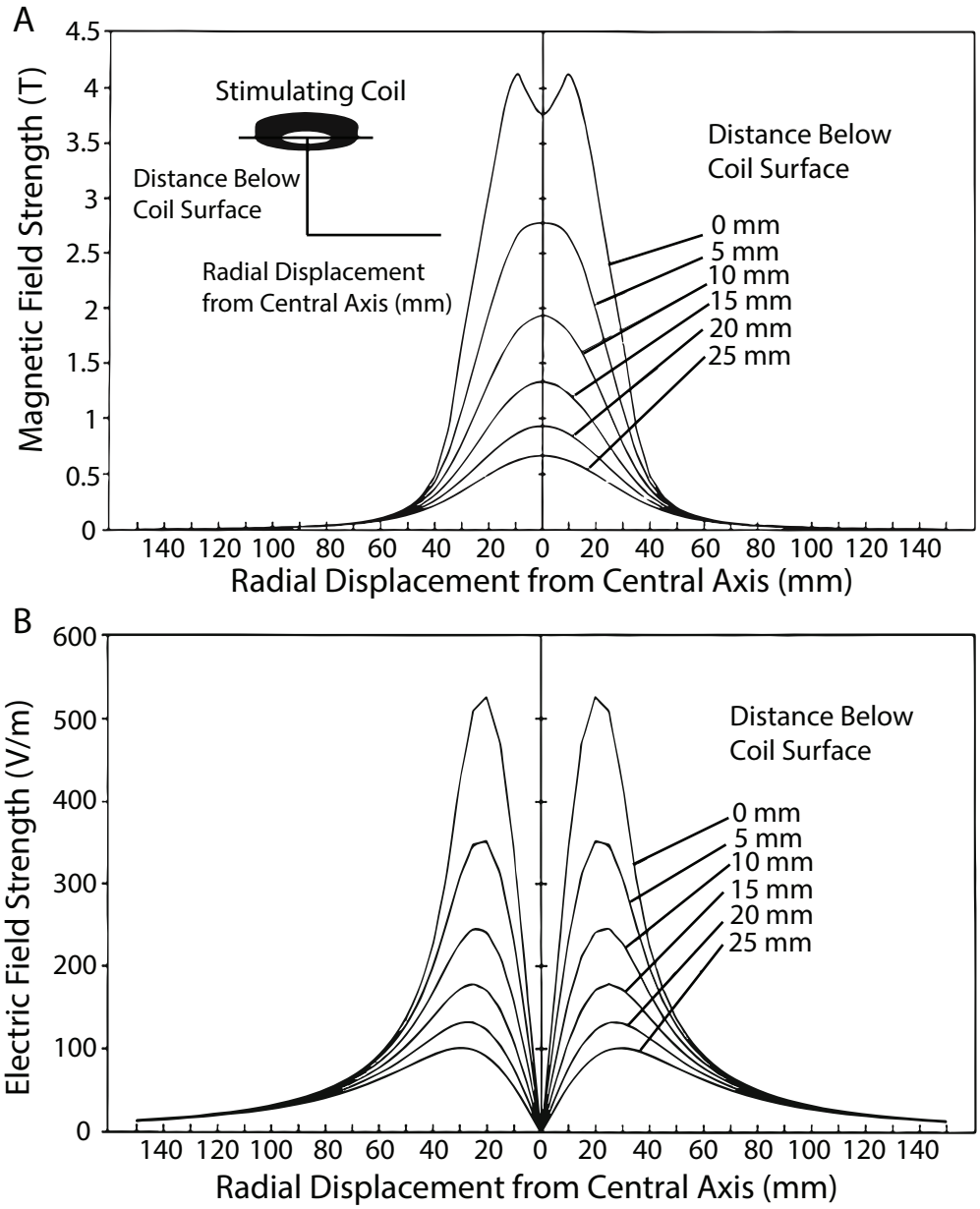

Figure 1.2: Magnetic and Induced Electric Field Strength
(A) Magnetic and (B) electric field strength as a function of radial displacement from the central axis and depth below the surface of a 62 mm outer diameter coil. With the exception of the plane on the bottom of the coil, the greatest magnetic field strengths are located directly along the center axis of the coil. In contrast, electric field strength is minimized along the central axis of the coil because the magnetic fields are radially symmetrical, resulting in zero net electric field. However, as the measurement point moves radially outward, the net magnetic flux lines become stronger until they are maximized directly below the turns of the stimulating coil before decreasing as the measurement point moves outside the outer diameter. Figure adapted from Jalinous [5] ©1991 American Electroencephalographic Society.

$$C_m \cdot d(V_{i,n} - V_{e,n})/dt + I_{i,n} + G_a(V_{i,n} - V_{i,n-1}) + G_a(V_{i,n} - V_{i,n+1}) = 0 \qquad (1.5)$$

where C_m is that compartment's membrane capacitance; $I_{i,n}$ is the ionic current (as opposed to the capacitive current from the first term), and is thus dependent on the internal and external voltages V_i and V_e, respectively; G_a is the inter-compartment resistance; n refers to an individual compartment. We may set V_r as the resting potential of the compartment, and change variables with Equation 1.6.

$$V_n = V_{i,n} - V_{e,n} - V_r \qquad (1.6)$$

Thus, V_n is the difference between the intracellular and extracellular voltages of a given compartment relative to the resting potential in that compartment. When V_n is substituted into Equation 1.5, we rearrange to get Equation 1.7.

$$dV_n/dt = (G_a \cdot (V_{n-1} - 2V_n + V_{n+1} + V_{e,n-1} - 2V_{e,n} + V_{e,n+1}) - I_{i,n})/C_m \qquad (1.7)$$

Here, $I_{i,n}$ represents the ionic current and can be modeled by the well-known Hodgkin-Huxley equations for unmyelinated axons [13] or the Frankenhauser-Huxley equations for myelinated axons [14]. When units are converted to specific resistances, conductances, and capacitances, and $G_a = 1/r_s\Delta x$, simplification yields Equation 1.8

$$\frac{dV_n}{dt} = \frac{1}{c_m} \cdot \{\frac{1}{r_s d\pi}(\frac{V_{n-1} - 2V_n + V_{n+1}}{\Delta x^2} + \frac{V_{e,n-1} - 2V_{e,n} + V_{e,n+1}}{\Delta x^2}) - I_{i,n}\} \qquad (1.8)$$

where c_m is specific capacitance ($C_m = \pi \cdot d \cdot \Delta x \cdot c_m$), r_s is specific resistivity of axoplasm, d is the axon diameter, and Δx is the intercompartment distance. Then, if we are only interested in the effect of external voltage (i.e., from an extracellular source like an induced electric field), we find Equation 1.9

$$\bar{S}(x,t) = (V_{e,n-1} - 2V_{e,n} + V_{e,n+1})/\Delta x^2 \tag{1.9}$$

and taking the limit of $\Delta x \to 0$, we are left with the activating function, Equation 1.10:

$$S = \partial^2 V_e / \partial x^2 \tag{1.10}$$

Thus, we can recognize that the second derivative of the external voltage along the length of the axon is the most important factor in determining the activation inside the axon.

Current State of the Art

Since 1965, most magnetic nerve stimulators have used a similar architecture for developing the necessary magnetic fields: Energy stored on a capacitor is rapidly discharged through a coil of wire [15]. These systems are, in any modern instantiation, less energy efficient at affecting neural tissue than their electrical counterparts for two reasons: First, heat is produced in the coil which serves no beneficial purpose, but it is a byproduct of the resistive losses in the coil due to the large electric currents necessary to develop the magnetic fields. Second, for small focal volumes of stimulation, the magnetic fields produced by the stimulating coils are less precisely controllable than electrical stimulation modalities. This is because with simple coil designs, we are limited by a tradeoff between depth and focality [16]. An important caveat to this is that there is no good electrical analog for large-focal-volume transcranial magnetic stimulation (TMS), in which case magnetic stimulation does have a unique use. In the first cases that describe required energies, it is reported that typically 400 J [17] or 500 J [5] of energy needs to be transferred from the energy storage capacitor to the stimulating coil to affect useful responses. Since then, in magnetic stimulation studies of peripheral nerves, the energies required to evoke axonal responses and useful neuromuscular responses are near 50 J [18, 19]. While there have been many other studies of magnetic stimulation, the vast majority use commercially available

stimulators which do not report energy use per stimulus, creating difficulty in comparing the relative performance of devices. Finally, coil design plays a large role in the efficacy and efficiency of every magnetic stimulation system, and the design should be optimized for each particular use case. Due to the interest in TMS research, most coil designs are intended to be used in that arena. Hence, even coils considered small for a TMS application are 60 mm in outer diameter [5]. While some smaller coils have been used to provide more focused excitation volumes at shallower depths of stimulation [18, 20], these are unusual for magnetic stimulation systems.

Applications of Magnetic Stimulation

D'Arsonval was the first to report on magnetic stimulation of the nervous system in 1896 by noting that phosphenes could be produced when an entire head was inside a coil [21]. The first modern magnetic stimulation system is found in the work of Bickford and Freeming in 1965 [15]. Since then, magnetic stimulation devices have been used in a wide range of applications, in both the central [22] and peripheral [6] nervous system, in clinical [23], *in vitro* [24], and *in vivo* [18] research applications. Furthermore, there has been substantial investigation into coil design, stimulus waveform optimization, stimulator circuitry optimization, coil placement optimization, and other similarly controllable parameters [25, 26, 19, 27, 20, 28, 29].

The most commonly reported use of magnetic stimulation is for TMS, in which a relatively large stimulation coil is placed outside the skull and is used to noninvasively stimulate the brain via electromagnetic induction [17]. This technology has been commercialized and used in clinical studies with goals of treating clinical depression, schizophrenia, and other nuanced disorders [23]. TMS has also been used in an investigational capacity to determine its effects on cortical excitability and inhibition [30]. Recently, studies have been conducted demonstrating that micro-scale coils are effective in exciting and modulating CNS activity *in vivo* [3] and *in vitro* [2] with energies in the mJ range, but the mechanisms at work in these studies are not well understood.

Alternatively, magnetic stimulation in the PNS has not yet been developed into a commercialized technology, and clinical uses have been minimal. Most studies are

investigational in nature, with goals of better understanding magnetic stimulation in the peripheral nervous system [18] and trying to improve on coil [27] or stimulator designs [31]. Additionally, computational simulation studies have played a large role in improving our understanding of these same topics [32, 33, 34].

Approaches to Improve Magnetic Stimulation

Based on the value of a magnetic stimulation device capable of treating sensorimotor loss, and the robustness of peripheral nerve preparations, we aimed to improve the state of the art of magnetic stimulating devices for PNS applications. The work described herein provides significant steps on the path towards developing safe magnetic stimulation devices that are ready to be tested chronically in an *in vivo* model. First, we developed and validated a simulation platform able to rapidly iterate on designs for fast first-order performance prediction of coil designs. Second, we used coils with geometries spanning from the large coils previously reported in the PNS to those with very low energy requirements in the CNS, and by leveraging the simulation model, we studied the effect of changing coil design parameters in an *in vivo* peripheral nerve application. Third, we reduced the energy required for stimulation by truncation the stimulation waveform using a new circuit architecture with an insulated gate bipolar transistor instead of a thyristor.

Thus, we have introduced a series of advancements to the state of the art that begin to translate the performance of magnetic stimulation systems in the CNS to the PNS with the ultimate goal of developing a clinically viable, chronically implantable peripheral nerve magnetic stimulator. While there has been much work in the area of electrical stimulation modeling to advance our understanding of neural excitation, electrode design, and other factors that determine the ideal stimulator type for a given application, there has been comparatively few investigations into magnetic stimulation systems for similar purposes. In particular, one of the most valuable contributions to the field of magnetic stimulation of peripheral nerves would be a simulation model for *in vivo* magnetic stimulation validated with experimental data. Past models were often limited by *ad hoc* parameter choice, the lack of *in vivo* or *in vitro* validating data, or the lack of a sufficiently physiologically and

anatomically accurate model. Here, we have developed a simulation platform that addresses these issues. All parameters, including stimulation circuit electrical characteristics, stimulating coil electrical and mechanical properties, nerve anatomy, axonal arrangement, and the related electromagnetic characteristics of the different types of tissues, are fully controllable, which leads to more accurate simulation results and a better understanding of the mechanisms and capabilities of peripheral magnetic stimulation. The multiresolution nature of the simulation platform means that the simulation includes the effects of anatomical features as small as 1 μm when the smallest resolutions are used, but computation time is not unnecessarily lengthened by simulating large volumes of homogeneous tissue when the largest resolutions are used. This multiphysics model also used the NEURON simulation environment to apply the induced transmembrane currents to nerve fibers [35]. The successful development and validation of our proposed multiresolution, heterogeneous model that addresses these issues allows for more rapid device development and testing without the immediate need for *in vivo* experimental data.

Several peripheral magnetic stimulation studies have investigated the effect of coil properties on magnetic field generation or neural tissue excitation in rabbit sciatic nerve *in vivo* [18], bullfrog sciatic and dog phrenic nerve *in vitro* [19], pig phrenic nerve *in vitro* [24], and generic human and rabbit nerves *in silico* [27], but they were too limited in scope to yield informative answers about coil designs for small, low energy peripheral magnetic stimulation. Thus, we have developed an *in vivo* rat sciatic nerve preparation to test a variety of coils so as to investigate which coil parameters are most important. This preparation is robust, consistent, and broadly accessible, ensuring that data collected from it would be reliable and easily comparable to work by other researchers. We used coils with a wide range of electrical and mechanical properties within a single animal so as to directly compare their performances and understand which properties are most important for effective magnetic stimulation. Notably, we used using coils with a range of sizes that spans from the mm-scale to the cm-scale, near the size of coils used in previous *in vivo* studies [18], to try to bridge the performance gap between magnetic stimulation in the CNS and PNS. In

this study, we were able to reduce the energy require to evoke a useful neuromuscular response from the 30 or more J reported in previous studies [18] to 20 J.

We were able to substantially improve the state of the art of magnetic stimulation by identifying coil parameters that improve performance and design new coils with those features, but this alone was not enough to reduce energy consumption and heat generation to the point that a magnetic stimulation device will be capable of being chronically implanted. Hence, we implemented a stimulation architecture used in repetitive TMS, specifically the one proposed by Peterchev et al. [36, 37] called controllable TMS that allowed current waveforms to be shaped beyond simply behaving as a second-order RLC oscillator. By adopting this stimulation architecture, we were able to fully halt current flow in the coil after neural excitation, reducing stimulation energies required to evoke a neural response by 33% or more, moving us closer to realizing the goal of clinically relevant peripheral magnetic stimulation devices. Additionally, by retaining charge on the capacitor as a result of truncating the current waveform, the capacitor could be recharged and discharged again more rapidly. This capability directly allows for higher frequency stimulation and the production of pulse trains, which is likely a requirement for a clinically useful implanted neurostimulator [38].

In summary, we have developed and validated a whole nerve, multiresolution simulation model of magnetic stimulation of peripheral nerves. We then leveraged this simulation platform to develop and test coils spanning a range of size so as to understand the importance of different coil design parameters. Finally, we adapted a stimulation architecture previously used in transcranial magnetic stimulation to directly halt the flow of current in the stimulating coil and substantially reduce the energy required to evoke use neuromuscular responses. Ultimately, we reduced this energy from 30 J to 7 J, a reduction of 77%.

References

[1] S. F. Cogan, "Neural stimulation and recording electrodes.," *Annu. Rev. Biomed. Eng.*, vol. 10, pp. 275–309, Jan. 2008.

[2] G. Bonmassar, *et al.*, "Microscopic magnetic stimulation of neural tissue," *Nat. Commun.*, vol. 3:921, pp. 1–10, Jan. 2012.

[3] H.-J. Park, *et al.*, "Activation of the central nervous system induced by micro-magnetic stimulation," *Nat. Commun.*, vol. 4:2463, pp. 1–9, Sep. 2013.

[4] L. A. Geddes, "History of magnetic stimulation of the nervous system," *J Clin Neurophysiol*, vol. 8, pp. 3–9, Jan. 1991.

[5] R. Jalinous, "Technical and practical aspects of magnetic nerve stimulation," *J. Clin. Neurophysiol.*, vol. 8, pp. 10–25, Jan. 1991.

[6] P. Basser and B. Roth, "Stimulation of a myelinated nerve axon by electromagnetic induction," *Med. Biol. Eng. Comput.*, vol. 29, pp. 261–268, May 1991.

[7] F. Rattay, "Analysis of models for external stimulation of axons," *IEEE Trans. Biomed. Eng.*, vol. 33, pp. 974–977, Oct. 1986.

[8] F. Rattay, "Analysis of models for extracellular fiber stimulation.," *IEEE Trans. Biomed. Eng.*, vol. 36, pp. 676–82, Jul. 1989.

[9] B. Roth and P. Basser, "A model of stimulation of a nerve fiber by electromagnetic induction," *IEEE Trans. Biomed. Eng.*, vol. 37, pp. 588–597, Jun. 1990.

[10] F. Rattay and M. Aberham, "Modeling axon membranes for functional electrical stimulation.," *IEEE Trans. Biomed. Eng.*, vol. 40, pp. 1201–9, Dec. 1993.

[11] F. Rattay, "The basic mechanism for the electrical stimulation of the nervous system," *Neuroscience*, vol. 89, pp. 335–346, Mar. 1999.

[12] C. R. Butson and C. C. McIntyre, "Current steering to control the volume of tissue activated during deep brain stimulation," *Brain Stimul.*, vol. 1, pp. 7–15, Jan. 2008.

[13] A. L. Hodgkin and A. F. Huxley, "A quantitative description of membrane current and its application to conduction and excitation in nerve," *J. Physiol.*, vol. 117, pp. 500–544, Aug. 1952.

[14] B. Frankenhaeuser and A. F. Huxley, "The action potential in the myelinated nerve fiber of xenopus laevis as computed on the basis of voltage clamp data," *J. Physiol.*, vol. 171, pp. 302–315, Jun. 1964.

[15] R. G. Bickford and B. D. Freeming, "Neuronal stimulation by pulsed magnetic fields in animals and man," *Dig. 6th Int. Conf. Med. Electron. Biol. Engeneering*, p. 112, Aug. 1965.

[16] Z. Deng, *et al.*, "Electric field depth–focality tradeoff in transcranial magnetic stimulation: simulation comparison of 50 coil designs," *Brain Stimul.*, vol. 6, pp. 1–13, Jan. 2013.

[17] A. Barker, "An introduction to the basic principles of magnetic nerve stimulation," *J. Clin. Neurophysiol.*, vol. 8, pp. 26–37, Jan. 1991.

[18] M. Yamaguchi and S. Yamada, "Electromagnetic mechanism of magnetic nerve stimulation," *J. Appl. Phys.*, vol. 66, pp. 1459–1465, Aug. 1989.

[19] S. S. Nagarajan, *et al.*, "Mapping location of excitation during magnetic stimulation: effects of coil position.," *Ann. Biomed. Eng.*, vol. 25, pp. 112–125, Jan. 1997.

[20] H. Tischler, *et al.*, "Mini-coil for magnetic stimulation in the behaving primate," *J. Neurosci. Methods*, vol. 194, pp. 242–251, Oct. 2011.

[21] A. D'Arsonval, "Dispositifs pour la mesure des courants alternatifs de toutes frequences," *C R Soc Biol*, vol. 3, pp. 450–457, 1896.

[22] E. M. Wassermann, "Risk and safety of repetitive transcranial magnetic stimulation: report and suggested guidelines from the International Workshop on the Safety of Repetitive Transcranial Magnetic Stimulation, June 5-7, 1996.," *Electroencephalogr. Clin. Neurophysiol.*, vol. 108, pp. 1–16, Jan. 1998.

[23] T. Burt, *et al.*, "Neuropsychiatric applications of transcranial magnetic stimulation: a meta analysis," *Int. J. Neuropsychopharmacol.*, vol. 5, pp. 73–103, Mar. 2002.

[24] E. R. Lontis, *et al.*, "In vitro magnetic stimulation of pig phrenic nerve with transverse and longitudinal induced electric fields: analysis of the stimulation site.," *IEEE Trans. Biomed. Eng.*, vol. 56, pp. 500–12, Feb. 2009.

[25] S. Nagarajan and D. Durand, "Determination of excitation sites during magnetic stimulation of nerve fibers," *Eng. Med. Biol. Soc. 1992 14th Annu. Int. Conf. IEEE*, vol. 4, pp. 1426–1427, Oct. 1992.

[26] J. Ruohonen, *et al.*, "Coil optimization for magnetic brain stimulation.," *Ann. Biomed. Eng.*, vol. 25, pp. 840–9, Sep. 1997.

[27] K.-H. Hsu, *et al.*, "Analysis of efficiency of magnetic stimulation.," *IEEE Trans. Biomed. Eng.*, vol. 50, pp. 1276–1285, Nov. 2003.

[28] S. M. Goetz, *et al.*, "Analysis and optimization of pulse dynamics for magnetic stimulation," *PLoS One*, vol. 8, p. e55771, Mar. 2013.

[29] A. V. Peterchev, *et al.*, "Controllable pulse parameter transcranial magnetic stimulator with enhanced circuit topology and pulse shaping.," *J. Neural Eng.*, vol. 11, p. 056023, Sep. 2014.

[30] P. B. Fitzgerald, *et al.*, "A comprehensive review of the effects of rTMS on motor cortical excitability and inhibition," *Clin. Neurophysiol.*, vol. 117, pp. 2584–2596, Dec. 2006.

[31] E. Basham, *et al.*, "Magnetic Stimulation of Neural Tissue: Techniques and System Design," in *Implant. Neural Prostheses 1* (E. Greenbaum and D. Zhou, eds.), Biological and Medical Physics, Biomedical Engineering, pp. 293–351, New York, NY: Springer US, 2009.

[32] S. S. Nagarajan, *et al.*, "Effects of induced electric fields on finite neuronal structures: a simulation study.," *IEEE Trans. Biomed. Eng.*, vol. 40, pp. 1175–88, Nov. 1993.

[33] S. S. Nagarajan and D. M. Durand, "Analysis of magnetic stimulation of a concentric axon in a nerve bundle.," *IEEE Trans. Biomed. Eng.*, vol. 42, pp. 926–33, Sep. 1995.

[34] J. Ruohonen, *et al.*, "A volume-conduction analysis of magnetic stimulation of peripheral nerves.," *IEEE Trans. Biomed. Eng.*, vol. 43, pp. 669–78, Jul. 1996.

[35] N. Carnevale and M. Hines, *The NEURON Book*. Cambridge, UK: Cambridge University Press, 2006.

[36] A. V. Peterchev, *et al.*, "A transcranial magnetic stimulator inducing near-rectangular pulses with controllable pulse width (cTMS)," *IEEE Trans. Biomed. Eng.*, vol. 55, pp. 257–266, Jan. 2008.

[37] A. Peterchev, *et al.*, "Repetitive transcranial magnetic stimulator with controllable pulse parameters," *J. Neural Eng.*, vol. 8, p. 036016., Jun. 2011.

[38] S. Hamid and R. Hayek, "Role of electrical stimulation for rehabilitation and regeneration after spinal cord injury: An overview," *Eur. Spine J.*, vol. 17, pp. 1256–1269, Sep. 2008.

CHAPTER 2

A μM-SCALE COMPUTATIONAL MODEL OF MAGNETIC NEURAL STIMULATION IN MULTIFASCICULAR PERIPHERAL NERVES

This chapter is a published journal article in the *IEEE Transactions on Biomedical Engineering*, Vol. 62, No. 3, pp. 2837-2849, 2015. Reprinted by permission, ©2015 IEEE. Authors of this chapter are A.K. Ramrakhyani, Z.B. Kagan, D.J. Warren, R.A. Normann, and G. Lazzi.

Abstract

There has been recurring interest in using magnetic neural stimulation for implantable, localized stimulation. However, the large stimulation voltages and energies necessary to evoke neuronal activity have tempered this interest. To investigate the potential of magnetic stimulation as a viable methodology and to provide the ability to investigate novel coil designs that can result in lower stimulation threshold voltages and energies, there is a need for a model that accurately predicts the magnetic field-tissue interaction that results in neuronal stimulation. In this work, we provide a computational framework to accurately estimate the stimulation threshold and have validated the model with *in vivo* magnetic stimulation experiments. To make such predictions, we developed a μm-resolution, anatomically-driven computational model of rat sciatic nerve and quantified the effect of tissue heterogeneity (i.e. fascicular organization, axon distribution and density) and axonal membrane capacitance on the resulting threshold. Using the multiresolution impedance method, we computed the spatial-temporal distribution of the induced electric field in the nerve and applied this field to a Frankenhaeuser-Huxley (FH) axon model in NEURON to simulate the nonlinear mechanisms of the membrane channels.

The computational model developed predicts the stimulation thresholds for four magnetic coil designs with different geometrical parameters within the 95% confidence interval (experiments count = 4) of measured *in vivo* stimulation thresholds for the rat sciatic nerve.

Introduction

Magnetic neural stimulation is emerging as a technique for transcranial [1, 2] and peripheral nerve stimulation [3], and for the investigation of cortical connectivity/ reactivity [4]. As most biological tissues have uniform relative magnetic permeabilities (close to that of air), applied magnetic fields are unaffected by tissue heterogeneity. Based on this property, non-invasive, extra-corporeal magnetic coils have been employed to evoke neural activity using time-varying magnetic fields. Performance of these designs is primarily limited by the ability of the magnetic coil and stimulator circuit to generate an effective spatial-temporal distribution of the induced electric fields inside tissue. Even though many studies have pursued the goal of optimizing coil designs [5] and circuit designs [6], the design parameters in these studies were chosen on an *ad hoc* basis, or by use of a simplified homogeneous (uniform conductivity) tissue model. The large sizes of the coils ($\sim$ 5 cm diameter) used in these studies [7, 1], the low stimulation focality [8], and the high stimulation energy ($\sim$100 J) [3, 7, 9] remain as key challenges in designing a safe and efficient magnetic stimulator.

Accurate prediction of stimulator performance in animal or human subjects is an important step in the design and optimization of coil and stimulator parameters. Previously, the understanding of the magnetic field's interaction with biological tissue had been based on *in vitro* experiments performed in peripheral [10, 11] and central [12, 13, 14] nervous systems. To study the effect of stimulation parameters (magnitude and pulse width of coil current), many studies used frog sciatic nerve in *in vitro* experiments, [11, 15, 16]. Other studies focused on *in vivo* experiments, performing peripheral stimulation of rabbit sciatic nerve [7] and transcranial stimulation in behaving primates [17]. These experiments established stimulation thresholds in terms of stimulation voltage [11] or induced electric field magnitude [7]. However, these values are highly susceptible to the operating conditions of the experiment (air-

tissue interface and the surrounding medium), which restricts stimulation threshold predictions under new experimental circumstances. In contrast, we propose that the pre-experiment performance of a magnetic stimulator can best be predicted using anatomically-driven computational models of the tissue and the experimental arrangement.

Although computational models to study transcranial magnetic stimulation [18] and peripheral nerve stimulation [19] have been developed, these models, with spatial resolution on the order of millimeters, did not include the interactions of neurons or axons with the magnetic fields and were not validated using *in vivo* experiments. Moreover, axonal membrane capacitance was not included in these models, thus potentially affecting the temporal distribution of the induced electric fields. Recently, we presented the induced field distribution inside a heterogeneous tissue environment and studied the effect of axon packing density on the magnitude of the induced field [20]. In the present work, we introduce a modeling framework that accurately predicts the stimulation thresholds during *in vivo* magnetic stimulation of rat sciatic nerve. To make such predictions, we developed a multiresolution impedance method to compute the induced electric fields resulting from an applied magnetic field and we combined this method with the Frankenhaeuser-Huxley (FH) axon model [21] to simulate active neuronal membrane mechanisms. To improve the simulation's prediction accuracy, we created a detailed μm-scale computational model of the rat sciatic nerve based on a histological image of the sciatic nerve cross-section. Moreover, the resulting modeling approach was validated for a variety of solenoid shaped magnetic coils, (each with different geometrical parameters) with *in vivo* magnetic stimulation experiments. Predicted magnetic stimulation thresholds were within the 95% confidence interval of the measured thresholds in magnetic stimulation experiments in rat sciatic nerve.

The proposed modeling framework is divided into three steps. First, a high resolution computational model of the nerve was created, which includes statistically distributed axon diameters and densities. The nerve was positioned in the simulation model in a manner that closely represents the setup for our *in vivo* magnetic neural stimulation experiments. Second, we implemented a multiresolution field simulator to resolve fine biological features (axon myelination and axonal membranes), and

used it to solve the electric field distribution in the multifascicular nerve. During this step, we also studied the effect of axon diameter and membrane capacitance on the induced field distribution. Third, we implemented the FH axon model in NEURON to estimate the minimum magnetic stimulator voltage that can elicit an action potential in the axon. Each step was individually validated by comparing the simulation predictions with analytical solutions.

Theory of Operation and Simulation Approach

Magnetic neural stimulation operates on Faraday's induction principle, which states that time-varying magnetic fields can induce electric field distributions inside a conductive medium, in this case biological tissue. To predict action potential thresholds in an axon, both the spatial and temporal distributions of the induced electric field need to be calculated. The spatial distribution of the electric field depends on the coil geometry and spatial distribution of the conductivities in the medium, particularly at boundaries between anatomical structures, while its temporal distribution is controlled by the time distribution of the current waveform in the magnetic coil. It is well accepted that the charge accumulation at the medium boundaries can significantly alter the distributions of induced electric fields [22, 23], and some studies have provided analytical solutions for the induced electric fields, including the effect of the semi-infinite, tissue-air interface [23, 24]. To predict the site of activation and the effect of the extracellular field, some studies also included analytical solutions based on a volume conduction analysis [25, 26, 27]. However, these analytical models were proposed for oversimplified boundary conditions (i.e., radial symmetry of the axon or a single axon inside a large homogeneous medium), which limited the accuracy of the predicted field distribution inside a realistic heterogeneous tissue environment. In contrast, we recently demonstrated that the induced electric field inside a densely packed axon can be 30% lower than the electric field for a single axon placed inside a homogeneous medium [20]. Therefore, we relied on a computational model instead of analytical solutions to quantify the spatial-temporal distribution of the induced electric fields in a nerve.

Additionally, we recently demonstrated *in vivo* magnetic stimulation of rat sciatic

nerve [28]. Inside such multifascicular sciatic nerves, axons are randomly located creating a random heterogeneity in the tissue's electrical properties. To validate our modeling framework using *in vivo* experiments, we created a computational model of sciatic nerve based on a histological image of the nerve's cross-section. We discretized the simulation space of the heterogeneous tissue environment using 3-dimensional voxels and computed the electric fields induced inside the voxels using a multiresolution impedance method. Our multiresolution field simulation is derived from the impedance method that was originally used to simulate the absorbed electromagnetic energy inside a conductive tissue caused by low-frequency magnetic fields [29]. The impedance method is a frequency-domain field solver, which uses the 3-dimensional magnetic field profile generated by the source (i.e., coil) to compute the induced electric field distribution inside the 3-dimensional tissue model. We simulated the tissue model at multiple frequencies and used Fourier analysis to create the temporal distributions of the induced electric fields. Compared to other algorithms for field calculations (spatial and temporal) such as the Finite Element Method (FEM) or the Finite-Difference Time-Domain (FDTD) method, the impedance method presents lower complexity for implementation, and it can be used to find a stable solution for large computational problems. Results from the field simulation were used to estimate the stimulus current across axonal membranes. The nonlinear behavior of the active ion channels were simulated using NEURON 7.3 software [30] and stimulation thresholds were predicted based on the minimum voltage for the stimulator circuit (pulse discharge based stimulator) that can evoke an action potential in the nerve fiber.

Methods

Computational Methods: Modeling of Heterogeneous Sciatic Nerve with Densely Packed Fascicles

Mammalian sciatic nerves are multifascicular structures with heterogeneous conductivities represented by boundaries between the nerve membrane and surrounding tissue, between the perineurium and the epineurium, and between the axonal membranes and the extraaxonal space. To make an accurate prediction of stimulation

thresholds, we employed an anatomically-driven computational model that included densely packed fascicles with statistically distributed axon diameters. As the basis for this computational model, we used the histological image of the cross-section of a rat's sciatic nerve from a previous study (Figure 3d of [31]). Additionally, we used this study's statistical parameterization of the axonal characteristics (distributions of the axonal diameters, axonal densities, and g-ratios) to populate fascicles with axons. Although we have only utilized the histological image found in [31], the fascicular arrangement is similar to that shown in another study [32]. The resulting computational model preserves the cross-sectional areas and boundary locations of the fascicles within the nerve, as illustrated in Figure 2.1(b).

Similar multiphysics computational modeling frameworks have been applied to the electrical stimulation of the peripheral nervous system (PNS) [32, 33, 34, 35]. Notably, FEM-based approaches were used to predict the stimulation selectivity for cuff electrodes [35] and penetrating microelectrodes [33]. Despite the advances in electrical stimulation modeling of the PNS, there is a lack of similar work in magnetic stimulation of peripheral nerves. Compared to the previous studies [32, 33, 34, 35], our work differed in terms of the underlying application, adopted algorithms, focus of the study, and excitation mechanisms. Using magnetic coils, we induce the stimulating currents directly inside the intracellular space of the axon instead of applying an extracellular potential as with electrical stimulation. Therefore, this modeling framework quantifies the μm resolution interaction between magnetic fields and groups of axons within a whole multifascicular nerve.

To incorporate the random distribution of axons inside the fascicles, the axons were randomly positioned and their diameters from 4 to 16 μm were randomly assigned (Figure 2.1(c)) based on the fiber distribution data presented in [31]. This achieved a high packing density of 67% or $\sim$11,000 axons/mm^2 [31, 36]. For this distribution, the g-ratio ($= \frac{\text{inner diameter of the axon}}{\text{outer diameter of the axon}}$) ranged from 0.45 to 0.7 [31]. To create the 3-dimensional (3-D) nerve model, the cross-sectional model was extruded in the x-direction (along the nerve). For each axon, the spacing between adjacent nodes of Ranvier was set at 100 times the outer diameter of the axon, as suggested in previous work [37, 38]. Additionally, to create a random distribution of nodes of

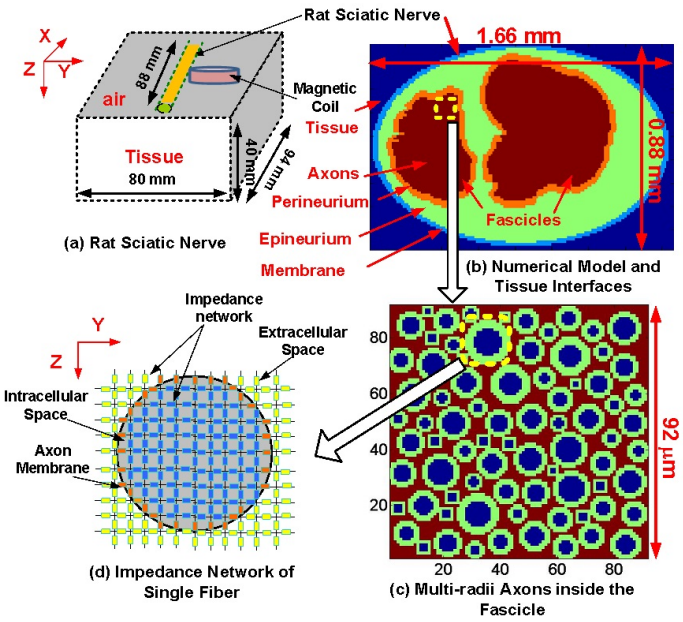

Figure 2.1: Simulation Setup

(a) Simulation model for magnetic stimulation consists of the sciatic nerve, the surrounding tissue, and the magnetic coil. The sciatic nerve is embedded inside tissue, while the magnetic coil is located in air. (b) Cross-sectional view of the sciatic nerve (c) Random placement of the different diameter axons inside a nerve fascicle (d) Cross sectional view of the individual axon's impedance network including the intracellular and the extracellular spaces.

Ranvier, the x position of the node of Ranvier closest to the origin of the model (i.e., where the coil is located) was uniformly distributed between ±0.5 times the distance between nodes for each axon.

The relative positions of the coil, nerve, and surrounding tissue in the simulation were arranged to mimic that of our *in vivo* experiments (Figure 2.1(a)). Thus, the magnetic coils were located in air and placed in close proximity to the nerve and tissue. The simulation model included an 88 mm long nerve embedded in the surface of a uniform tissue (Figure 2.1(a)). The key focus of this work was to accurately estimate the effect of anatomical boundaries inside the heterogeneous nerve. Therefore, the surrounding tissue was represented as a uniform muscle medium with a conductivity of 0.5 S/m [39].

Table 2.1 includes the conductivities of specific media inside the nerve compiled from previous work [40, 41, 39, 34]. The conductivity of the axon membrane was calculated based on the transmembrane leakage conductance of $\sim 61.4 mS/cm^2$ at an operating temperature of 37^oC [40]. Figure 2.1(b) shows a cross section of the elliptical nerve (typical shape during the *in vivo* experiments), with dimensions of 1.66 mm x 0.88 mm. Individual fascicles were populated with myelinated axons of different diameters as shown in Figure 2.1(c). To solve for the field distribution in the presence of different media boundaries, an impedance network of individual axons was created as shown in Figure 2.1(d) (cross-section view).

To reduce the overall volume of the simulated space and the resulting computation time, we constrained the simulated volume to where the magnetic field strength was negligible at its boundaries, which we defined as 2% of the peak magnetic field strength. For a coil positioned at the center of the model and with an outer diameter around 2 cm (the largest tested here), the region of simulation was a cube with 7 cm edges. In these simulations, such tradeoffs were made to ensure that the boundary effects will have a negligible impact on the electric field distribution. If a nerve were in a more constrained environment such as a petri dish, this framework could easily be modified to include those conditions.

To resolve μm feature sizes in a 7x7x7 cm cube, the simulation will require more than 300×10^{12} voxels, which is computationally intensive. Therefore, we developed a

multiresolution impedance method that was applied in multiple iterations. Simulation models were created with fine resolution at the region of high heterogeneity (inside a fascicle, Figure 2.1(b), (c)) and with coarse resolution for the more homogeneous regions (outside the nerve) [20]. To compute the field distribution inside the finer resolution model, the simulation results from the coarse resolution model were applied as the boundary conditions to the finer resolution models. Successive simulations, with resolutions 1 mm $\rightarrow$ 200 μm $\rightarrow$ 40 μm $\rightarrow$ 10 μm $\rightarrow$ 1 μm, were performed to increase resolution from 1mm to 1μm (Table 2.2, Step 1 to 5). Table 2.2 shows the model resolution and size for each simulation step. For the tissue model with $\sim 4\times10^6$ voxels, the simulation took 16 hours on a 24 CPUs server (Intel® Xeon®, 3.3. GHz) to achieve an absolute difference below 0.0001% between two sequential iterations. Therefore, using this multi-step approach, the voxel count of the peak computational model was kept below 5 million without sacrificing the fine heterogeneous features of the nerve.

To include the effect of active ion channels of the axon and to estimate the magnetic stimulation thresholds, we used an active nerve model [22, 21]. As the ion channels open during the stimulus pulse, the effective membrane conductance increases non-linearly. For the peak membrane conductance of 1200 mS/cm^2 [37], the induced stimulus current increases only by 19% compared to the current at its resting conductance of 61.4 mS/cm^2. Moreover, the peak conductance is achieved $\sim$100 μs after the end of the stimulus pulse. Therefore, the effect of nonlinear membrane conductance on the stimulus current is small and was dismissed for the computation of the stimulus current.

Rat sciatic nerves primarily consist of myelinated fibers [31, 36]. Multiple models have been proposed to simulate the behavior of the myelinated axon for electrical neural stimulation [42, 43, 41, 38, 44]. Generally, electrical models of a myelinated axon characterize the active nodes of Ranvier with fixed capacitance and variable conductances that represent voltage gated ion channels (sodium, potassium, and leakage), and characterize the myelinated internodal regions with passive components (Figure 2.2). Two models commonly used to simulate mammalian myelinated axons are the double cable model [44] and the Frankenhaeuser-Huxley (FH) model [21]. The

Table 2.1: Tissue Properties

Tissue Type	Conductivity $(\sigma_x, \sigma_y, \sigma_z)$ S/m	Reference
Surrounding tissue	(0.5, 0.5, 0.5)	[39]
Nerve membrane	(0.02, 0.02, 0.02)	[39]
Epineurium	(0.1, 0.1, 0.1)	[34]
Perineurium	(0.01, 0.01, 0.01)	[34]
Intracellular space	(0.91, 0.91, 0.91)	[41]
Extracellular space	(0.33, 0.33, 0.33)	[41]
Myelination	$(2 \times 10^{-4}, 5 \times 10^{-9}, 5 \times 10^{-9})$ High impedance myelination	
Axon membrane	$(2 \times 10^{-4}, 4 \times 10^{-6}, 4 \times 10^{-6})$ Based on the membrane impedance of rat's myelinated axon	[40]

Table 2.2: Multiresolution Model Simulation Parameters

Step No.	Model Resolution (x-, y-, z-)	Model Size (x-, y-, z-)	Voxels Count ($\times 10^6$)
1	(1 mm, 1 mm, 1 mm)	(100, 80, 40)	0.32
2	(1 mm, 200 μm, 200 μm)	(98, 50, 50)	0.245
3	(1 mm, 40 μm, 40 μm)	(96, 110, 80)	0.845
4	(1 mm, 10 μm, 10 μm)	(94, 188, 94)	1.66
5	(0.2 mm, 1 μm, 1 μm)	(460, 92, 92)	3.89

more complex double cable model has been shown to accurately simulate the threshold fluctuations that occur after spiking [44] and has been used in a multiphysics model of extraneural electrical stimulation of human femoral nerve [35]. The relatively simpler FH model has been used in a multiphysics model of intrafascicular electrical stimulation of rat sciatic nerves [33] and has been subsequently experimentally validated [32]. In this work, we chose to use the simpler FH model because (a) we could directly compare our results of modeling magnetic stimulation of the rat sciatic nerve to the previous modeling study of electrical stimulation of rat sciatic nerve, including the use of similar conductance parameters, [33], (b) we are principally interested in characterizing initiation of an active response, which occurs at similar stimulus levels for both the FH and the double cable models, and (c) the more accurate characterization of the post-spike threshold fluctuations afforded by the cable model was of little value as the time course of these fluctuations (<100 ms) is orders of magnitude lower than our experimental interpulse period (>10 s). Nevertheless, our modeling framework can readily be modified to use a double cable model to support future studies. The mathematical representations of the ion channels are adopted from the Frankenhaeuser-Huxley's original work [21] and the model parameters of the FH node (Table 2.5 in Appendix 2) are based on rat sciatic nerve experiments [40]. We modeled active membrane ion channels in the rat myelinated fiber using NEURON 7.3 software [30].

Experimental Methods

All procedures described here were approved by the University of Utah Institutional Animal Care and Use Committee. Sciatic nerves were prepared via surgical exposure from adult male Sprague-Dawley rats (n = 4). Anesthesia was induced and maintained with Isofluorane gas (1-5%). Depth of anesthesia and animal condition were evaluated via continuous monitoring of heart rate, blood oxygen saturation, respiration, and rectal temperature. A 5 cm section of the sciatic nerve was exposed between the hip and knee. Surgical procedures for exposing the nerve were similar to those previously described [45].

Stimulation was provided via a custom capacitive discharge system (Figure 2.3(a))

similar to previous designs [46] with a total capacitance of 6.85 mF. Four air-core solenoid shaped magnetic coils with different geometrical and electrical parameters were built and used in sequence during all experiments. Table 2.3 includes the mechanical and electrical properties of these magnetic coils. As the key focus of this work is the creation and validation of the modeling toolset, the effectiveness of individual coils for threshold reduction was kept outside the scope of this work. The stimulating coils, which were insulated from tissue by a $\sim$5 cm by $\sim$5 cm square of 13 μm thick insulating polyimide film, were positioned in place directly above the nerve approximately halfway between the hip and knee with a stereotactic 3-dimensional positioning system. The insulation integrity of the film was verified before and after each experiment. During experiments, the magnetic coil was positioned to within 0.5 mm of the optimal placement (location of minimum stimulation threshold) by testing the coil at five positions, each 1 mm apart, perpendicular to the long axis of the nerve. Generally, this position was where the nerve ran parallel to solenoid turns between the inner and outer diameters (Figure 2.3(b)). Stimulation trials were performed with capacitor voltages between 60 and 160 V in 20 V increments.

Electromyography (EMG) data was recorded differentially from the major extensor and flexor muscles of the ankle: Lateral gastrocnemius (LG), medial gastrocnemius (MG), tibialis anterior (TA), and soleus (Sol) as natural indicators of neural activity. Fine wire EMG electrodes were made as described in prior work [47] and inserted as pairs into each muscle. EMG recordings were bandpass filtered between 10 Hz to 1 kHz with a differential AC amplifier (Model 1700, A-M Systems, Sequim, WA) with a gain of 100. Amplifier ground was provided via either a Ag/AgCl 15 AWG wire or a deinsulated 18 AWG needle inserted under the skin near the hip. Data was recorded using a Cerebus data acquisition system (Blackrock Microsystems, Salt Lake City, UT) at a sampling rate of 30 kHz per channel. EMG amplitude for a trial was defined as the peak minus trough value in a window from 2 ms to 16 ms post-stimulus. Maximal muscle activation was determined via whole nerve electrical excitation using bipolar hook electrodes. Recruitment curves were generated by linearly interpolating between adjacent points on EMG amplitude vs stimulus intensity plots. Stimulus threshold of a muscle was defined as the stimulus intensity at which 20% of the

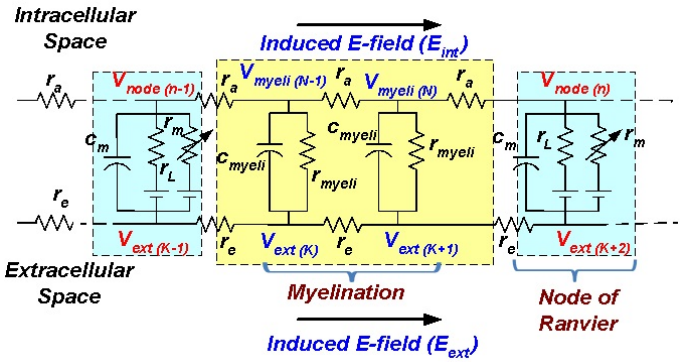

Figure 2.2: Circuit Model
Circuit model of a myelinated axon including the nodes of Ranvier and myelination. The active node of Ranvier includes voltage controlled ion gates and membrane capacitance.

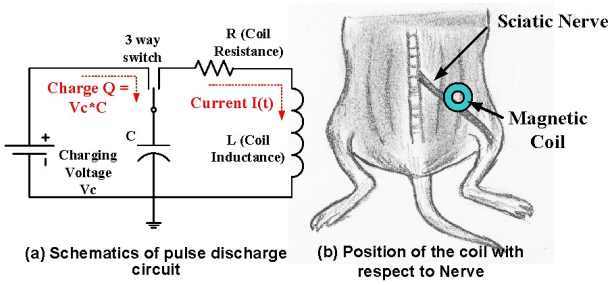

Figure 2.3: Experimental Setup
(a) Basic schematic of the pulse discharge circuit that includes a DC voltage source, charging capacitor C and a magnetic coil. (b) Exposed sciatic nerve of the rat and the position of the magnetic coil with respect to the nerve.

Table 2.3: Coil Geometrical Parameters of four Coils Used in Simulations and *In Vivo* Experiments

Coil	O.D (mm)	I.D. (mm)	H (mm)	N_t turns	N_a layers	L_{exp} (μ H)	R_{exp} (mΩ)
C1	16.4	8.00	13.3	9	3	4.28	17.3
C2	16.0	3.00	10.7	8	5	5.34	28.0
C3	11.7	7.00	27.4	23	2	5.27	39.0
C4	11.8	2.24	16.8	13	4	4.38	26.0

O.D. = outer diameter, I.D. = inner diameter, and H = height of the coil. Measured L_{exp} = inductance and R_{exp} = resistance of the coil. Wire Type: single strand magnetic wire, C1:AWG 17; C2,C3,C4: AWG 18.

maximal EMG response was observed for that muscle in that experiment for either magnetic or electrical stimulation (maximum EMG value is expected when 100% of the motor fibers were excited).

Results

Using this multiresolution hybrid model, we performed field and neuronal simulations for all four magnetic coils described in Table 2.3. However, for purposes of brevity, in the first five subsections only the details of the simulation with coil C1 are shown as a typical example of the collective results. In the first three subsections, the effects of fascicle distribution, axon diameter, and axon heterogeneity on the induced fields and transmembrane current density (J_m) at the nodes of Ranvier are investigated using the multiresolution impedance method model. In the fourth subsection, the effect of transmembrane capacitance on the temporal distribution of J_m at the nodes of Ranvier is presented. In the fifth subsection, the resulting spatial and temporal values of J_m at the nodes of Ranvier are applied to a NEURON model to investigate neuronal activation. In the last subsection, the stimulus thresholds produced by the modeling framework for all four magnetic coils are compared to those arising from experiments conducted in sciatic nerve of four rats.

Effect of Fascicle Distribution

To quantify the effect of fascicle boundaries in the heterogeneous model, the multiresolution impedance method was applied to a modeled rat sciatic nerve as described in Section 2 and the 3-D distribution of the 3-D induced electric field at the whole nerve level (Table 2.2, step 4) was studied. As the input to the frequency domain impedance method model, we used the magnetic field arising from exciting the coil with a 600 A magnitude, 2 kHz sine wave. For reference, the cross-sectional view of induced electric field along the nerve (E_x) for the heterogeneous model and the fascicle boundaries are shown in Figure 2.4(a). To illustrate that the electric fields are affected by tissue boundaries having low conductivity (e.g., nerve membrane and perineurium), the difference between E_x for the heterogeneous and homogeneous models is plotted in Figure 2.4(b) and for E_y in Figure 2.4(c). These results demonstrate that the induced eddy currents in the y and z directions are

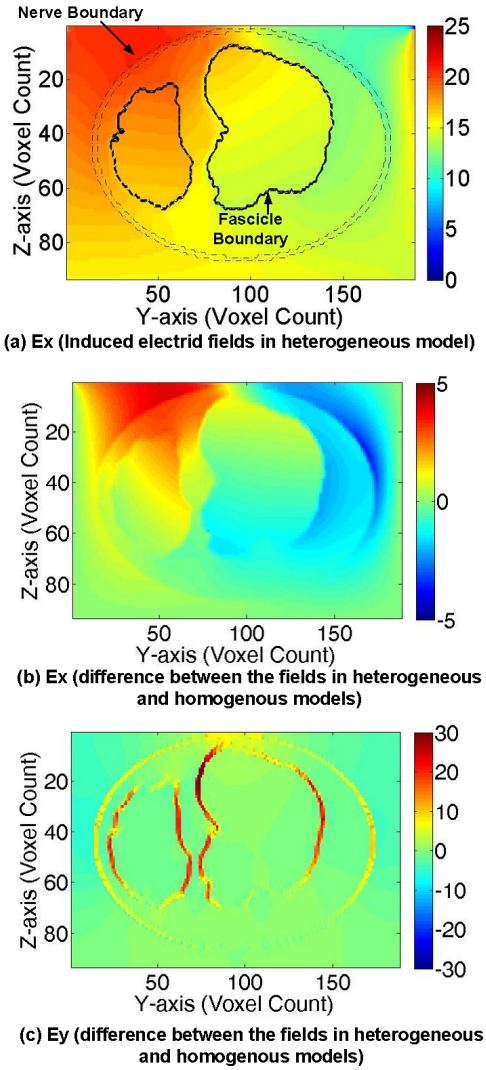

Figure 2.4: Effect of Fascicle Distribution and Heterogeneity on the Induced Electric Fields (a) X-directed electric field $\vec{E_x}$ distribution. Difference between (b) The x-directed electric field $\vec{E_x}$ and (c) The y-directed electric field $\vec{E_y}$ for the heterogeneous and homogeneous tissue models (Difference defined as heterogeneous model minus homogeneous model.) Due to the low conductivity of the nerve membrane and perineurium, the induced current in y- and z- direction is redirected toward the x-direction resulting in the difference between the heterogeneous and homogeneous tissue model results. All fields are in V/m. Y-axis and Z-axis are the voxel count in y- and z- direction, respectively (resolution 10 μm).

redirected towards the x direction at the medium boundaries, causing a change in the induced electric field along the nerve. Clearly, the induced electric field in the heterogeneous model is substantively different compared to the homogeneous model.

Between experiments, there may be variations in the preparation outside of our control such as fascicular arrangement and perineurium thickness. According to previous work [48], such variation can significantly alter stimulation thresholds of electric stimulation. However, magnetic stimulation does not require a direct conductive path between the magnetic coil and region of stimulation, making the induced electric field less susceptible to fascicular organization inside the nerve and perinurium properties. To investigate the effect of fascicular organization on magnetic stimulation thresholds, the x-axis directed electric field (E_x) of the initial organization (Model-1, Figure 2.1(b)) was compared to E_x for both a rotated version of the initial model (Model-2) and a translated version of the initial model (Model-3). For both the organizations, the difference in E_x between Model-1 and Model-2, and Model-1 and Model-3 were 10% or less, as shown in Figure 2.5(a) and 2.5(b), respectively. This indicates that for cm-sized magnetic coils, the fascicular arrangement has little impact on the induced electric field distribution inside the nerve. A similar sensitivity analysis was performed to quantify the effect of perineurium thickness on electric field variation. The perineurium thickness was varied to 2%, 6% and 12% of the effective fascicle diameter D ($D = 2 * \sqrt{\frac{FascicleArea}{\pi}}$). It was found that the peak electric field variation for both conditions (2% and 12 % perineurium thickness) from its nominal value (6% perineurium thickness, Model-1) is less than 5%. This analysis of fascicular variation suggests that variability in peak electric field distributions is not strongly influenced by fascicular organization and perineurium thickness.

Equally well, the results of this model are dependent upon the tissue conductivities used. In particular, the conductivity values of the perineurium and epineurium we used were gathered from prior work [34] (Table 2.1) that created a computational model of a mammalian sciatic nerve. There were some differences in the conductivity values used from [49] (Perineurium = 0.002 S/m, epineurium = 0.083 S/m). Thus, we analyzed the effect of these differences on the induced electric field distribution. The results showed that even if perineurium conductivity was changed by a factor of

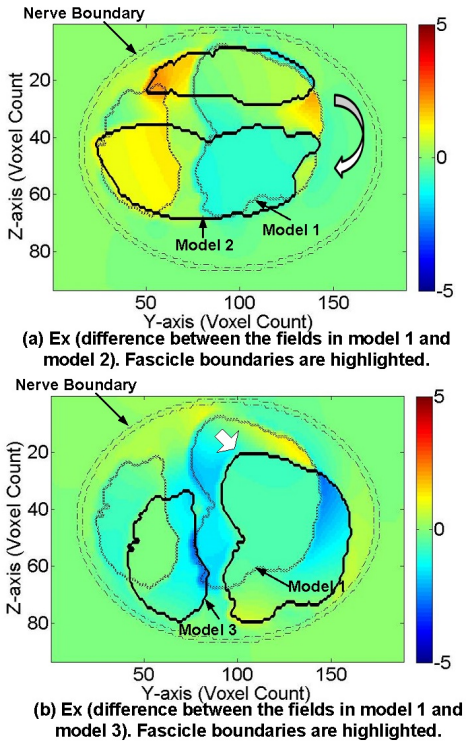

Figure 2.5: Effect of Fascicle Distribution Inside the Nerve
(a) Difference between the x-directed electric field $\vec{E_x}$ in Model-1 and Model-2 configurations. (b) Difference between the x-directed electric field $\vec{E_x}$ in Model-1 and Model-3 configurations. Fascicle boundaries are highlighted. All fields are in V/m. Y-axis and Z-axis are the voxel count in y- and z- direction, respectively (resolution 10 μm).

5 (0.01 S/m to 0.002 S/m), the peak induced electric field magnitude did not change by more than 10 % of the maximum magnitude of model 1. This limited dependency of the induced field on the fascicle distribution, and perinurium conductivity, and perienurium thickness is a key benefit of magnetic neural stimulation. This occurs because biological tissues are highly permeable to magnetic fields.

Electric Field Distribution Inside a Myelinated Axon

To study the interaction between the different sized myelinated axons inside a densely populated fascicle, a 92 mm $\times$ 92 μm $\times$ 92 μm subsection of the fascicle was taken as a simulation model. The μm resolution model (Figure 2.1(c)) was extracted from the highlighted fascicle shown in Figure 2.1(b), which is located 0.3 mm (in z-direction) from the tissue-air interface. Figure 2.1(c) shows a cross section (Y-Z

plane) of the model with a resolution of 0.2 mm, 1 μm, and 1μm in x-, y-, and z- directions, respectively (Table 2.2, step 5). Using the impedance method, the induced electric fields and the induced currents were computed in different regions (intracellular, extracellular, and axon membrane). The induced transmemebrane current i_m (intracellular to extracellular) for each axon was calculated at each segment location along the nerve (x-direction). The transmembrane current density J_m for each axon was calculated based on the axon radius and nodal length (δ) of 1μm ($J_m = i_m/2\pi a\delta$). Figure 2.6(a) shows the distribution of the transmembrane current density J_m along the selected axon (Figure 2.1(c)) of 16 μm diameter. As expected, the membrane current (and J_m) passes only through the nodes of Ranvier which are separated by 1.6 mm. The peak intracellular induced electric field value of 17.2 V/m was achieved at the midpoint of the axon. In previous works, it was shown that stimulation starts at the position where $-\frac{\partial E_x}{\partial x}$ is a maximum [25, 22]. Figure 2.6(b) shows the spatial derivative of the induced electric field (intracellular and extracellular) along the axon (x-direction). Comparing Figure 2.6(a) and 2.6(b) indicates that the peak positive J_m (stimulation site) is achieved at the location of $-\frac{\partial E_x}{\partial x}|_{peak}$, which supports the performance of the proposed computational model.

Effect of Axon Diameter on Induced Current Density

To study the recruitment order of axons inside the nerve, the peak membrane current density was computed for all axons. Induced transmembrane current density J_m varies exponentially with the axon radius, as shown in Figure 2.7. The solution indicates that larger axons experience higher induced current densities, and as such are excited first. Field simulations were performed for three different templates of randomly distributed axons to study the effect of axon positions and their proximity on the current density. For all the simulations, the simulated J_m was well fit with the polynomial relationship $J_m(mA/cm^2) = Ka^n$, where K = 0.03 ± 0.0012, n = 1.86 ± 0.0268, and a is the radius of the axon in μm. We also derived an analytical solution for the transmembrane current density (Equation 2.8 presented in Appendix 2). From this equation, the maximum current density $J_{m-max}(mA/cm^2) = 0.015 * |\frac{\partial E_x}{\partial x}|_{max} * a^2$, where $\frac{\partial E_x}{\partial x}$ is in mV/mm^2 and a is axos radius in μm. For coil C1,

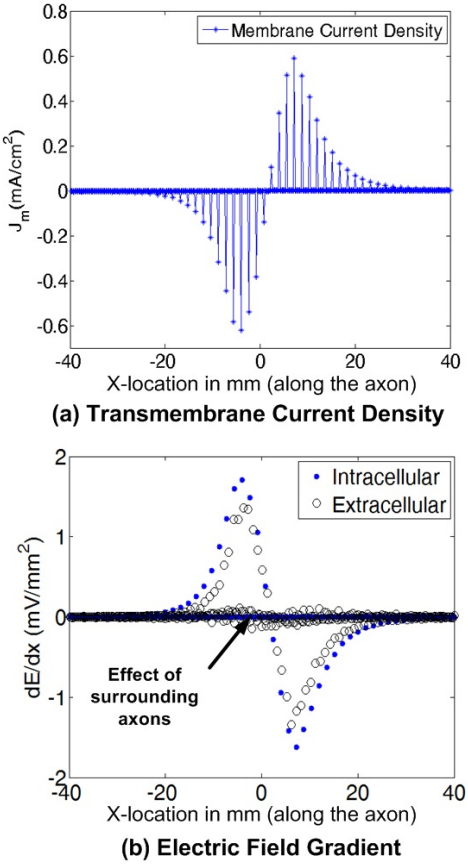

Figure 2.6: Transmembrane Current Density and Induced Electric Fields
(a) Transmembrane current density J_m at the nodes of Ranvier along the selected axon (b) Spatial derivative of the induced electric fields (intracellular and extracellular) along the axon (x-direction). The induced electric field is maximum at the position x = 0. From simulations, $J_m \propto -\frac{\partial E_x}{\partial x}$.

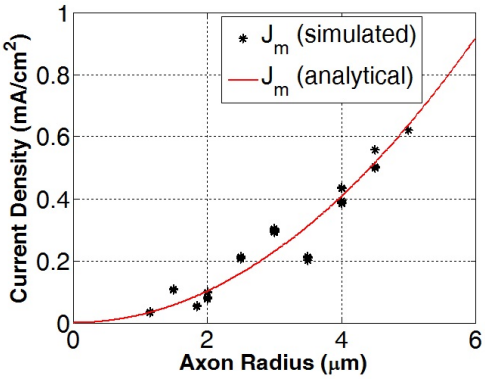

Figure 2.7: Simulated Peak Transmembrane Current Density
J_m as function of axon inner radius. The simulated data can be fitted with curve $J_m = 0.03 * radius^{1.86}$. The analytical solution: $J_m = 0.0255 * radius^2$ (Appendix 2).

$\frac{\partial E_x}{\partial x} = 1.7\ mV/mm^2$, which indicates $K = 0.0255$ and $n = 2$ using the analytical solution. The analytical and simulated values of the parameters (K,n) are in good agreement and indicate that the present simulations are capable of predicting the behavior of axons with different radii in the presence of magnetic fields. There is a small difference between the simulated and analytical values of induced J_m (Figure 2.7), which is due to the non-constant value of the g-ratio ranging from 0.45 to 0.7, compared to the value 0.6 used in the analytical solution.

Effect of Membrane Capacitance

Magnetic stimulation uses pulsed current in the magnetic coil to induce transmembrane current across the axon membrane. For the charging capacitance of 6.85 mF, an overdamped pulse current was delivered by the magnetic stimulator to the coil C1 by discharging the capacitor from a voltage of 120 V. To study the contribution of individual frequency components of the current pulse, a Fourier transform was taken and is shown in Figure 2.8(a). To study the impact of membrane capacitance on the temporal distribution of the induced electric fields (or membrane current densities), the membrane's capacitive and resistive components need to be compared. In this simulation, the nodes of Ranvier were modeled as parallel membrane resistances and capacitances. Based on the nerve model of rat sciatic nerve at 37^oC [40], the leakage transconductance g_L of 43 nS ($G_L = 61.4\ mS/cm^2$) and membrane capacitance c_m of 1.4 pF ($C_m = 2\ \mu F/cm^2$ [37], node area = 70 μm^2) were used to calculate the resistivity and dielectric constant of the axon membrane. This results in a time constant of 32.5 μs (3-db frequency of 4.8 kHz). The capacitive component ($2\pi f \epsilon_r \epsilon_0$, $\epsilon_r = 23$) reaches 10% of the resistive component (conductivity $\sigma = 4 \times 10^{-6}$ S/m) for a frequency as small as 500 Hz, and therefore, the effect of the capacitance needs to be included for frequencies above this. For other tissue media (fascicle membrane, intracellular and extracellular space) inside the nerve, the resistive components are significantly larger than the capacitive components for all the frequency components of the pulse. Due to its high resistivity and low capacitivity, the myelination layer has a comparable time constant as the axon membrane but with high impedance at all frequencies. Consequently, the induced stimulus current primarily exists through

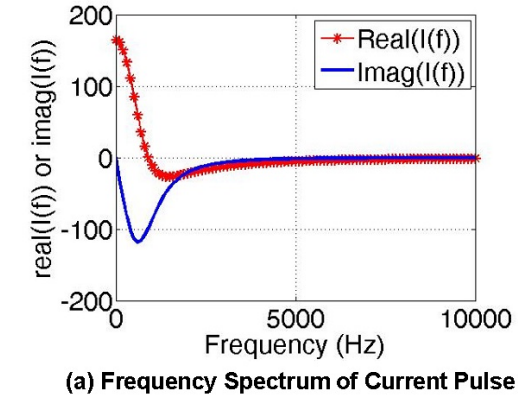

Figure 2.8: Current Pulse Characteristics
(a) Real and imaginary frequency components of the current pulse. Current pulse in the simulated magnetic coil (L = 4.32 μH, R = 45 mΩ, $V_{capacitor}$ = 120 V. (b) Normalized temporal distribution of the induced electric fields with and without including the effect of membrane capacitance. Comparison between the capacitive (=$2\pi f \epsilon_r \epsilon_0$, f = frequency, ϵ_r = 23) and resistive (= conductivity σ) components of the transmembrane impedance showed that the capacitive component reaches 10% of the resistive component for a frequency as small as 500 Hz.

the node of Ranvier and the current density across the myelination is 4-5 orders of magnitude smaller than the transmembrane current density (as seen in Figure 2.6(a)). Therefore, the spatial-temporal distribution of the myelination current has a negligible effect on the stimulus current and only the effect of the axon membrane was considered in this simulation. To achieve the empirical formulation of J_m versus frequency, transmembrane currents were simulated for multiple frequencies ({0.5, 2, 4, 6, 8, 10, 20, 40} kHz) for the real and imaginary components of the current pulse. To recreate the temporal distribution of induced current densities, the contributions from each frequency component were included in the inverse Fourier transform. The normalized (to peak value) induced current densities, with and without the effect of membrane capacitance are shown in Figure 2.8(b). Compared to the traditional models of the temporal distribution of induced current densities [6, 5, 7, 37], our simulations demonstrate that membrane capacitance increases the pulse width (PW) of the stimulus current and can not be ignored for the correct estimation of the temporal distribution of the induced current density.

Effect of Axon Radius on Stimulation Threshold

For a fixed length nerve, the number of nodes of Ranvier depends on the axon diameter $\left(\text{Node count} = \frac{\text{Length of nerve } (= L_{nerve})}{\text{Internodal distance}}\right)$. To estimate the stimulation threshold as a function of axon radius (or diameter), neuron simulations were performed for the magnetic coils' field distributions (spatial and temporal), and stimulation thresholds were estimated for axon radius varying from 1 to 5 μm (outer diameter 4 to 16 μm). Figure 2.9 shows the stimulation threshold J_m versus the axon radius for coil C1's field distribution. Compared to electric stimulation in which the stimulating electrodes excite only one or two nodes of Ranvier, a cm-sized magnetic coil induces transmembrane current at multiple nodes (Figure 2.6(b)). As the node count decreases with axon diameter, the field distribution around the smaller axon spreads to higher numbers of nodes. This reduces stimulation threshold current densities $J_{m(threshold)}$ for the smaller axons. From the NEURON based simulations for different radii axons, the stimulation threshold $J_{m(threshold)}$ is linearly proportional to the axon radius ($J_{m(threshold)}$ = 0.249*radius + 0.637 mA/cm^2, Figure 2.9).

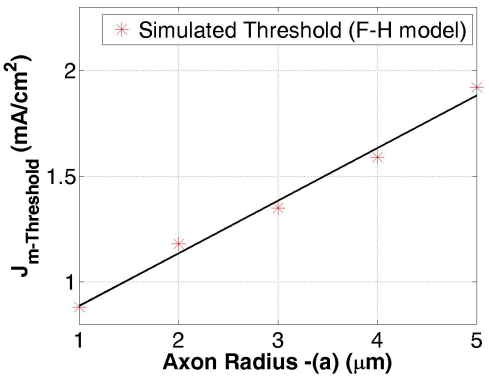

Figure

2.9: Stimulation Thresholds for Myelinated Axons as a Function of Axon Radius The axon model was created based on the Frankenhaeuser-Huxley (FH) model for rat sciatic nerve [21, 40]. The threshold shows a linear relation (fitted curve: 0.249*radius + 0.637 mA/cm^2).

Using the analysis presented in Figures 2.7 and 2.9, the recruitment order of the different radius axons is deduced. Under the same electric field distributions (or same operating voltage), the induced current density $J_m \propto a^2$ and $J_{m(threshold)} \propto a$. Therefore, $E_{x(threshold)}$ (or $V_{stimulation}$) $\propto 1/a$. This analysis shows that the larger radius axons tend to become excited for lower stimulation voltages applied to the magnetic stimulator. To validate the NEURON based simulation, the dynamics of the generated action potentials were recorded and compared with the known neuronal behavior. For example, the action potential starts at the location of peak depolarization and propagates in both axonal directions. Moreover, the propagation velocity of the action potential increases with the increase in axon radius as expected from previous work [50].

Experimental Validation of the Modeling Framework

To validate our simulations we used experimental data to compare the model's ability to predict stimulation thresholds. We performed experiments in four rat sciatic nerves as discussed in Section 2. Four magnetic coils were used in each experiment and measured stimulation thresholds were compared with the predicted values. Simulations were performed based on the proposed heterogeneous model and a traditional homogeneous model. The heterogeneous model included the effects of

fascicle and axon heterogeneity, axon proximity, and membrane capacitance. In our simulations, we found that the effect of fascicle distribution and perineurium thickness was small (less than 10 %) on the induced electric field. Therefore, the fascicular geometries in the model were not adjusted post hoc to match the geometries of an experiment. Nevertheless, we experimentally tested the coil at multiple positions perpendicular to the long axis of the nerve to reduce the variability in response due to the relative position of the coil to the unknown positions of fascicles within the nerve. The homogeneous model was based on previous studies [22, 37], which considered an axon inside an infinite homogeneous medium without including the membrane capacitance and the axons' interactions with other axons. For all coils used, the stimulation thresholds were computed based on the minimum charging voltage of the capacitor required for excitation of 20% of the motor fibers ($\sim$6% of total fiber count [51], diameter 13-16 μm). Table 2.4 and Figure 2.10(a) provide the stimulation thresholds for the four experiments and the simulations.

The variation in experimental data can be attributed to minor surgical differences and animal size and weight. If the nerve slightly curved in an experiment, stimulations thresholds were reduced [52, 53, 16], which may also contribute to differences in the threshold values between experimental and predicted data. Despite this difference, the heterogeneous model's predictions were closer to the experimental values than those of the homogeneous model (Figure 2.10(a)).

In seeking to optimize size and stimulation parameters of magnetic coils, it is important to know each coil's performance relative to one another. Therefore, we chose coil C1 as a baseline coil and normalized the stimulation thresholds of the other investigated magnetic coils (C2, C3 and C4). Using such normalization, the effects

Table 2.4: Stimulation Threshold

Coil No.	Animal 1 (V)	Animal 2 (V)	Animal 3 (V)	Animal 4 (V)	Heterogen. model (V)	Homogen. model (V)
C1	116	79	105	108	122	166
C2	114	81	118	106	121	143
C3	169	142	185	158	206	253
C4	138	114	145	141	158	176

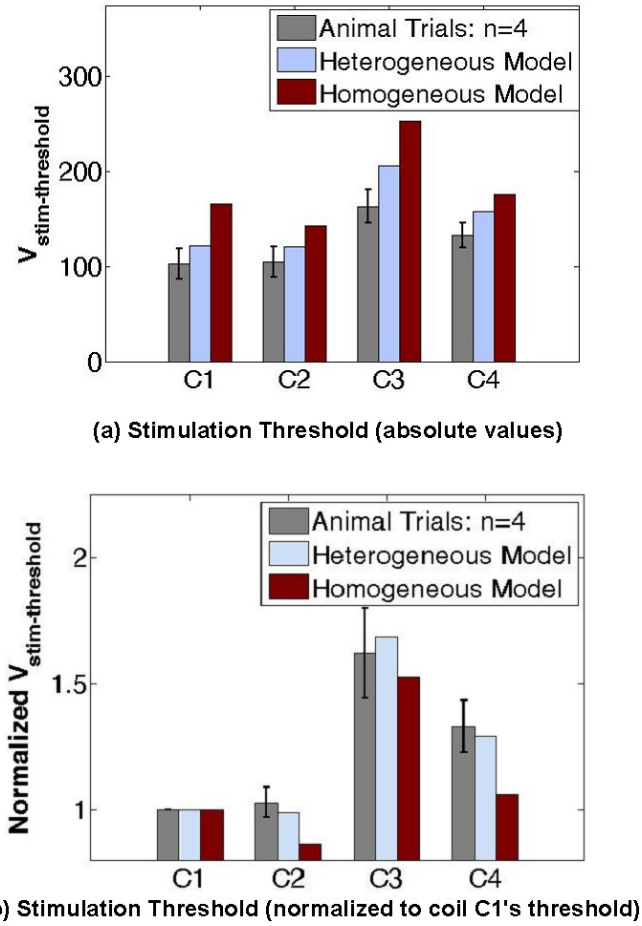

Figure 2.10: *In Vivo* vs. Simulated Stimulation Thresholds
Comparison between the (a) Absolute and (b) Normalized stimulation threshold for the *in vivo* experiment and the proposed heterogeneous and homogeneous models. The experiments were performed for four magnetic coils in four separate animals and normalization is done for the baseline coil C1.

of non-ideal scenarios (i.e., nerve curvature, surrounding tissue of the nerve) can be mitigated without increasing the complexity of the simulation. Moreover, with the knowledge of C1's stimulation threshold during one experiment, the thresholds of the other magnetic coils can be predicted. The normalized thresholds for coil C2, C3 and C4 with respect to baseline coil C1 are shown in Figure 2.10(b). Figure 2.10(b) also shows that the heterogeneous model accurately predicts threshold voltages of our *in vivo* experiments. We also considered other coils (C2, C3, and C4) as the reference coil and normalized the stimulation thresholds of the coils with respect to the threshold of each reference coil. For all these cases, the heterogeneous model based threshold prediction was a better indicator of the experimental thresholds. Moreover, predicted simulated thresholds were within the 95% confidence interval of *in vivo* experimental thresholds for all the investigated magnetic coils during four separate experiments.

The design of the magnetic coil is a multivariable optimization problem that includes coil shape, total coil volume, wire type, and capacitance of the charging capacitor. Each of these parameters can significantly alter the spatial and temporal distribution of an induced electric field. Using this comprehensive model, there is a strong correlation between the predicted threshold values and those observed in *in vivo* experiments. Compared to previous models, the current study included the effect of tissue heterogeneity, recruitment order of different diameter axons, and the effect of membrane capacitance on stimulation thresholds. We used this framework as a predictor of coil performance before using various coils during *in vivo* experiments. In the future, we intend to develop an optimization algorithm to function in conjunction with this framework to develop smaller, more energy efficient coils compared to those used in this study.

Conclusion

In this work, a computational framework for the prediction of the threshold level for magnetic stimulation of peripheral nerve tissue is presented. To make these predictions, a μm resolution heterogeneous model of rat sciatic nerve was simulated using a multiresolution impedance method to quantify the magnetically induced electric fields. The proposed model includes the effect of fascicle distribution,

axon distribution including the spacing between adjacent axons, and axon membrane resistance and capacitance in the estimation of the spatial-temporal distribution of the induced fields. Using this model, the transmembrane current density was computed as a function of axon diameter and compared with an analytical solution. To estimate the magnetic stimulation thresholds for the myelinated axon, a Frankenhaeuser-Huxley (FH) mechanism was used at the axon's nodes of Ranvier, and the behavior of the ion channels were simulated in NEURON software. Using the impedance method for the field simulation and NEURON for the active ion channel mechanisms, stimulation thresholds were predicted for four magnetic coils and compared with traditional homogeneous nerve models. Using *in vivo* magnetic stimulation in four separate rat sciatic nerve experiments, it was shown that *in vivo* measurements of magnetic stimulation thresholds can be accurately predicted using the proposed heterogeneous modeling within a 95% confidence interval (trials count=4). The presented simulation toolset describes a multi-scale model for magnetic stimulation and therefore, is capable of studying the interaction of individual neurons/axons or neuronal networks with the incident magnetic field. This modeling toolset can be effectively utilized in clinical settings (i.e., transcranial magnetic stimulation, spinal cord or peripheral nerve stimulation) to generate specific neuronal response (e.g., stimulation selectivity) in the tissue depending on the coil's shape, orientation, and position.

Appendix

Membrane Current Density versus Axon Radius

In this section, the relationship between the spatially distributed induced transmembrance current density and axon radius is derived. Figure 2.11 shows a drawing of a section of a myelinated axon containing one node of Ranvier surrounded by myelinated internodal regions. The transmembrane current (i_m) is calculated from the intracellular currents I_1 and I_2 by Kirchhoffs Current Law and each intracellular current is calculated from its induced electric field distribution, (E_K) by Ohms Law (Equations 2.1 and 2.2). Due to the high resistivity of the myelination compared to the node of Ranvier, the induced intracellular current I_K primarily passes through the node of Ranvier causing I_K to stay constant between each node. Therefore, for

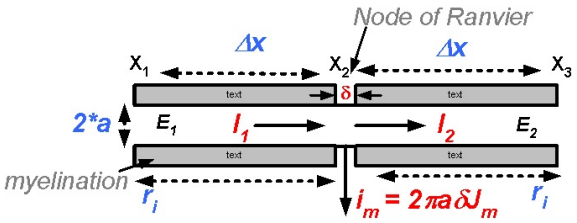

Figure 2.11: Myelinated Axon with Transmembrane Current Density
Drawing of the myelinated axon (inner radius a) with transmembrane current density J_m. r_i is the intracellular resistance between the adjacent nodes of Ranvier.

constant conductivity σ_{axon} inside the axon, E_K stays constant between consecutive nodes ($I_K = \sigma_{axon} E_K * \pi a^2$).

$$i_m = I_1 - I_2 \tag{2.1}$$

$$I_K = \frac{\Delta V}{r_i} = \frac{\int_{X_K}^{X_{K+1}} E dx}{r_i} = \frac{E_K \Delta x}{r_i} \tag{2.2}$$

where, r_i is the intracellular resistance between the adjacent nodes of Ranvier and can be represented as a function of the intracellular resistivity R_i, the internodal distance Δx, and the axon inner radius a (Equation 2.3).

$$r_i = \frac{R_i(\Delta x)}{\pi a^2} \tag{2.3}$$

where inter-nodal distance $\Delta x = 100 D_{out} = \frac{200}{0.6}\text{a} \sim 333\text{a}$ for $\frac{D_{in}}{D_{out}} = 0.6$. D_{in} and D_{out} are the inner diameter and outer diameter of the myelinated axon.

Using Equations 2.1, 2.2, and 2.3, the induced transmembrane current i_m, in response to the applied time varying magnetic fields, is shown in Equation 2.4.

$$\begin{aligned} i_m &= \frac{\Delta x}{r_i}(E_1 - E_2) \\ &= \frac{\pi a^2}{R_i}(E_1 - E_2) = \frac{\pi a^2}{R_i}\Delta E_{1-2} \end{aligned} \tag{2.4}$$

where ΔE_{1-2} is the induced electric field difference between consecutive node 1 and 2.

Multiplying Δx in the numerator and denominator of the Equation 2.4 and replacing Δx in the numerator by 333a, transmembrane current i_m and current density J_m for a general node of Ranvier can be written as:

$$i_m = \frac{333\pi a^3}{R_i}\frac{\Delta E}{\Delta x} \tag{2.5}$$

$$J_m = \frac{i_m}{2\pi a\delta} = -\frac{333}{2\delta}\frac{a^2}{R_i}\left(\frac{\Delta E}{\Delta x}\right) \quad (A/m^2) \tag{2.6}$$

where δ is the length of node of Ranvier. All parameters are in SI units.

To achieve J_m in units of mA/cm^2 (as used by NEURON) and expressing the values for $\left(\frac{\Delta E}{\Delta x}\right)$ in mV/mm^2 and axon radius a in μm (typically used for magnetic stimulation [9, 26, 11]), the following conversion factors were applied ($1\ A/m^2 = 0.1\ mA/cm^2$, $1\ V/m^2 = 0.001\ mV/mm^2$, 1 m $= 10^6 \mu m$). Therefore,

$$J_m = \frac{i_m}{2\pi a\delta} = -\frac{333\times 10^{-10}}{2\delta}\frac{a^2}{R_i}\left(\frac{\Delta E}{\Delta x}\right) \quad (mA/cm^2) \tag{2.7}$$

For $\delta = 1\times 10^{-6}$ meter, $R_i = 1.1\ \Omega - meter$, transmembrane current density J_m at the node of Ranvier is calculated using Equation 2.8.

$$J_m = -0.015\left(\frac{\Delta E}{\Delta x}\right)a^2 \quad (mA/cm^2) \tag{2.8}$$

where $\left(\frac{\Delta E}{\Delta x}\right)$ is the spatial derivative of intracellular electric field in the long axis of the axon (x-direction in the model). The spatial derivative of induced electric fields is in mV/mm^2 and a is the axon radius in μm.

Frankenhaeuser-Huxley (FH) Model

A Frankenhaeuser-Huxley (FH) model was first proposed to model the membrane's ion channel activity in myelinated axons [21]. Compared to the traditional Hodgkin-

Huxley (HH) model, the myelinated axon has lower contributions from the potassium channels [54]. The FH model based node of Ranvier includes one sodium channel, potassium channel, leakage channel, and the membrane capacitance [40]. Equation 2.9 includes the transmembrane current density contributed by sodium (J_{Na}), potassium (J_K), leakage (J_L), and stimulation (J_m) currents.

$$J_{membrane} = J_{Na} + J_K + J_L + C_m dV/dt + J_m \tag{2.9}$$

Individual currents were calculated based on the sodium and potassium concentrations in the intracellular ($[Na]_i$ or $[K]_i$) and extracellular ($[Na]_o$ or $[K]_o$) spaces [21]. Table 2.5 includes the parameter values used for the rat FH model.

Table 2.5: Frankenhaeuser-Huxley (FH) Model Parameters

Temp:	37^{o}C		
E_{rest}	-78 mV	V_L	-78 mV
$[Na]_i$	8.71 mM	$[Na]_o$	154 mM
$[K]_i$	155 mM	$[K]_o$	5.9 mM
G_L	61.4 mS/cm^2	C_m	2 $\mu F/cm^2$
$\bar{P}_{Na}$	$7.32 \times 10^{-3} cm/sec$	$\bar{P}_K$	$0.288 \times 10^{-3} cm/sec$
Q_{10}:	$\tau_m = 2.2$	$\tau_h = 2.9$	$\tau_n = 3.0$
	A	B	C
	(ms^{-1})	(mV)	(mV)
α_m	0.49	25.41	6.06
β_m	1.04	21.0	9.41
α_h	0.09	-27.74	9.06
β_h	3.7	56	12.5
α_n	0.02	35	10
β_n	0.05	10	10
D_{axon}	4-16 μm	$d_{node-node}$	$100 * D_{out-axon}$
δ_{node}	1 μm	L_{nerve}	88 mm

References

[1] M. Kobayashi and A. Pascual-Leone, "Transcranial magnetic stimulation in neurology," *Lancet Neurol.*, vol. 2, no. 3, pp. 145–156, 2003.

[2] P. M. Rossini and S. Rossi, "Transcranial magnetic stimulation: Diagnostic, therapeutic, and research potential," *Neurology*, vol. 68, pp. 484–488, Feb. 2007.

[3] J. Reilly, "Peripheral nerve stimulation by induced electric currents: exposure to time-varying magnetic fields," *Med. Biol. Eng. Comput.*, vol. 27, pp. 101–110, Mar. 1989.

[4] R. J. Ilmoniemi, *et al.*, "Neuronal responses to magnetic stimulation reveal cortical reactivity and connectivity.," *Neuroreport*, vol. 8, pp. 3537–40, Nov. 1997.

[5] K.-H. Hsu, *et al.*, "Analysis of efficiency of magnetic stimulation.," *IEEE Trans. Biomed. Eng.*, vol. 50, pp. 1276–1285, Nov. 2003.

[6] E. Basham, *et al.*, "Circuit and coil design for in-vitro magnetic neural stimulation systems," *IEEE Trans. Biomed. Circuits Syst.*, vol. 3, pp. 321–331, Jun. 2009.

[7] M. Yamaguchi and S. Yamada, "Electromagnetic mechanism of magnetic nerve stimulation," *J. Appl. Phys.*, vol. 66, pp. 1459–1465, Aug. 1989.

[8] T. Pashut, *et al.*, "Mechanisms of magnetic stimulation of central nervous system neurons.," *PLoS Comput. Biol.*, vol. 7, p. e1002022, Mar. 2011.

[9] S. S. Nagarajan, *et al.*, "Effects of induced electric fields on finite neuronal structures: a simulation study.," *IEEE Trans. Biomed. Eng.*, vol. 40, pp. 1175–88, Nov. 1993.

[10] E. R. Lontis, *et al.*, "In vitro magnetic stimulation of pig phrenic nerve with transverse and longitudinal induced electric fields: analysis of the stimulation site.," *IEEE Trans. Biomed. Eng.*, vol. 56, pp. 500–12, Feb. 2009.

[11] S. S. Nagarajan, *et al.*, "Mapping location of excitation during magnetic stimulation: effects of coil position.," *Ann. Biomed. Eng.*, vol. 25, pp. 112–125, Jan. 1997.

[12] H.-J. Park, *et al.*, "Activation of the central nervous system induced by micro-magnetic stimulation," *Nat. Commun.*, vol. 4:2463, pp. 1–9, Sep. 2013.

[13] G. Bonmassar, *et al.*, "Microscopic magnetic stimulation of neural tissue," *Nat. Commun.*, vol. 3:921, pp. 1–10, Jan. 2012.

[14] T. Pashut, *et al.*, "Patch-clamp recordings of rat neurons from acute brain slices of the somatosensory cortex during magnetic stimulation," *Front. Cell. Neurosci.*, vol. 8, pp. 1–12, Jun. 2014.

[15] E. Corthout, *et al.*, "Transcranial magnetic stimulation: Which part of the current waveform causes the stimulation?," *Exp. Brain Res.*, vol. 141, pp. 128–132, Nov. 2001.

[16] P. Maccabee, *et al.*, "Magnetic coil stimulation of straight and bent amphibian and mammalian peripheral nerve in vitro: locus of excitation," *J. Physiol.*, vol. 460, pp. 201–219, Jan. 1993.

[17] H. Tischler, *et al.*, "Mini-coil for magnetic stimulation in the behaving primate," *J. Neurosci. Methods*, vol. 194, pp. 242–251, Oct. 2011.

[18] T. A. Wagner, *et al.*, "Three-dimensional head model simulation of transcranial magnetic stimulation.," *IEEE Trans. Biomed. Eng.*, vol. 51, pp. 1586–98, Sep. 2004.

[19] V. T. Z. Krasteva, *et al.*, "Peripheral nerve magnetic stimulation: influence of tissue non-homogeneity.," *Biomed. Eng. Online*, vol. 2, p. 19, Dec. 2003.

[20] A. K. RamRakhyani, *et al.*, "A m-resolution Heterogenous Tissue Model for the Magnetic Stimulation of Multifascicular Sciatic Nerve," *Conf. Proc. IEEE Eng. Med. Biol. Soc.*, vol. 2014, 2014.

[21] B. Frankenhaeuser and A. F. Huxley, "The action potential in the myelinated nerve fiber of xenopus laevis as computed on the basis of voltage clamp data," *J. Physiol.*, vol. 171, pp. 302–315, Jun. 1964.

[22] B. Roth and P. Basser, "A model of stimulation of a nerve fiber by electromagnetic induction," *IEEE Trans. Biomed. Eng.*, vol. 37, pp. 588–597, Jun. 1990.

[23] D. Durand, *et al.*, "Effect of surface boundary on neuronal magnetic stimulation.," *IEEE Trans. Biomed. Eng.*, vol. 39, pp. 58–64, Jan. 1992.

[24] K. P. Esselle and M. a. Stuchly, "Neural stimulation with magnetic fields: analysis of induced electric fields.," *IEEE Trans. Biomed. Eng.*, vol. 39, pp. 693–700, Jul. 1992.

[25] J. Ruohonen, *et al.*, "A volume-conduction analysis of magnetic stimulation of peripheral nerves.," *IEEE Trans. Biomed. Eng.*, vol. 43, pp. 669–78, Jul. 1996.

[26] S. Nagarajan and D. Durand, "A generalized cable equation for magnetic stimulation of Axons," *IEEE Trans. Biomed. Eng.*, vol. 43, no. 3, pp. 304–312, 1996.

[27] S. S. Nagarajan and D. M. Durand, "Analysis of magnetic stimulation of a concentric axon in a nerve bundle.," *IEEE Trans. Biomed. Eng.*, vol. 42, pp. 926–33, Sep. 1995.

[28] Z. B. Kagan, *et al.*, "Magnetic stimulation of mammalian peripheral nerves in vivo: An alternative to functional electrical stimulation," *Conf. Proc. IEEE Eng. Med. Biol. Soc.*, pp. 2573–2576, Aug. 2014.

[29] N. Orcutt and O. P. Gandhi, "A 3-D impedance method to calculate power deposition in biological bodies subjected to time varying magnetic fields.," *IEEE Trans. Biomed. Eng.*, vol. 35, pp. 577–83, Aug. 1988.

[30] N. Carnevale and M. Hines, *The NEURON Book*. Cambridge, UK: Cambridge University Press, 2006.

[31] M. B. Christensen and P. A. Tresco, "Differences exist in the left and right sciatic nerves of naïve rats and cats," *Anat. Rec.*, vol. 298, no. 8, pp. 1492–1501, 2015.

[32] S. Raspopovic, *et al.*, "Experimental validation of a hybrid computational model for selective stimulation using transverse intrafascicular multichannel electrodes," *IEEE Trans. Neural Syst. Rehabil. Eng.*, vol. 20, pp. 395–404, May 2012.

[33] S. Raspopovic, "A computational model for the stimulation of rat sciatic nerve using a transverse intrafascicular multichannel electrode," *Neural Syst. ...*, vol. 19, pp. 333–44, Aug. 2011.

[34] C. R. Butson, *et al.*, "Selective neural activation in a histologically derived model of peripheral nerve.," *J. Neural Eng.*, vol. 8, p. 036009, Jun. 2011.

[35] M. A. Schiefer, *et al.*, "A model of selective activation of the femoral nerve with a flat interface nerve electrode for a lower extremity neuroprosthesis," *IEEE Trans. Neural Syst. Rehabil. Eng.*, vol. 16, pp. 195–204, Apr. 2008.

[36] P. Y. C. N. Mazzer, *et al.*, "Morphologic and morphometric evaluation of experimental acute crush injuries of the sciatic nerve of rats," *J. Neurosci. Methods*, vol. 173, pp. 249–258, Aug. 2008.

[37] P. Basser and B. Roth, "Stimulation of a myelinated nerve axon by electromagnetic induction," *Med. Biol. Eng. Comput.*, vol. 29, pp. 261–268, May 1991.

[38] J. P. Reilly and R. H. Bauer, "Application of a neuroelectric model to electrocutaneous sensory sensitivity: parameter variation study.," *IEEE Trans. Biomed. Eng.*, vol. 34, pp. 752–4, Sep. 1987.

[39] D. Andreuccetti, *et al.*, "An Internet resource for the calculation of the dielectric properties of body tissues in the frequency range 10 Hz - 100 GHz," 1997.

[40] J. Schwarz and G. Eikhof, "Na currents and action potentials in rat myelinated nerve fibres at 20 and 37 C," *Pflügers Arch.*, pp. 569–577, Aug. 1987.

[41] D. R. McNeal, "Analysis of a model for excitation of myelinated nerve.," *IEEE Trans. Biomed. Eng.*, vol. 23, pp. 329–37, Jul. 1976.

[42] F. Rattay and M. Aberham, "Modeling axon membranes for functional electrical stimulation.," *IEEE Trans. Biomed. Eng.*, vol. 40, pp. 1201–9, Dec. 1993.

[43] J. H. Frijns, *et al.*, "A quantitative approach to modeling mammalian myelinated nerve fibers for electrical prosthesis design.," *IEEE Trans. Biomed. Eng.*, vol. 41, pp. 556–66, Jun. 1994.

[44] C. C. McIntyre, *et al.*, "Modeling the excitability of mammalian nerve fibers: influence of afterpotentials on the recovery cycle.," *J. Neurophysiol.*, vol. 87, pp. 995–1006, Feb. 2002.

[45] A. Branner and R. A. Normann, "A multielectrode array for intrafascicular recording and stimulation in sciatic nerve of cats.," *Brain Res. Bull.*, vol. 51, pp. 293–306, Mar. 2000.

[46] A. Barker, "An introduction to the basic principles of magnetic nerve stimulation," *J. Clin. Neurophysiol.*, vol. 8, pp. 26–37, Jan. 1991.

[47] H. A. C. Wark, *et al.*, "Selective activation of the muscles of micturition using intrafascicular stimulation of the pudendal nerve," *IEEE J. Emerg. Sel. Top. Circuits Syst.*, vol. 1, pp. 631–636, Dec. 2011.

[48] Y. Grinberg, *et al.*, "Fascicular perineurium thickness, size, and position affect model predictions of neural excitation.," *IEEE Trans. Neural Syst. Rehabil. Eng.*, vol. 16, pp. 572–81, Dec. 2008.

[49] A. Q. Choi, *et al.*, "Selectivity of multiple-contact nerve cuff electrodes: A simulation analysis," *IEEE Trans. Biomed. Eng.*, vol. 48, pp. 165–172, Apr. 2001.

[50] L. Goldman and J. S. Albus, "Computation of impulse conduction in myelinated fibers; theoretical basis of the velocity-diameter relation.," *Biophys. J.*, vol. 8, pp. 596–607, May 1968.

[51] H. Schmalbruch, "Fiber composition of the rat sciatic nerve," *Anat. Rec.*, vol. 215, pp. 71–81, May 1986.

[52] J. P. Reilly and A. M. Diamani, "Spatial relationships in electrostimulation: application to electromagnetic field standards.," *IEEE Trans. Biomed. Eng.*, vol. 50, pp. 783–5, Jun. 2003.

[53] A. Rotem and E. Moses, "Magnetic stimulation of curved nerves.," *IEEE Trans. Biomed. Eng.*, vol. 53, pp. 414–420, Mar. 2006.

[54] S. Chiu, *et al.*, "A quantitative description of membrane currents in rabbit myelinated nerve," *J. Physiol.*, pp. 149–166, Jul 1979.

CHAPTER 3

IN VIVO MAGNETIC STIMULATION OF RAT SCIATIC NERVE WITH CENTIMETER- AND MILLIMETER-SCALE SOLENOID COILS

This chapter is a journal article in press in the *IEEE Transactions on Neural Systems and Rehabilitation*. Reprinted by permission, ©2016 IEEE. Authors of this chapter are Z.B. Kagan, A.K. Ramrakhyani, G. Lazzi, R.A. Normann, and D.J. Warren.

Abstract

Previous reports of magnetic stimulation of the peripheral nervous system (PNS) used various coil geometries, all with outer diameters larger than 35 mm, and stimulation energies in the 50 J range to evoke neural excitation. Recent reports of central nervous system (CNS) activation used sub-mm-scale solenoid coils with mJ energy levels. The goal of this study was to translate the lower energy levels from the CNS to the PNS via using smaller coils placed in closer proximity to the neural tissue. Such a performance improvement would advance the state of the art of magnetic stimulation and provide a path towards new neuroprosthetic devices. Primarily, we investigated the range of coil outer diameters from 25 mm down to 5 mm to better understand the dependence of coil diameter on energy required for PNS activation. Nine cm- and mm-scale copper solenoid coils, with various resistances, inductances, inner and outer diameters, and heights were compared by quantizing neuromuscular responses to magnetic stimulation via capacitive discharge excitation of rat sciatic nerves *in vivo*. Additionally, the effects of stimulus duration and coil position were investigated. As opposed to prior work, this study compares a subset of stimulation parameters in an intact nerve preparation, and shows that magnetic stimulation with coils that abut the nerve is a reliable, effective method of neuromuscular stimulation. Although we observed different energies required for

neuromuscular activation depending on the coil and excitation parameters used, for the experimental configuration, devices, and stimulus waveform shapes presented in this manuscript, no systematic dependence of PNS activation on coil diameter was found, even for the mm-scale coils investigated herein. However, there was a clear relationship between discharge circuit capacitance and energy required to evoke a neuromuscular response. Coils approximately 12 mm in outer diameter and larger consistently evoked responses, whereas coils 5 mm in outer diameter did not. Furthermore, we observed meaningful neuromuscular excitation when stimulating with energies as low as 20 J. Although this is an improvement over prior work, it is still orders of magnitude greater than the energy required for conventional electrical stimulation, suggesting that these devices are presently not suitable for use in an application requiring continued pulsed stimulation. Nevertheless, these devices are suitable for basic research and as clinical tools that infrequently stimulate, such as in diagnostic applications.

Introduction

Magnetic stimulation of neural tissue has been investigated as a diagnostic, therapeutic, or research tool. The primary motivation to use magnetic stimulation instead of electrical stimulation is that magnetic stimulation does not require direct electrical contact to the neural tissue. However, the most notable drawback of magnetic stimulation is the large energy required to evoke neural activity, often orders of magnitude higher than conventional electrical microstimulation. Recent studies have demonstrated that magnetic stimulation of the central nervous system (CNS) is possible with energies below 1 mJ [1, 2], providing a substantial impetus to achieve these low stimulus energies in the peripheral nervous system (PNS). Previously, magnetic stimulation coils used in the PNS [3, 4] and CNS [5] were several centimeters in outer diameter, with energies required for peripheral nerve stimulation larger than 30 J. The coils used in recent reports of low-energy magnetic stimulation experiments in the CNS were of sub-millimeter size. Successfully using sub-millimeter scale coils at very low energies in the PNS, as has been done in CNS, would provide a notable improvement to the state of the art of peripheral magnetic stimulation, potentially

allowing for these sub-millimeter coils to be used in implanted device applications.

Thus, in an effort to achieve low energy magnetic stimulation of the PNS, we have investigated coil geometries ranging from the cm-scale to the mm-scale, smaller than any coils previously reported in studies of magnetic stimulation of the PNS [3, 4]. An *in vivo* rat sciatic nerve model was developed and used as it is robust, consistent, and widely available. Additionally, computational methods of peripheral magnetic stimulation [6] corroborated findings from the *in vivo* experiments.

Methods

Coil Designs

Nine copper wire solenoid coils with various electrical properties and geometries were used. Six of these were hand wound cm-scale coils made by wrapping single strand copper magnet wire around wooden dowels. The other three coils were mm-scale commercially available surface-mount-device (SMD) air-core solenoid inductors (AIAC-4125C series, Abracon, Irvine, CA). Coil geometries were selected so as to span the range of coils that have been shown to work in the PNS to those recently shown to work in the CNS. This range provides a methodical approach to investigating the dependence of coil geometry on magnetic stimulation energies. The hand wound coils were designed to have inductances in a range that other researchers have found to be effective for magnetic stimulation. The SMD coils utilized were selected as having the highest current carrying capacity among commercially available air-core SMD inductors. Geometrical and electrical properties of all coils used are provided in Table 3.1.

Stimulation Electronics

To generate sufficient currents within the coils to induce neuromuscular activity, a capacitive discharge stimulation system similar to those employed in prior studies [6, 7, 8, 9] was used (Figure 3.1A). A custom-built high voltage DC power supply with a maximum voltage of 400 V charges a capacitor bank to a preset voltage and the solid-state relay is opened. Stimulation occurs when the thyristor connects the charged capacitor bank to the stimulating coil. For initial designs, a stimulus duration of approximately 200 μs was chosen based on a prior study in rabbit sciatic

Table 3.1: Solenoids Used and Their Geometrical and Electrical Properties and Cross Sectional Views

Coil Size Class	Small		Medium		Large		SMD Class		
Coil Identifier	A	B	C	D	E	F	G	H	I
OD (mm)	11.6	11.7	16	16.4	23.5	24.7	5	5	5
PW @ 6.6 mF (μs)	185	203	203	200	311	361	85	81	73
ID (mm)	2.2	7.0	3.0	8.0	9.4	9.7	4.6	4.6	4.6
L (μh)	4.6	5.3	5.4	4.3	10.3	12.6	0.491	0.538	0.422
R (mΩ)	34	33	35	17	30	32	40	42	39
Total Turns	52	46	30	27	30	30	19	20	18
Wire Thickness (mm)	1.02	1.02	1.02	1.15	1.15	1.02	0.40	0.38	0.40
Height (mm)	16.8	27.4	10.7	13.3	8.8	11.0	9.0	9.0	9.0
Used in N animals	11	6	6	20	6	10	3	3	3

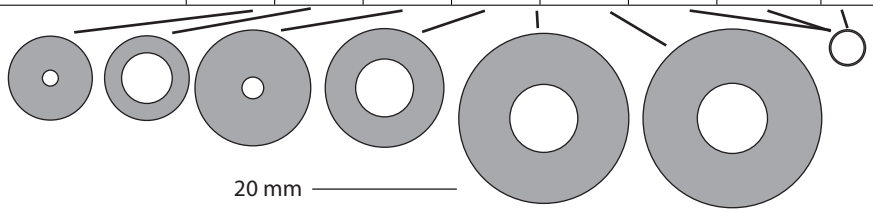

nerve [3], which found that increasing the stimulus duration substantially beyond 200 μs did not meaningfully reduce the stimulation intensity necessary to develop a given response. To accommodate this stimulus duration with the manufactured coils, as well as provide other stimulus durations, a capacitor bank that provided five different capacitance options was used (0.73 mF, 1.1 mF, 2.2 mF, 4.4 mF, and 6.6 mF). Stimulus duration was defined as the time from when current is zero to the time that current reaches its maximum (Figure 3.1B) as has been done previously [10].

Surgical Procedure

All procedures were approved by the University of Utah Institutional Animal Care and Use Committee. Sprague-Dawley rats (male, 250-450 g) were used (n = 20). Anesthesia was induced and maintained with Isoflurane gas (1-5% MAC). Vital signs (heart rate, blood oxygen saturation, respiration rate, and rectal temperature) were monitored to assess the depth of anesthesia and animal condition. Surgical procedures

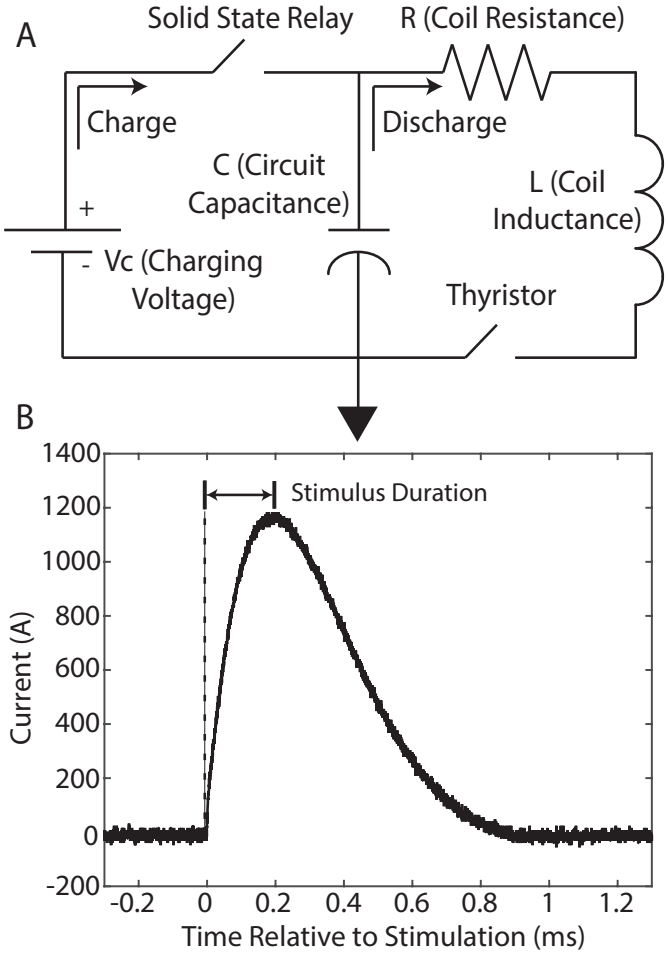

Figure 3.1:
Circuit Diagram of Stimulator and Current through Coil after Capacitor Discharge (A) The high voltage power supply (left branch) charges the capacitor (middle branch) through the closed solid state relay to a desired voltage at which time the solid state relay opens. Then, the thyristor between the capacitor and the discharge path (right branch) is closed, rapidly delivering energy in the capacitor to the coil. (B) Stimulus duration is defined from stimulus onset to when the current reaches its maximum (i.e., the first time $di/dt = 0$) as indicated. Current was experimentally measured with a series 5 mΩ resistor. For these data, Coil D was used, discharge circuit capacitance was 6.6 mF, and charging voltage was 100 V.

for exposing the nerve were similar to those previously described [11]. A segment of the sciatic nerve at least 2.5 cm long was exposed between the hip and the knee. The stimulating coil, which was electrically insulated from tissue by a 3 cm x 3 cm x 13 μm thick polyimide film, was positioned directly above the nerve approximately halfway between the hip and knee with a stereotactic 3-dimension positioning system. Care was taken to maintain the nerve in a linear geometry to reduce the effects of nerve curvature on stimulation criterion responses [12, 13]. The coil was placed such that the turns of the coil were tangent to the length of the nerve when viewed from above, with the nerve laying beneath the inner and outer diameters of the coil, as illustrated in Figure 3.2. In this position, the coil was connected to the stimulator such that current in turns closest to the nerve flowed distally. Further details are described in the experimental procedures section.

In addition to the electrical insulation provided by the polyimide film, the film also provided a surface that covered the nerve to reduce dehydration for the duration of the magnetic stimulation trials. The nerve was directly exposed to air for the trials of electrical stimulation and some parts of the surgical exposure, typically for about 20 minutes out of the entire experiment. Additionally, the EMG response to electrical stimulation was tested before and after the magnetic stimulation portion of all experiments. If the evoked EMG responses changed dramatically (15% or more) between these two sets of control trials, those data from the experiment were not used. These control experiments were used to assure changes in response to magnetic stimulation were only minimally impacted by dehydration, physical damage, or inflammation of the nerve.

As natural indicators of evoked neural activity, electromyography (EMG) data was recorded differentially from the major extensor and flexor muscles of the ankle: lateral gastrocnemius (LG), medial gastrocnemius (MG), tibialis anterior (TA), and soleus (Sol). EMG wires were made as described in prior work [14] and inserted as pairs into each muscle. EMG recordings were bandpass filtered between 10 Hz and 1 kHz with a differential AC amplifier (Model 1700, A-M Systems, Sequim, WA) with a gain of 100. Amplifier ground was provided via a Ag/AgCl 15 AWG wire or a non-insulated 18 gauge syringe needle inserted under the skin near the hip. Data

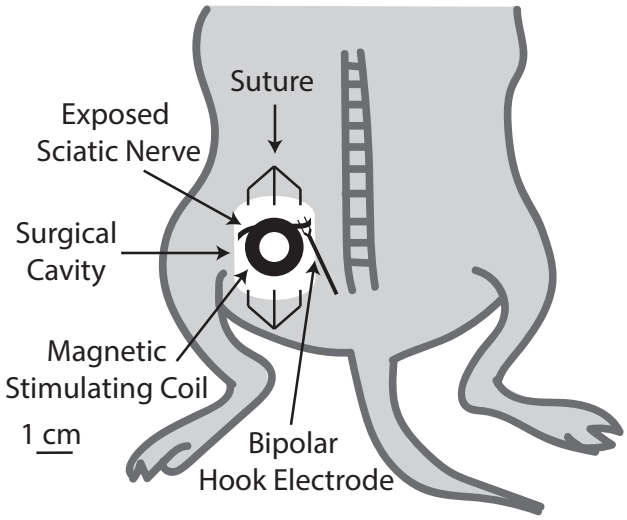

Figure 3.2: Surgical Cartoon
Illustration of surgical preparation and coil position. The magnetic stimulating coil was positioned with the turns of wire tangent to the exposed sciatic nerve.

were sampled using a Cerebus data acquisition system (Blackrock Microsystems, Salt Lake City, UT) at 30 kHz.

Experimental Procedures for Investigating the Effects of Coil Parameters on Criterion Response

EMG amplitude for a trial was defined as the peak minus trough value over a window from 2 ms to 16 ms post-stimulus. In all experiments, an EMG criterion response was defined as the stimulation intensity at which 20% of the maximal EMG amplitude was observed. We characterized the stimulus intensity in both voltage and energy based on the voltage stored on the discharge circuit capacitor and the discharge circuit capacitance. Maximal EMG amplitudes were established via 50 μs constant voltage electrical stimulation by an SD-9 stimulator (Grass Products, Warwick, RI) using a bipolar hook electrode with stimulation starting from 0.1 V and increasing until EMG saturation was observed. This was performed once prior to any magnetic stimulation trials to establish a baseline comparison between electrical stimulation and magnetic stimulation and again at the end of the experiment as a return to control to ensure that the quality of the preparation was maintained throughout. Typically, there were about 4 hours of magnetic stimulation trials between these

electrical stimulation control trials. As described earlier, only data from experiments in which the change in response amplitude from electrical stimulation before and after magnetic stimulation was 15% or less were used. The stimulation intensity evoking the 20% criterion response was calculated by linearly interpolating between the two data points directly below and above 20% responses. Additionally, latency and duration of the EMG response were defined as the time from stimulation to EMG waveform onset, and the time from EMG waveform onset to EMG waveform return to baseline, respectively.

Magnetic stimulation trials were performed with each of the coils, coil positions, capacitor configurations, and capacitor charging voltages in order to assess the influence of these factors on EMG criterion response voltages and energies. To ensure the coil was placed no further than 0.5 mm from the position at which stimulation produced the lowest EMG criterion energies, each time a coil was introduced it was first tested at 5 positions, separated by 1 mm, with the middle position corresponding to the assumed optimal position. These positioning trials were performed in every experiment. The coil was positioned over the nerve such that the nerve appeared tangent to a turn of wire approximately in the middle of the inner and outer diameters of the coil when viewed from above, as illustrated in Figure 3.2 [15]. All stimulation trials, including coil positioning trials, were performed three times to record the consistency of EMG amplitude responses to magnetic stimulation.

After optimizing coil position, response EMG amplitude was measured as a function of magnetic stimulation intensity (i.e., by measuring EMG recruitment curves) by stepping capacitor voltage in 20 V increments over the range from 80 V to 400 V (depending on capacitor configuration). Full EMG recruitment curves (in which EMG amplitudes reflect the full range of muscle activation, from zero to saturation) were obtained in 8 animals. In other experiments, an air gap between the nerve and coil was introduced by raising the coil above the nerve. The effect of this air gap on EMG criterion response was investigated by generating EMG recruitment curves for air gaps of 1, 2, and 3 mm (n = 4 animals). In order to study the effects of excitation stimulus duration on criterion response energy, EMG criterion response energies were measured for each of the five different capacitance values used (n = 4

animals). Lastly, to investigate the effect of coil geometry on criterion response, all six of the hand wound coils were used within the same animals (n = 5) to compare the capacitor voltages needed to evoke criterion responses. Each of the 3 SMD coils were tested in 3 separate animals, for a total of 9 SMD experiments. In an attempt to reach EMG criterion responses with these small coils, testing was continued up to their failure point, defined as any stimulus evoked mechanical deformation of the coil. These coils typically failed for stimulation energies near 60 J. For this reason, SMD coils were only tested with the two lowest capacitance values (0.73 mF and 1.1 mF). If an SMD coil mechanically failed, a new coil with the same properties replaced the damaged coil for subsequent experiments. The larger coils were used in many trials with energies over 100 J. Most data presented here was collected using Coil D.

Thermal Response of Coils to Capacitive Discharges

The magnetic stimulation currents needed to induce neuromuscular activity for the experimental configuration and exposure conditions presented herein are on the order of 1 kA with durations on the order of hundreds of microseconds or less. Despite these short durations, heat may be generated in the coils that is sufficient to damage the nerves, preventing conduction of action potentials. To characterize the thermal kinetics of these coils, and the temperatures to which a nerve may be exposed, a T420 infrared thermal imaging camera with a one second frame rate (FLIR, Wilsonville, OR) was used to capture thermal images of coils D and G. To hasten coil cooling, a vacuum port developing a flow rate of approximately 0.08 m^3/s at the nozzle was placed within 5 mm of the coil to circulate air around the coil. After completing all magnetic stimulation trials in an experiment, the coil was removed. The bipolar hook electrode, which was used for control electrical stimulation, was then positioned proximal to the previous location of the magnetic coil before it was removed. Hence, if the nerve had been damaged during magnetic stimulation trials, neuromuscular activity from electrical stimulation would have been suppressed or prevented entirely. This damage was observed in two experiments not reported in this study which led to the inclusion of vacuum cooling.

Simulation Methods

Voltages and energies required to elicit an action potential in a single axon were simulated for all 9 coils used in the *in vivo* experiments using the multiphysics modeling approach delineated in Ramrakhyani et al. [6]. In response to the magnetic field generated by the coil, the induced transmembrane current was simulated and applied as a stimulus in NEURON software [16]. The induced transmembrane current density followed the spatial field profile of the induced electric field (i.e., the current density was proportional to the derivative of the electric field along the length of the axon) [6]. To simulate the dynamics of active ion channels, biophysical parameters were based on the Frankenhauser-Huxley myelinated axon model. Circular magnetic coils created the depolarization and hyperpolarization sites along the axon. The action potential started at the site of the greatest depolarization and propagated in both directions of the axon. The spatial distribution of the depolarization and hyperpolarization sites depended on the coil diameter.

Results

While our primary goal was to reduce criterion response energies via modification of coil geometries ranging from the cm-scale to the mm-scale, we first wanted to characterize peripheral magnetic stimulation more broadly so it could be compared to more conventional electrical stimulation. Thus, we investigated more general aspects of magnetic stimulation via the resulting EMG response, including EMG waveform amplitude, latency, and duration.

Comparison of Magnetic and Electrical Stimulation

As the most common method of neuromuscular stimulation, functional electrical stimulation (FES) was used as a benchmark for magnetic stimulation (MS). Both electrical and magnetic stimulation with increasing intensities were capable of producing small, intermediate, and saturating levels of EMG responses in the rat lateral gastrocnemius muscle (Figure 3.3A). Furthermore, the response kinetics evoked by both stimulation modalities were very similar, with the exception of a stimulus artifact produced during magnetic stimulation visible from stimulus onset to approximately 1.4 ms later. This magnetic stimulation artifact was visible because

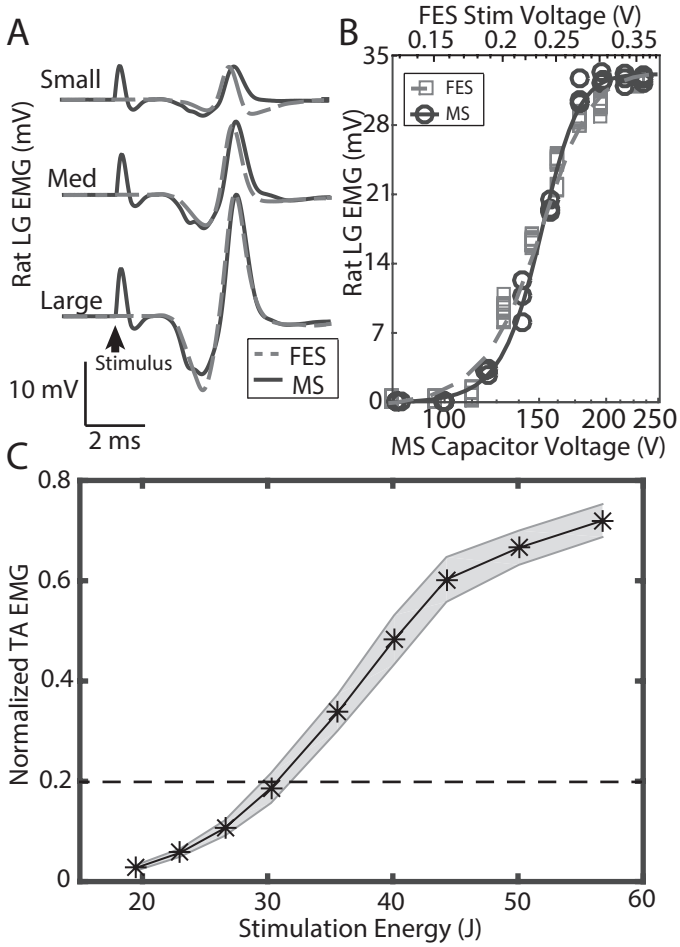

Figure 3.3: Comparison of Electrical and Magnetic Stimulation
Electrical and magnetic stimulation (FES and MS, respectively) produced similar muscle activation. EMG responses and subsequent EMG recruitment curves of rat lateral gastrocnemius (LG) for FES and MS (stimulation with Coil D and 6.6 mF capacitance). (A) Samples evoked by each stimulation modality demonstrating similar muscle activation, similar muscular output kinetics, and graded responses. Data show responses with amplitudes just above threshold, at an intermediate value, and near-maximal (Small, Med, and Large in A). An arrow indicates when stimulation was delivered in every trial. The events immediately following stimulation in the MS traces are stimulation artifacts. (B) Both stimulation modalities show a dynamic range of approximately half of a logarithmic decade. Sigmoidal curves were generated with a nonlinear regression function using least squares estimation in Matlab (MathWorks, Natick, MA) (C) Variability of MS of tibialis anterior (TA) across 8 animals. At the coil position where MS produced the largest response in each animal, the EMG criterion response (20% of maximum) occurred at about 30 J. The dashed horizontal line indicates the criterion response of 20% of maximum EMG amplitude. Stimulation was performed with Coil D and 0.73 mF capacitance. The other instrumented muscles showed similarly consistent responses to TA.

of the strong magnetic fields that induced currents in the EMG electrodes. In contrast, there was a high impedance pathway from the electrically stimulating electrode to the EMG electrodes, significantly attenuating any electrical stimulation artifact. Both magnetic and electrical stimulation evoked compound muscle action potential responses having a latency of approximately 1.6 ms from stimulus onset to the beginning of the compound muscle action potential response, which had a duration lasting another 4 ms. When the direction of current flow in Coil D was reversed, the latency from stimulus onset to EMG onset increased by an average of 220 μs (data not shown). With a conduction velocity of 53 m/s, a reasonable assumption based on the work of Thomas et al. [17], this corresponds to a 12 mm shift proximally of the excitation site. For FES and MS, the EMG response amplitude as a function of intensity manifested curves with similar dynamic ranges (Figure 3.3B). These recruitment curves had similar maximum values and shapes across half a logarithmic decade, suggesting that common biophysical mechanisms underlie FES and MS.

The characterization of the remainder of the results in the study is based on the amplitude of the EMG signal, due to the similarities of EMG latency, width, and shape between electrical and magnetic stimulation as shown in Figure 3.3A. Furthermore, the report by Nagarajan and Durand [18] contains data demonstrating the similarity between the compound nerve action potential resulting from FES and MS. This demonstrates that magnetic stimulation could achieve similar performance compared to electric stimulation. Furthermore, the majority of the variation in latency can be attributed to the varying distances between the stimulation and recording sites, as well as biophysical characteristics, which change slightly between every animal. EMG waveform width and shape, measured as the EMG width at half height, had narrower dynamic ranges than EMG amplitude as a function of stimulus intensity. Hence, EMG shape was a less suitable output metric to characterize neuromuscular responses. Thus, EMG amplitude was used as our index of FES and MS activation because it was a simple quantifiable measure of neuromuscular activation with a wide dynamic range.

Variability of Magnetic Stimulation Across Animals

There are two notable sources of variance in the data recorded during experiments performed in this study. The first is the variability in stimulation parameters, including coil parameters, and the second is inter-animal variability resulting from physiological differences between animals. To identify the contribution of variance from inter-animal variability, we compiled EMG recruitment curves from all animals in which curves containing the full range of EMG responses were generated using Coil D and the same range of stimulation intensities (n = 8). The expected variability of EMG responses would be manifested as a horizontal shift of the recruitment curves along the stimulation intensity axis (i.e., a change in the stimulus intensity needed to evoke activity) or as a scaling in EMG amplitude (after normalization to the maximum EMG response in that experiment). We observed only modest changes in stimulus intensity needed to evoke criterion responses across animals (Figure 3.3C). For the illustrated muscle (TA), a 19% of maximal response (near the criterion level of 20%) was achieved with a stimulus delivering about 30 J using Coil D. The standard error of the mean about this point was 3% of the largest EMG response, indicating criterion levels of activation can be achieved with little variation. As another example, the variance in EMG response seen for 50 J intensities of MG stimulation, the standard error of the mean was 6% of the largest EMG response. The other instrumented muscles showed similarly consistent responses to TA (data not shown). With the consistency of magnetic stimulation established, it becomes plausible to explore more detailed aspects of this stimulation modality. These results indicate we can reliably and repeatably evoke activation via magnetic stimulation. For all the experiments described in subsequent results sections, we first verified the ability to evoke criterion responses at similar intensities of magnetic stimulation prior to testing other coils and/or stimulating conditions.

Effect of Coil and Nerve Separation

In an effort to understand how to minimize energies at the EMG criterion response in cases where the distance between the coil and nerve cannot be controlled, we investigated the effect of an air gap on criterion response energies for peripheral

magnetic stimulation. In previous work, an air gap was present but its relationship to a criterion response was not explicitly studied [3]. When these air gaps were introduced, the stimulus intensity needed to reach criterion response increased approximately linearly as a function of the nerve-coil separation, reaffirming Barker's observations [7] (Figure 3.4). The cartoon in the lower right corner of the figure explicitly illustrates the nerve-coil separation distance. It was noted that this effect was strongly dependent on coil geometry: namely, we found that stimulating with larger coils was more effective at evoking EMG criterion responses than smaller coils at a particular nerve-coil separation (data not shown), which was to be expected given that the depth of magnetic field penetration is proportional to coil diameter [7]. Adding this air gap provides additional validation that the mechanism of action of neuromuscular excitation is indeed magnetic stimulation, and not another modality such as electrical excitation via a leakage current or via thermal excitation. Further, this information is relevant in the context of an experimental device in which the coil may not always perfectly abut the nerve.

Relationship Between Capacitor Charge Voltage, Stimulation Energy, and Stimulus Duration

With a primary goal of reducing energy usage for effective magnetic stimulation, the stimulus duration was altered to determine its effect on criterion energies. The capacitance values used here, ranging from 0.73 to 6.6 mF, produced stimulus durations ranging from 83 to 370 μs, respectively, for Coils A, D, and F. Increasing the stimulus duration resulted in lower capacitor discharge voltages needed to produce EMG criterion responses (Figure 3.5A). Conversely, a positive relationship was found between these longer stimulus durations and their corresponding criterion energies, shown in the stimulus duration/energy curves (Figure 3.5B). A common trend across all coils was that the energy required to evoke EMG criterion responses approached a lower bound as pulse duration reached the lower values tested. This result suggests that there are diminishing returns if stimulus duration is further reduced.

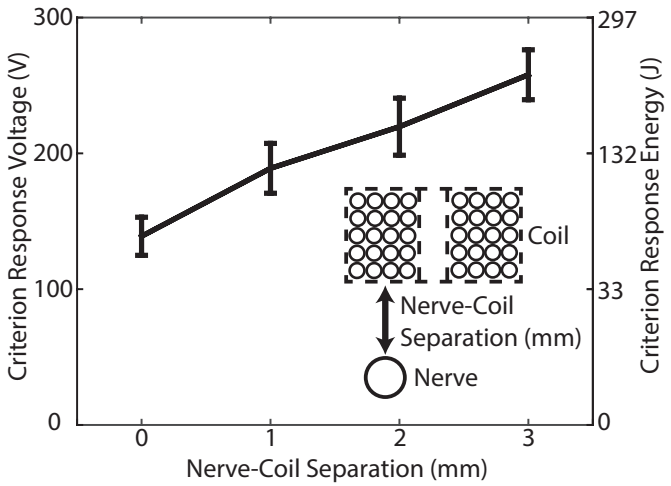

Figure 3.4: Effect of Nerve-Coil Separation on Criterion Response
Increasing the distance between nerve and coil resulted in a near-linear increase in stimulation criterion energies and voltages measured in LG in 4 animals. Observing responses after introducing an air gap validates that the mechanism of excitation is magnetic stimulation. Stimulation was performed with Coil D (16.4 mm OD) and 6.6 mF capacitance. The other instrumented muscles had criterion energies that showed a similar dependence on nerve-coil separation. Error bars represent standard error of the mean. The cartoon embedded in the lower right corner of the figure illustrates nerve-coil separation, the vertical distance between the bottom of the stimulating coil to the top of the nerve.

Geometric Factors for Effective Magnetic Stimulation Using cm-Scale Coils

Stimulation energy necessary to evoke criterion EMG responses is impacted by coil design parameters such as geometry, electrical resistance, and inductance. These coil design parameters can be chosen to construct a coil capable of providing EMG criterion responses at lower energies compared to less optimally designed coils. However, with this reduction of stimulation energy needed to evoke useful responses as a primary goal, there is not a single design parameter that can be optimized to meet this goal. To illustrate this, the mean criterion energies of the six hand wound coils across 5 animals, using the smallest criterion energy of the four instrumented muscles, was examined as a function of the coil's outer diameter (Figure 3.6A). The smallest cm-scale coils required higher energies to reach criterion excitation: however, there was not a systematic relationship between coil outer diameter and criterion stimulation energy that is independent of other design parameters. Similarly, when

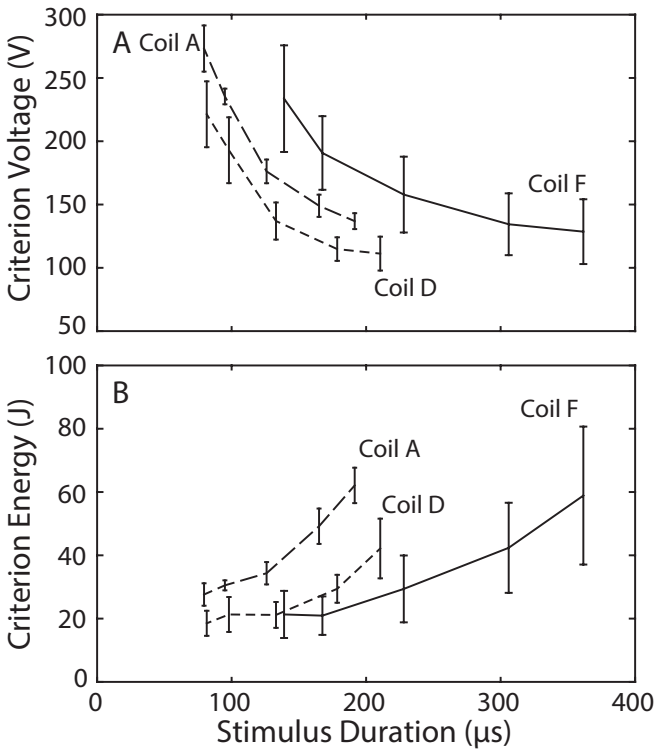

Figure 3.5: Effect of Stimulus Duration on Criterion Response
Increasing stimulus durations produces smaller criterion response voltages (A) but larger criterion energies (B) measured in medial gastrocnemius (MG). Because energy, not voltage, is proportional to heat produced in the coil, greater emphasis was placed on reducing total energy rather than voltage. Stimulation was performed with Coils A, D, and F. Means +/- standard error of the mean (n = 3) are shown.

mean criterion energy was examined as a function of the number of coil turns (Figure 3.6B) there was a positive relationship between coil turns and criterion energy. Thus criterion energy for neural excitation of a nerve with a given diameter is not exclusively a matter of coil size, but rather it includes other factors (such as number of turns, number of layers of wire, and coil inner diameter) as well. Notably, Coils A and B had markedly different criterion energies, despite their similar outer diameter. In this case, the height of Coil B is likely the main reason for the difference in criterion energies between Coils A and B. Coil B, being taller, has turns of wire further from the nerve that contribute less to the induced electric field. To expound on the complex relationship between stimulation parameters, increasing the number of turns in a coil increases the coil's inductance and resistance, which reduces the current in the coil under the same operating voltage; however, for the same current in the coil,

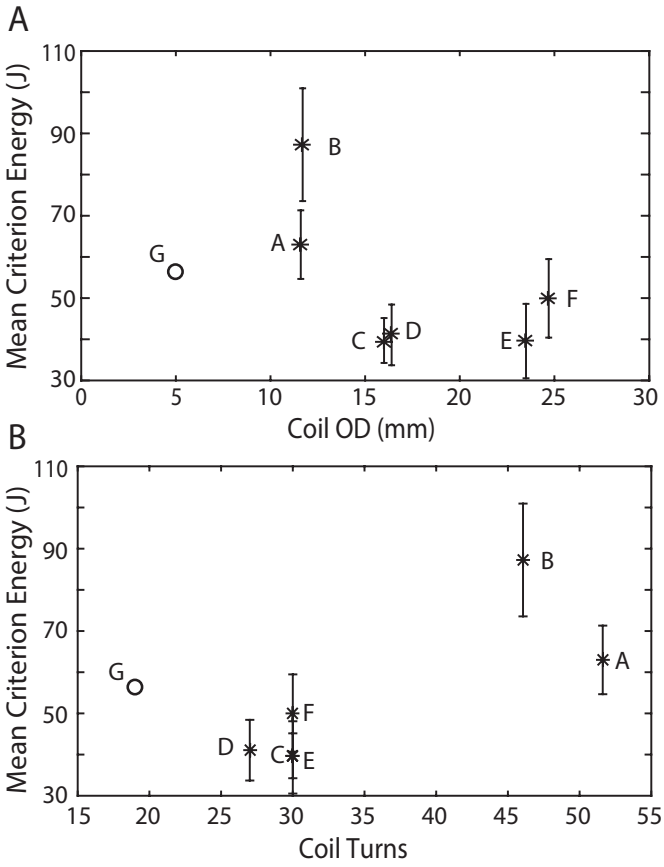

Figure 3.6: Effect of Coil Geometrical Parameters on Criterion Response
Mean EMG criterion energies for all 6 hand-wound coils tested within the same animal (n = 5). (A) MS with the smallest coils (11.6 and 11.7 mm OD) required higher criterion energies than MS with larger coils (16 and 24 mm). (B) The coils with the fewest turns (27 to 30) all have mean criterion stimulation energies of about 50 J or less, whereas the coils with more turns (above 45) have criterion stimulation energies of at least 60 J. Capacitance in these trials was 6.6 mF. The circle indicates 3% of maximum EMG response measured using one SMD coil in one successful experiment with a discharge circuit capacitance of 0.73 mF. Letters refer to individual coils (Table 3.1). Error bars show standard error of the mean.

increasing the number of turns results in a higher amplitude of the induced electric field in the nerve. Therefore, there is a complex effect of the number of turns in the coil on the induced electric field in the tissue. Similar effects can be observed for other parameters such as coil diameters and height.

Millimeter-Scale Coils

Due to the small size and the relatively thin wire used in the construction of mm-scale coils, caution was exercised when testing them, as the large currents and resultant heating of the wires often lead to mechanical deformation of the coil. Due to their relatively fragile structure and the desire to have consistent coil performance across experiments, we elected to purchase commercially available SMD coils instead of hand-winding our mm-scale coils. In all experiments in which SMD coils were used, Coil D was first used to verify our ability to evoke criterion responses at energy levels similar to those shown in Figure 3.3C. Only in one experiment was stimulation with an SMD inductor able to elicit a response, and while it was reliable within that experiment, it only excited one of the four instrumented muscles (medial gastrocnemius), and only up to approximately 3% of the maximum amplitude observed in that experiment (i.e., the response did not meet the 20% criterion response of the cm-scale coils). The 3% EMG response measured for this SMD coil is shown with a circle labeled 'G' in Figure 3.6.

Three rats were used in testing the mm-scale coils, so it is possible that the relatively small sample size studied with mm-scale coils could affect the results of the experiments. However, the three SMD coils investigated in each rat were very similar, and when the results are taken as a group, only 1 of 9 SMD experiments produced an EMG response distinguishable from noise, that EMG response had an amplitude of 3% of the maximum EMG response. Even if this low sample size did not adequately sample the population, these results are suggestive that for the experimental setup used in the present study, the SMD coils were not capable of causing substantial neuromuscular excitation with stimulus levels up to and including the failure point of the coils. As noted above, we were able to evoke EMG criterion responses with Coil D prior to stimulating with any SMD coil in the same animal, indicating that that failure to evoke activity with the SMD coils was not due to inter-animal variability.

Thermal Kinetics of Coils after Stimulation

Coil heating during stimulation will play a major role in determining the viability of magnetic stimulation for future clinical applications. As the thermal response of

any coil is directly proportional to the capacitor discharge energy, priority was given to finding lower energy criterion levels over voltage criterion levels. The temperatures of two coils were measured to characterize the potential impact of this heating on neural tissue. The differences in coil assemblies lead to very different thermal kinetics after stimulation, as shown in Figure 3.7.

Comparison of Experimental and Model Predicted Stimulation Intensities

To provide a basis for interpreting the relative performance of the hand-wound coils and to explain the lack of observed response with the SMD coils, the simulation methods of Ramrakhyani et al. [6] were used to predict the activation intensities for magnetic stimulation (Table 3.2). An asterisk in Table 3.2 indicates the 3% of maximum EMG response which did not meet the 20% criterion response. To simplify the model, the tissue properties were assumed to be homogeneous and the neural membrane capacitance was ignored. Additionally, this model predicts the intensities necessary for activation of a single axon, not the multiple axons necessary to reach the criterion response levels utilized in the *in vivo* experiments. Jointly, the consequences of these three assumptions are predictions that substantively exceed those observed experimentally, similar to those in Table IV of [6].

To account for the prediction of larger energy levels and to allow for more meaningful predicted criterion energy levels for the SMD coils, we normalized all predicted energy levels to the mean ratio of the predicted energy by simulation to the in vivo measured criterion energy for the size hand-wound coils. On average, the in vivo criterion energies required only 46.2% of the energy predicted for the cm-scale coils. The normalized predicted energy levels for 5 of the 6 coils were within 10% of the in vivo measured energy levels. Using the same normalization factor, the normalized predicted energy levels for the 3 SMD coils ranged from 71 to 82 Joules.

Discussion

To investigate the feasibility of achieving low-energy magnetic stimulation in the peripheral nervous system using millimeter-scale coils, we systematically tested coils in a range of sizes from cm-scale coils previously shown to work in the PNS at

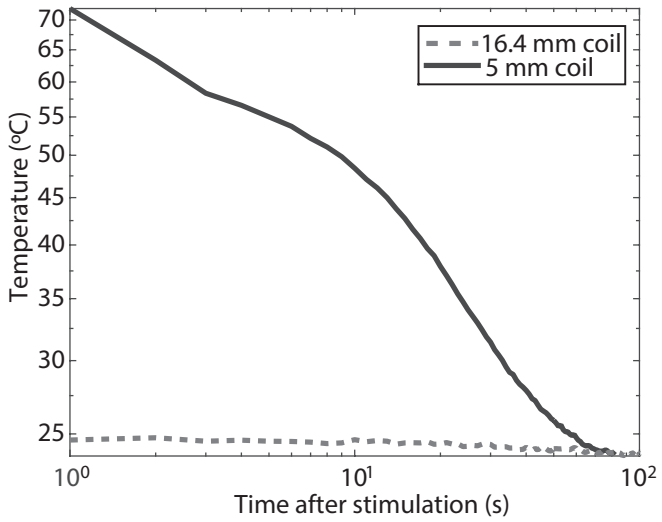

Figure 3.7: Thermal Response of Coils After Stimulation
Thermal response to stimulation varied greatly across coils. A 1.1 mF capacitor bank was charged to 250 V then discharged through Coil D (16.4 mm OD coil, dashed line) or Coil G (5 mm OD, solid line) for a 34.3 J stimulus duration. The smaller coil, with a much lower thermal capacity, had a 47 °C rise above room temperature with a single stimulus and returned to room temperature after about 100 s, whereas the larger coil warmed up by about 1 °C with a similar time (about 100 s) before returning to room temperature. Thermal data were recorded at 1 Hz.

Table 3.2: *In Vivo* and Simulation Results

Coil Identifier	A	B	C	D	E	F	G	H	I
In Vivo Energy (J)	62	86	39	40	38	48	N/A*	N/A	N/A
In Vivo Voltage (V)	137	161	109	110	107	121	N/A*	N/A	N/A
Simulation Energy (J)	137	220	84	78	87	93	162	153	177
Simulation Voltage (V)	204	258	160	154	162	168	666	648	696
Capacitance (mF)	6.6						0.73		

higher energies [3] to millimeter-scale coils such as those that have only been shown to work in the CNS [1, 2]. This was performed by abutting these coils against the nerve similar to the way low-energy stimulation was achieved in the CNS, an approach that has not previously been done for *in vivo* PNS studies. Our results are examined in the context of creating an investigative device that may be used in animal experimentation, and eventually, in humans with implanted neuroprosthetic

devices or other biomimetic systems. The *in vivo* rat sciatic nerve preparation used here is simple to perform, provides reliable results, is a suitable model for human applications, and allows for comparison to existing and future studies. The reliability of this preparation provides consistent data, so that accurate predictions can be made about neuromuscular responses to MS.

Comparing FES and MS

Graded and maximal EMG responses to MS similar to those produced by FES were observed, which corroborates and extends compound nerve action potential data reported previously [18]. These features are desirable in a clinical device for reanimation of motor function, recreation of sensory percepts, or modulation of ongoing activity of the autonomic nervous system [19]. Furthermore, in the same animal, EMG responses to MS and FES have similar kinetics, including latency (given the same excitation sites for FES and MS), waveform width, and shape suggesting similar mechanisms and sites of activation [20]. Thus, it may be possible to use the larger body of literature about FES to productively direct future experiments investigating MS.

Selectivity of MS

Intrafascicular FES has been shown to be able to selectively activate muscles [21], a valuable feature for a clinical device. Here, single-coil MS was capable of selectively activating muscles in only 1 of 6 experiments by translating the coil across the nerve and adjusting stimulation intensities (data not shown). These 6 experiments were performed with Coil D (16.4 mm OD). Our observation that selective activation of LG was achieved in only 1 experiment is likely the result of the large fields produced by the 16.4 mm OD coil relative to the size of the nerve (1 mm). Selectivity may be more reliably achieved with smaller coils, as the smaller size of the electric fields they produce could preferentially activate axons innervating different muscles via a more focal excitation volume. Moreover, selectivity via MS might be better accomplished with arrays of coils, where one can take advantage of the homogeneous and unitary relative magnetic permeability of biological tissues to control the distribution of the field induced in the tissue.

Millimeter-Scale Coils

Millimeter-scale inductors did not evoke criterion responses for stimulus levels up to and including those causing coil damage. Limited studies have reported that microscale coils activated retinal ganglion cells of the rabbit retina *in vitro* [1] and neurons in rat dorsal cochlear nucleus *in vivo* [2] with energies on the order of 1 mJ. Thus, in the CNS, submillimeter-scale coils appear to require stimulation energies about 5 orders of magnitude less than those of cm-scale coils (1 mJ vs 100 J) [3, 4]. However, there are some differences in experimental preparations and methods between these studies and the present study that may account for the large differences in stimulation energies needed to evoke responses. In Bonmassar et al. [1], single spike events from a patch-clamp recording of retinal ganglion cells were used as indicators of neural activation. In the present study, we used the less specific 20%-of-maximum EMG activation as our criterion of neural activation. Thus, although a single spike event meets the criterion for neural activation from a patch-clamp recording, reaching the 20%-of-maximum metric used here requires the activation of many axons within the sciatic nerve. Park et al. [2] used extracellular electrophysiological recordings at inferior colliculus when stimulating the dorsal cochlear nucleus, upstream from the inferior colliculus, as their response metric. This indirect response to stimulation leaves open the possibility of this being a neuromodulatory effect as opposed to strict excitation [22]. Both studies by Park et al. and Bonmassar et al. used microscale coils to stimulate tissue in the central nervous system whereas herein axons in a peripheral nerve were stimulated. This is particularly noteworthy as excitation at threshold energies typically occurs at the initial segment or first node of Ranvier of the axon, rather than in the soma [23, 24] or further along the axon. Hence, activation may have occurred at the initial segment of the axon in the CNS, but must occur along the axon in the PNS, which would require more energy to reach excitation threshold. Additionally, in the CNS, the induced electric field magnitude is the primary factor responsible for achieving magnetic stimulation, as suggested by Bonmassar et al. [1], but in the PNS, it is the relationship between the derivative of the electric field magnitude along the length of the nerve and the fiber diameter [6, 10, 25, 26]. Moreover, differences between *in vivo* and *in vitro* animal preparations

may result in endpoint stimulation instead of an action potential developing along the length of the axon [4]. This endpoint stimulation may be due to the short axonal lengths present in many neurons of the CNS, or due to the thin brain slicing in *in vitro* experiments. Further, there are large differences in the cytoarchitecture of peripheral and central nervous systems. In the CNS, there may be local recurrent neural activity but no such similar activity exists in the peripheral nervous system [27]. Finally, differences in electric field geometries as a result of different coil designs [28] and/or other selectable stimulation parameters are obvious factors that influence stimulation efficacy [10, 29].

Design Parameters for the Reduction of Stimulation Energies

From our investigation with multiple cm- and mm-scale coils, each with unique geometrical and electrical parameters, we cannot readily establish rules or guidelines for choosing specific design parameters that will reliably reduce energies needed to evoke a criterion response. However, shorter stimulus durations (via lower circuit capacitance) were found to reduce energies required for a criterion response. Our results indicate that only marginal returns are possible from further reductions in the circuit capacitance, but if stimuli could be truncated immediately at the point of excitation, (i.e., immediately after the peak of the current waveform) it may be possible to save half or more of the total energy in the stimulus. The model proposed by RamRakhyani et al. [6] can be used to approximate the effectiveness of new coil designs and iterate upon them, then test and validate the best designs with *in vivo* experiments like those performed in this study.

Thermal Limitation of MS

Even when stimulation was performed with a 16.4 mm OD coil using short stimulus durations, the coil temperature still increased about 1 °C. A single 1 °C rise may be acceptable, but stimulus trains, which are expected to be required for clinical applications, will require a better heat distribution mechanism to keep the coil's and nerve's temperatures in a safe range. That is, with the set-up and coils presented herein, heating of the coil represents a hurdle to be overcome should MS be considered for clinical applications involving continuous pulsed stimulation. In contrast, for

applications that only use infrequent stimulation, the modest temperature increase for a single pulse is well within the acceptable range for an implantable device.

Millimeter-Scale Performance in the Context of Model Predicted Excitation Energies

In general, the predicted energies required to evoke activity are always larger than the experimental criterion energies. This is likely due to the simplifications in the model such as not accounting for tissue heterogeneity and membrane capacitance, and despite the simulations only requiring activation of a single axon. In the context of the mm-scale coils tested, no direct comparison could be made to in vivo data because these coils never produced a criterion response. To accommodate the bias in the prediction, we applied a normalization factor of 0.462 to all predicted energies levels, which resulted in most predictions being within 10% of the measured energy levels. After normalization, we may have expected to see criterion EMG responses for the SMD coils at energy levels in the range of 71 to 82 J (reduced from the unnormalized predicted range of 153 to 177 J). However, we were unable to test stimuli of this energy, as the mm-scale coils typically failed when 60 J stimuli were used. We were likely using stimuli with energies near those required to excite some axons in the nerve, as suggested by the single experiment that produced an EMG response, even if it was not a 20% criterion response.

Conclusion

In this study we have investigated magnetic stimulation in the peripheral nervous system (PNS) using coils with a range of outer diameters, from the cm-scale to the mm-scale, that have not been previously studied. We have shown consistent performance of magnetic stimulation of rat sciatic nerves *in vivo* with six cm-size copper solenoid coils. Energies necessary to evoke criterion EMG responses for these cm-scale coils occurred at 20 J or more, whereas the three mm-scale coils were not effective at evoking responses for currents up to and including their failure point. Consequently, we were unable to translate the performance of sub-mm coils reported in the CNS to the PNS. In particular, we found that activation of peripheral nerve tissue via magnetic stimulation by a single, air-core, copper-wire, solenoid coil excited

by a capacitive discharge system required relatively large energies, compared to those necessary for other stimulation modalities or other target tissues. Furthermore, the sizes of the coils that were able to produce neuromuscular responses were also too large to be implanted in small animals. Moreover, the energy levels required with the experimental stimulation system presented herein result in potentially unsafe temperature increases that preclude the clinical use of these coils and excitation methods in a PNS application. However, we have studied only a limited range of all possible stimulator parameters (i.e., values of the discharge capacitance) and solenoid coil design parameters, and we recognize that other parameter sets potentially could result in the multiple order of magnitude decrease in energy necessary to make this approach viable for a clinical PNS application. Examination of the parameter space is best performed through simulation methods and we are actively pursuing those studies, although the results of the present study do not indicate which of the parameters might individually provide the largest improvement. Equally, reduction in energy and/or heating may be achieved by alternative coil designs, using highly conductive wires, cores with high permeability and saturation levels, non-solenoid coil designs, and multi-coil designs, as well as alternative stimulation methods, such as temporally controlled current application. Nevertheless, until more optimal solenoid coil design parameters are found or alternative coil and stimulator designs are available, we conclude the heat produced in the coils as a result of stimulation will continue to be a major obstacle to using MS in clinical applications requiring continued pulsed stimulation.

Acknowledgment

The authors would like to thank Dr. Faisal Khan for his technical advice in designing the stimulation system. The authors also gratefully acknowledge helpful discussions with Mr. Zachary Wach regarding the simulation methods.

References

[1] G. Bonmassar, *et al.*, "Microscopic magnetic stimulation of neural tissue," *Nat. Commun.*, vol. 3:921, pp. 1–10, Jan. 2012.

[2] H.-J. Park, *et al.*, "Activation of the central nervous system induced by micro-magnetic stimulation," *Nat. Commun.*, vol. 4:2463, pp. 1–9, Sep. 2013.

[3] M. Yamaguchi and S. Yamada, "Electromagnetic mechanism of magnetic nerve stimulation," *J. Appl. Phys.*, vol. 66, pp. 1459–1465, Aug. 1989.

[4] S. S. Nagarajan, *et al.*, "Mapping location of excitation during magnetic stimulation: effects of coil position.," *Ann. Biomed. Eng.*, vol. 25, pp. 112–125, Jan. 1997.

[5] H. Tischler, *et al.*, "Mini-coil for magnetic stimulation in the behaving primate," *J. Neurosci. Methods*, vol. 194, pp. 242–251, Oct. 2011.

[6] A. Ramrakhyani, *et al.*, "A um-scale computational model of magnetic neural stimulation in multifascicular peripheral nerves," *IEEE Trans. Biomed. Eng.*, vol. 62, pp. 2837–2849, Dec. 2015.

[7] A. Barker, "An introduction to the basic principles of magnetic nerve stimulation," *J. Clin. Neurophysiol.*, vol. 8, pp. 26–37, Jan. 1991.

[8] C. Reuter and J. Battocletti, "Magnetic stimulation of peripheral nerves," *IEEE Eng. Med. Biol. Soc. 10th Annu. Int. Conf.*, pp. 928–929, Nov. 1988.

[9] K. Davey and C. M. Epstein, "Magnetic stimulation coil and circuit design," *IEEE Trans. Biomed. Eng.*, vol. 47, pp. 1493–1499, Nov. 2000.

[10] K.-H. Hsu, *et al.*, "Analysis of efficiency of magnetic stimulation.," *IEEE Trans. Biomed. Eng.*, vol. 50, pp. 1276–1285, Nov. 2003.

[11] H. Wark, *et al.*, "A new high-density (25 electrodes/mm) penetrating microelectrode array for recording and stimulating sub-millimeter neuroanatomical structures.," *J. Neural Eng.*, vol. 10, p. 045003, May 2013.

[12] M. Abdeen and M. Stuchly, "Modeling of magnetic field stimulation of bent neurons," *IEEE Trans. Biomed. Eng.*, vol. 41, pp. 8–11, Nov. 1994.

[13] A. Rotem and E. Moses, "Magnetic stimulation of curved nerves.," *IEEE Trans. Biomed. Eng.*, vol. 53, pp. 414–420, Mar. 2006.

[14] H. A. C. Wark, *et al.*, "Selective activation of the muscles of micturition using intrafascicular stimulation of the pudendal nerve," *IEEE J. Emerg. Sel. Top. Circuits Syst.*, vol. 1, pp. 631–636, Dec. 2011.

[15] E. Basham, *et al.*, "Magnetic Stimulation of Neural Tissue: Techniques and System Design," in *Implant. Neural Prostheses 1* (E. Greenbaum and D. Zhou, eds.), Biological and Medical Physics, Biomedical Engineering, pp. 293–351, New York, NY: Springer US, 2009.

[16] N. Carnevale and M. Hines, *The NEURON Book*. Cambridge, UK: Cambridge University Press, 2006.

[17] P. K. Thomas, *et al.*, "Nerve conduction velocity in experimental diabetes in the rat and rabbit.," *J. Neurol. Neurosurg. Psychiatry*, vol. 44, pp. 233–8, Aug. 1981.

[18] S. Nagarajan and D. Durand, "Determination of excitation sites during magnetic stimulation of nerve fibers," *Eng. Med. Biol. Soc. 1992 14th Annu. Int. Conf. IEEE*, vol. 4, pp. 1426–1427, Oct. 1992.

[19] P. H. Peckham and J. S. Knutson, "Functional electrical stimulation for neuromuscular applications.," *Annu. Rev. Biomed. Eng.*, vol. 7, pp. 327–360, Jan. 2005.

[20] J. C. Kincaid, "The compound muscle action potential and its shape," *Muscle and Nerve*, vol. 22, pp. 4–5, Jan. 1999.

[21] A. Branner, *et al.*, "Selective stimulation of cat sciatic nerve using an array of varying-length microelectrodes," *J. Neurophysiol.*, vol. 85, pp. 1585–1594, Dec. 2001.

[22] J. Ranck, "Which elements are excited in electrical stimulation of mammalian central nervous system: a review," *Brain Res.*, vol. 98, pp. 417–440, Nov. 1975.

[23] C. C. McIntyre and W. M. Grill, "Excitation of central nervous system neurons by nonuniform electric fields.," *Biophys. J.*, vol. 76, pp. 878–888, Feb. 1999.

[24] C. C. McIntyre and W. M. Grill, "Extracellular stimulation of central neurons: influence of stimulus waveform and frequency on neuronal output.," *J. Neurophysiol.*, vol. 88, pp. 1592–1604, Oct. 2002.

[25] S. S. Nagarajan and D. M. Durand, "Analysis of magnetic stimulation of a concentric axon in a nerve bundle.," *IEEE Trans. Biomed. Eng.*, vol. 42, pp. 926–33, Sep. 1995.

[26] J. Reilly, "Peripheral nerve stimulation by induced electric currents: exposure to time-varying magnetic fields," *Med. Biol. Eng. Comput.*, vol. 27, pp. 101–110, Mar. 1989.

[27] V. B. Mountcastle, "The columnar organization of the neocortex," *Brain*, vol. 120, pp. 701–722, Apr. 1997.

[28] Z. Deng, *et al.*, "Electric field depth–focality tradeoff in transcranial magnetic stimulation: simulation comparison of 50 coil designs," *Brain Stimul.*, vol. 6, pp. 1–13, Jan. 2013.

[29] P. J. Maccabee, *et al.*, "Influence of pulse sequence, polarity and amplitude on magnetic stimulation of human and porcine peripheral nerve.," *J. Physiol.*, vol. 513, pp. 571–585, Dec. 1998.

CHAPTER 4

REDUCING HEAT PRODUCED IN MAGNETIC STIMULATING COILS VIA CURRENT WAVEFORM TRUNCATION

This chapter is a journal article to be submitted to *Muscle and Nerve*. Authors of this chapter are Z.B. Kagan, G. Lazzi, R.A. Normann, and D.J. Warren.

Abstract

The high energy needs and resultant heating of magnetic stimulating coils have been long-standing problems in the field of magnetic neurostimulation. While this heating is tolerable for extracorporeal applications such as transcranial magnetic stimulation, it presents a serious challenge to the use of magnetic stimulation in an implanted neuroprosthetic system. We present in this manuscript a magnetic stimulation system that truncates the stimulating coil current, thereby producing peripheral neuromuscular activation using less stimulus energy and coil heating than observed in previous reports. To evaluate the energy reduction using truncation, we performed 6 *in vivo* experiments in rats where the magnetic stimulating coil abutted the sciatic nerve. We used a metric of 20%-of-maximum electromyographic activation as a criterion response of a useful level of neuromuscular activation. The energy required to evoke this criterion response from muscles innervated by the sciatic nerve was reduced from 10.7 J with a waveform lasting 300 μs to 7.1 J with a waveform lasting 50 μs. Despite this 33% reduction in energy, magnetic stimulation systems for the peripheral nervous system still require energies orders of magnitude larger than comparable electrical stimulation systems. Nonetheless, truncated-waveform magnetic stimulation systems can be used in basic research and clinical applications not requiring rapidly pulsed stimuli.

Introduction

Magnetic stimulation of the nervous system has been shown to have useful diagnostic and clinical applications [1, 2, 3, 4]. However, because electrical stimulation is considerably more effective at evoking neural excitation, magnetic stimulation in the peripheral nervous system (PNS) has not been adopted as readily as electrical stimulation. Nevertheless, magnetic stimulation of the PNS does have two distinct advantages over electrical stimulation; magnetic stimulation does not require direct electrical contact with neural tissue (i.e., electrodeless stimulation), and the magnetic permeability of biological tissues is relatively uniform, unlike the wide range of resistivity of biological tissues. The prior advantage implies no buildup of potentially damaging byproducts at the electrode-electrolyte interface; the latter advantage suggests that it may be possible to use an arrangement of multiple coils to evoke neural activity in localized volumes of tissue. However, magnetic stimulation of the PNS does have the disadvantage of requiring significantly larger amounts of energy compared to electrical stimulation. Electrical stimulation has been shown to excite peripheral nerves with energies in the nJ and μJ range for penetrating microelectrodes and cuff electrodes, respectively [5, 6, 7]. Additionally, recent reports show effective magnetic stimulation of the central nervous system with micro-coils using energies in the 1 mJ range [8, 9, 10, 11]. Comparatively, magnetic stimulation systems for the PNS requires more than 20 J of energy to effectively excite nerves [12, 13, 14]. These relatively large energies, expressed as currents moving through a magnetic stimulating coil, produce heat in the coil due to resistive losses. This heating has precluded magnetic stimulating coils from being implanted in the body due to potential damage to the nerve and surrounding tissues. Typically, magnetic stimulation is achieved by producing large currents in the stimulating coil via capacitive discharge [15, 16]. These currents in the stimulating coil then induce current flow in and around the nerve that evokes neural responses. As opposed to fully discharging the energy storage capacitor, stimulation circuit architectures that truncate the flow of current in the coil have been developed for use in transcranial magnetic stimulation. This current truncation is achieved using an insulated gate bipolar transistor (IGBT) to enable pulse width control [17, 18, 19, 20]. Our modeling of neural currents induced with

magnetic stimulation has shown that the accumulation of induced charge, which is what ultimately excites neural tissue [21], is related to the initial increase of current flow in the coil produced by capacitive discharge. Stopping current flow in the coil after neural excitation occurs conserves a substantial portion of the energy stored in the capacitor, thus reducing heating of the coil. This idea is specifically dependent on the fact that the nontruncated current waveform and its first derivative both reach a maximum value while there is still substantial charge remaining in the capacitor, and this charge can be conserved. Continuing the flow of current after these maximums have occurred only results in resistive losses in the coil, and coil heating, without a substantive increase in the neural response. To investigate the reduction of coil heating via current truncation, we have adapted the TMS current-truncating magnetic stimulation circuit architecture for use in the PNS. Using this new circuit, our goal is to develop a magnetic stimulation system that is capable of evoking useful neural responses using less energy. We present herein the characterization of the circuit's performance both in bench testing and in an *in vivo* rat sciatic model, and demonstrate that the circuit leads to effective stimulation with less energy.

Materials and Methods

Coil Designs

In previous work, we compared the ability of nine copper solenoid coils in the cm- to mm-scale range to activate sciatic nerve fibers [12]. From the results of that study, we propose that a coil could be constructed with (1) a smaller total volume that would be more appropriate for chronic implantation, and (2) would be at least as effective in exciting axons in the PNS as any coil investigated in that study. To that end, we developed and tested a new coil in the present study based on parameters from our prior study (e.g., multiple turns in each layer and a mechanically robust design). Further, this new coil, like the coils with 5-mm outer diameter from that study, were constructed with smaller diameter wire and had a smaller total volume compared to the best coil from the previous study. Finally, numerical techniques described by RamRakhyani et al. were used to provide a first-order estimate of the energy required to evoke neural activity for several new coil designs using a single

axon model before finalizing the design [22]. By using both the new coil and the most effective coil from the previous study in the same experiments, we were able to compare the results of the present study with our previous work. Both coils were custom made by wrapping solid core magnet wire around a wooden dowel. Relevant coil properties are shown in Table 4.1, where OD, ID, R, and L are the coil outer diameter, inner diameter, resistance, and inductance, respectively. Notably, the best coil from the previous study had an outer diameter of 16.4 mm whereas the new coil had an OD of 9.7 mm. We will refer to the best coil from the previous study as the "previous coil" throughout the remainder of this study.

Stimulation Electronics

Previous studies of magnetic stimulation in the PNS have used relatively simple capacitive discharge systems to develop the large currents in the coil necessary to induce electric fields strong enough to excite neural tissue. The current flowing through the coil can be well approximated by the second-order response of a series RLC circuit with an initial voltage on the capacitor. Although the capacitance used in the circuit is user selectable, smaller values of capacitance require larger initial voltages in order to evoke the same level of neural activity [12]. Hence, relatively large capacitance values typically have been used and these result in an overdamped second order response. In earlier reports of magnetic stimulation, a silicon controlled rectifier (SCR) was used to initiate capacitive discharge through the coil [15, 16]. However, once an SCR begins conducting, it does not stop conducting until the current flowing through the device falls to nearly zero. Given an overdamped response, this implies that the SCR will not stop conducting until the initial charge on the capacitor is nearly depleted. Hence, in these systems, no attempt can be made to alter the flow of current in the coil once capacitive discharge began. In contrast, an insulated gate bipolar transistor (IGBT) is an actively controlled electronic switch, and conducts as long as the IGBT is sufficiently positively biased. Consequently, an IGBT may be used to stop or start the current flowing through the stimulating coil with temporal resolution on the order of microseconds or less. In previous work, pulse duration (or stimulus duration) was defined as the time from the start of capacitor discharge to

Table 4.1: Mechanical and Electrical Properties of Coils Used

Coil Name	OD	ID	R	L	Turns	Height	Wire Size
Previous	16.4 mm	8 mm	25 mΩ	4 μH	30	13.3 mm	17 AWG
New	9.7 mm	2 mm	123 mΩ	5 μH	60	6.4 mm	22 AWG

when the coil current reaches its maximum [23]. However, in this study, due to the explicit truncation of the current waveform, we defined stimulus duration to be the duration that the IGBT is fully conducting, i.e., the duration for which current flows uninterrupted through the stimulating coil.

Many of the design parameters used in developing the stimulation circuit in this study were influenced by the work of Peterchev et al. [17]. A schematic of the stimulation electronics is shown in Fig 4.1. The charging section (left side) is primarily composed of a 400 V DC power supply (U400Y20, Acopian Technical Company, Easton, PA), a solid state relay (SSR, CPC1779J IXYS, Milpitas, CA), and C1, a 680 μF 500 V capacitor (LNU2H681MSEF, Nichicon, Kyoto, Japan) that stores the energy for neural stimulation. When the SSR is closed, C1 begins charging at a rate set by the time constant of R_{Charge} (3 kΩ, 50 W) and C1, and charging stops when the SSR is opened. The functional discharging section (right side) is primarily composed of C1, an IGBT (Q1, CM600HA-24A, Powerex, Youngwood, PA), and the stimulating coil (L1). When the IGBT is biased, current flows from C1 through the IGBT and stimulating coil to circuit ground. Additionally, there are two snubber sub-circuits to reduce the effects of large voltage transients during IGBT shutoff. The first snubber sub-circuit is capacitor C2 (5 μF Film), which is placed in parallel with C1. As per Peterchev et al., one side of C2 is mounted as close as possible to the collector terminal of Q1 to prevent the collector voltage from overshooting during turn off as a result of the parasitic inductance of C1 and the connecting wires [17]. The second snubber sub-circuit, which reduces high-frequency high-voltage spikes and facilitates current commutation to D1 and R1, consists of two branches in parallel with Q1. First, capacitor C3 (0.68 μF Film) is placed across Q1. The second parallel branch of the sub-circuit consists of D1 (60EPF12, Vishay, Malvern, PA) and R2 (2 Ω 1 W) in parallel, which is then in series with C4 (3 μF Film). Finally, R1 (1 Ω 50 W)

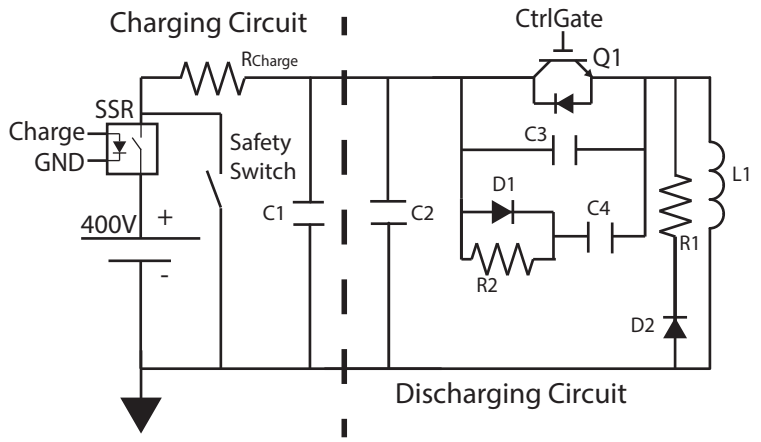

Figure 4.1: Schematic of Stimulation Electronics
The circuit is principally composed of a charging sub-circuit (SSR, R_{Charge}, and C1), a discharging sub-circuit (Q1 and L1), snubber sub-circuits (C2, C3, C4, D1, and R2), and an energy dissipation sub-circuit (R1 and D2).

and D2 (VS-VSKD91/16, Vishay, Malvern, PA) provide a local path for current to flow after the IGBT has been opened but there is still energy stored in the magnetic field of L1. The voltage on C1 was recorded for programmable control of the stimuli via a voltage divider. A myDAQ (National Instruments, Austin, TX) was used with custom software to control system charging and discharging. A manual safety switch was also added to slowly discharge the capacitor.

Stimulation Circuitry Validation

To evaluate system performance, five initial capacitor voltages, 200, 250, 300, 350, and 400 V, and seven stimulus durations, 50, 75, 100, 125, 150, 200, and 300 μs, were tested. Current was measured through the new coil with a series 5 mΩ resistor and recorded via a TDS 3014 B oscilloscope (Tektronix, Beaverton, OR) at 25 MHz. Data were smoothed with a fifty-sample moving average filter. These data indicated that the capacitor was nearly fully discharged with a stimulation duration of 300 μs and, hence, this duration was selected to be the maximal duration examined.

Animal Preparation

All procedures were approved by the University of Utah Institutional Animal Care and Use Committee. Many of the aspects of the preparation used in this study are the

same as those described in prior work [24, 25]. To briefly summarize: A 2.5 cm section of the left sciatic nerve was exposed in 6 anesthetized adult male Sprague-Dawley rats (350-500 g). A 100 μm thick polyimide film covering the nerve was used to electrically insulate the coil from the nerve and protect the nerve from dehydration. A custom-built plastic nerve trough was used to slightly raise the nerve out of surrounding tissue and straighten it to allow for more accurate positioning of the coil with respect to the nerve [26]. Intramuscular electromyography (EMG) data were recorded differentially via custom-made pairs of fine wire electrodes with each pair inserted into one of four muscles of the lower leg innervated by the sciatic nerve: lateral gastrocnemius (LG), medial gastrocnemius (MG), tibialis anterior (TA), and soleus (Sol). EMG data were bandpass filtered between 10 Hz and 1 kHz (Model 1700 Amplifier, A-M Systems, Sequim, WA). Amplifier ground was provided with a deinsulated 18 gauge syringe needle inserted under the skin near the hip. EMG data were sampled at 30kSa/s (Cerebus Data Acquisition System, Blackrock Microsystems, Salt Lake City, UT). EMG amplitude was defined as the maximum minus minimum EMG values in the period of 2 to 16 ms post-stimulation. The stimulating coil was positioned over the nerve with the nerve laying tangent to turns of the coil near its outer diameter when viewed from above (Fig. 4.2), which is near the theoretical optimal position [27]. At the beginning of each experiment, the nerve was stimulated with the stimulating coil at five positions, each translated by 1 mm in a direction orthogonal to the length of the nerve. We selected the position in which the coil evoked the largest average EMG response with a given stimulus intensity, and the coil was kept in this position for all subsequent trials. We defined 20% of the maximum EMG response observed in a given experiment to be a criterion response used in our analysis. This criterion response provides a level of neuromuscular activation that evokes useful muscular activity that is clearly above the noise. Electrical stimulation of the nerve was performed with a bipolar hook electrode before magnetic stimulation to determine maximal EMG activation. Magnetic stimulation trials using 50 μs stimulus duration were performed before and after all other magnetic stimulation trials as a control. If the energy required to evoke a mean EMG criterion response across all 4 muscles differed by 15% or more between the magnetic control trials, data from that experiment were not

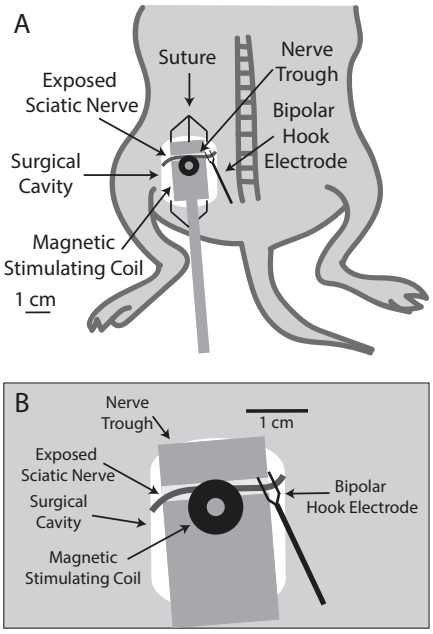

Figure 4.2: Illustration of Surgical Preparation and Coil Position with Nerve Trough The magnetic stimulating coil was positioned with the turns of wire tangent to the exposed sciatic nerve. (A) Illustration showing position of rat and surgical site. (B) Magnified view of surgical site showing relationship between the stimulating coil, nerve, nerve trough, and hook electrode used for electrical stimulation. The stimulating coil and hook electrode were never placed in their stimulating positions simultaneously during an experiment, as magnetic and electrical stimulation were performed at different times during the experiment.

used. All data reported herein came from experiments which passed these controls. All stimulation trials with the same experimental conditions were performed three times to avoid an aberrant single trail from affecting the results. A vacuum port developing an air flow rate of 0.08 m^3/s was placed near the coil to hasten coil cooling.

Characterization and Quantification of EMG Response to Stimulus Energy

Energy consumption for each stimulus pulse was calculated according to Equation 4.1, where E is the energy delivered to the coil, C is capacitance of the energy storage capacitor, and V_i and V_f are the voltages stored on the capacitor before and after discharge, respectively.

$$E = \frac{C(V_i^2 - V_f^2)}{2} \tag{4.1}$$

To characterize the difference in stimulation efficacy between the coils, EMG response curves were developed by plotting EMG responses from zero amplitude to either EMG saturation or to an amplitude evoked by the maximal energy capable of being provided in a single stimulus as a function of the energy contained in a given stimulus (i.e., EMG recruitment curves.) These recruitment curves were quantified by fitting a logistic function to all of the data points in a given stimulation set. The `nlinfit` command in MATLAB (MathWorks, Natick, MA) was used to estimate the parameters A, B, and C in Equation 4.2 that best fit the observed data in a least squares sense.

$$y = \frac{A}{1 + e^{B(x-C)}} \tag{4.2}$$

In Equation 4.2, x is the energy contained in an individual pulse, y is the EMG amplitude resulting from that pulse, and A, B, and C are the maximum value, steepness, and midpoint parameters of the logistic function, respectively. The energy needed to evoke the 20%-of-maximum criterion response was determined from the best-fit logistic curve.

We used statistical analyses to examine the effects of stimulating coils and stimulus duration on the criterion response and best-fit EMG recruitment curves. We performed one-way analyses of variance with repeated measures to compare the parameters of the recruitment curves (A, B, and C from Equation 4.2) with stimulating coil or stimulus duration as the within-subject factor. A paired-sample two-tailed t-test was used to determine whether there were significant differences between the mean energies needed to evoke a criterion response for stimuli with durations 300 μs and 50 μs. The same test was also used to determine whether there were significant differences between the mean energies needed to evoke a criterion response when stimulating using the new coil and the previous coil. All analyses were performed in MATLAB, using the `fitrm` command to develop the repeated measures model, `ranova` to perform the repeated measures ANOVA, and `ttest` to perform the t-tests. All tests were performed with a significance level of $\alpha = 0.05$.

Comparison with Prior Work

In order to compare results from this study with our prior work [24], we used the coil from the previous study with the lowest energy required for neural excitation as well as the new coil designed for this investigation. The effectiveness of both coils was evaluated in all 6 animals by measuring the evoked EMG amplitude as a function of the energy contained in the stimulus pulse as described previously. The energy storage capacitor, C1, was charged between 80 and 400 V in 40 V steps, and then was discharged through the coil with a 300 μs duration to develop the currents necessary to evoke neural excitation.

Neuromuscular Response to Truncated Current Waveforms

In order to characterize the effect of truncating current waveforms on stimulation efficacy, we measured the evoked EMG amplitude as a function of the energy contained in each stimulus pulse. The effectiveness of each stimulus pulse was evaluated in all 6 animals by measuring the evoked EMG amplitude as a function of the energy contained in the stimulus pulse as described previously. Initial capacitor voltages of 80 to 400 V in 40 V steps and stimulus durations of 50, 75, 100, 125, 150, 200, and 300 μs were tested.

Thermal Response to Truncated Current Waveforms

The new coil's temperature change from baseline was recorded in air with an infrared temperature sensing camera (T420, FLIR Systems, Wilsonville, OR) for each of the stimuli shown to be capable of producing a 20% criterion response. Given the memory limitation of the camera, we acquired both a fast and slow acquisition data set. In the first set of trials, the camera was set to record at 30 frames per second from at least 1 s prior to stimulation to at least 5 s after stimulation to capture the rise in coil temperature. In the second set, it was set to record at 3 frames per second from at least 1 s prior to stimulation to at least 100 s after stimulation to capture the decay of the coil temperature. A bitmap mask was used to select only pixels of the coil. The mean temperature of these pixels was defined as the overall coil temperature. The coil's temperature was also recorded in a deionized water bath to approximate an implanted use case. Because the infrared camera cannot capture temperatures inside a

water bath, a small thermistor (NXFT15WF104FA2B100, Murata Electronics North America, Smyrna, GA) was fixed to the coil with tape and used in a voltage divider to determine coil temperature. Data from the thermistor were recorded at 500 Sa/s (Cerebus DAQ System, Blackrock Microsystems, Salt Lake City, UT) from at least 1 s prior to stimulation to at least 60 s after stimulation.

Results

Stimulation Circuitry Performs as Designed

Currents developed in the coil as a result of capacitive discharge were recorded to ensure the responses were as expected based on the capacitor discharge voltage and commanded stimulus duration. Stimulation with each of the 35 voltage-duration pairs (i.e., 5 initial capacitor voltages and 7 stimulus durations) was tested through the new coil and the resulting currents were recorded. For example, for stimuli with the same initial capacitor voltage of 250 V and differing stimulus durations (Fig. 4.3A), the resulting current waveforms are nearly overlapping until the IGBT stops conducting, at which point the current immediately decreases, falling to 0 A within 20 μs. For stimuli with the same stimulus duration of 150 μs and differing initial capacitor voltages (Fig. 4.3B), the current waveforms are very similar in shape to each other, with all of the waveforms showing an immediate decrease in current at 150 μs. We also observed that the maximum current of a stimulus pulse linearly scales with the initial capacitor voltage. In summary, the current waveforms produced in the coil for all 35 voltage-duration pairs were truncated as expected.

New Coil Performance is Comparable to Previous Best Coil Performance

By using both coils with the modified animal preparation and stimulation circuitry, we were able to evaluate the difference in efficacy between the two coils under the same experimental conditions. To evaluate the effectiveness of the new coil at stimulating PNS fibers, we measured the EMG response evoked by the new coil as a function of stimulation energy and compared the responses to those evoked by the previous coil. EMG activity was recorded from four muscles in each of 6 rats after stimulating using a 300 μs duration, which is effectively a non-truncated waveform for the new

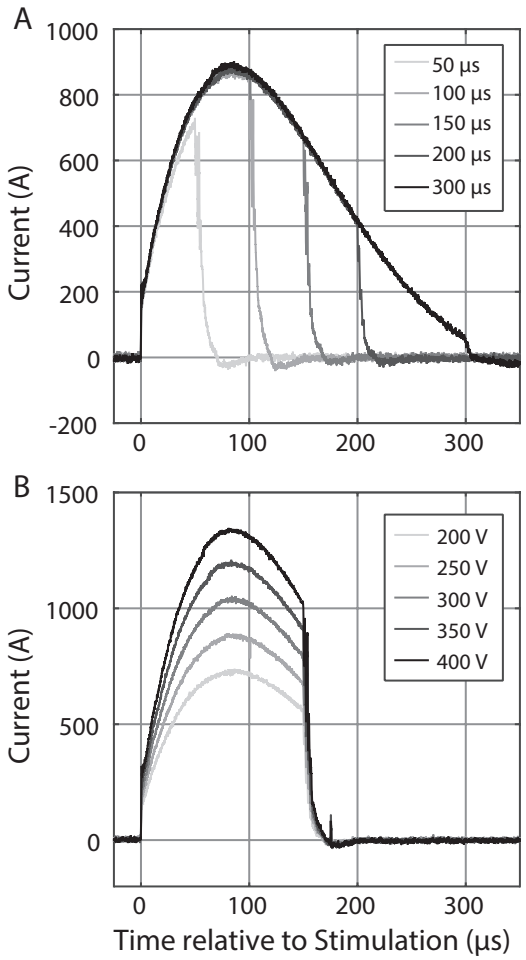

Figure 4.3: Truncated Current Waveforms
Current through the stimulating coil after stimulating with (A) a 250 V initial discharge voltage and various stimuli durations and (B) a 150 μs stimulus duration with various initial discharge voltages. Stimulation efficacy can be explored by selecting combinations of initial discharge voltage and stimulation duration. Current was measured with a 5 mΩ resistor in series with the coil.

coil and the previous coil. The resulting EMG recruitment curves show that the new coil evoked the same level of EMG activity at lower levels of stimulation energy, compared with the previous coil, over the range of observed values (Fig. 4.4). For example, in one muscle (TA) of one rat, we observed that the new coil had a similar threshold energy value but grew faster and came to maximum EMG response at a lower energy (Fig. 4.4A). Reductions in stimulus energy with the new coil generalized for this muscle across all rats (Fig. 4.4B). In the other three muscles examined, the

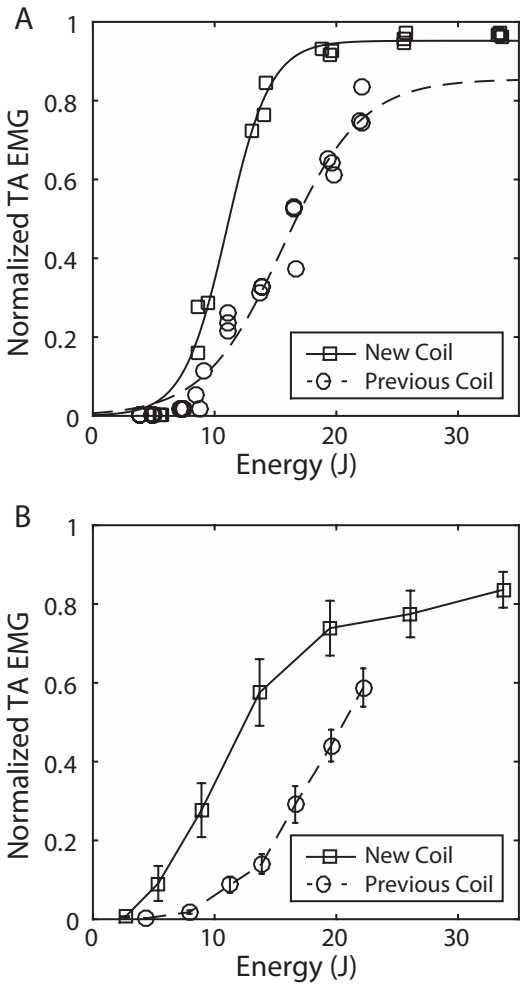

Figure 4.4: Comparison Between Previous Best and New Coil
Comparison of new coil and previous coil using the new stimulation system shown by normalized TA EMG response amplitudes as a function of stimulus energy. At every stimulus intensity, the new coil produced a larger amplitude EMG response than the previous coil. (A) Data are shown from an individual animal with each marker indicating an individual trial and the best fit logistic function shown. (B) Summary data from all 6 animals are shown. Markers indicate the mean energy and EMG data at each clustered energy value used. Error bars show the standard error of the mean about each point. Solid and dashed lines show the best-fit logistic curves (A) and linear interpolations between grouped data (B) for the new and previous coil, respectively.

new coil produced the same level of EMG at lower or similar levels of stimulation energy over the range of observed EMG values.

From the best-fit logistic curve for each muscle in each rat, we compared both the 20% criterion response and the parameters of the fit (maximum value, steepness, and curve midpoint). Across 6 animals, 20% criterion responses in tibialis anterior were achieved at mean values of 10.7 ± 5.1 and 15.8 ± 2.8 J (mean ± SD) for the new and previous coils, respectively, but this was not found to be a significant difference (t-test, $p < 0.11$). This is an improvement from the performance of the previous best coil in our last study [12] in which the best coil produced a 20% criterion response at about 20 J with a capacitance of 733 μF. Despite this apparent difference between the previous and new coil (Fig. 4.4B), the parameters (maximum value, steepness, or curve midpoint) were not significantly different for the best-fit logistic curves (see Equation 4.2) between the new and previous coil in any muscle (repeated measures ANOVA, stimulating coil as the within-subjects factor, $p > 0.11$ for all 12 parameter-muscle pairs). Despite the lack of significance between the coils performance, the new coil developed for this study had a reduction in top-view area (assuming no inner diameter) and volume (assuming a solid cylinder) of about 65% and 83% of the previous coil, respectively. The area and volume were calculated without inner diameter because this is the effective total volume the coil would occupy in tissue. Even though we have no evidence that the two coils differ in their effectiveness, the volume occupied by the new coil is more than 5 times smaller than that of the previous coil.

Truncated Waveforms Evoke Neuromuscular Responses at Lower Energy Levels

To determine the effectiveness of the truncated current waveforms in evoking neuromuscular excitation, full EMG recruitment curves were developed using the new coil for stimulus durations of 50, 75, 100, 125, 150, 200, and 300 μs. We observed a consistent pattern of shorter stimulus durations requiring the same or less energy to evoke a given EMG response across the range of EMG values observed, an example

of which is shown for one muscle (TA) in one rat (Fig. 4.5). Similar results were observed for each muscle of each rat.

From the best-fit logistic curve for each muscle in each rat, we compared both the 20% criterion response and the parameters of the fit (maximum value, steepness, and curve midpoint). A repeated measures ANOVA was used to determine whether any of the maximums, steepness, or midpoints of the best-fit logistic curves were different from the mean for each of the stimulus durations that were tested. None of the muscles showed significant differences in the maximum values of the best-fit logistic curve (repeated measures ANOVA, stimulus duration as a within-subject factor, $p <$ 0.59, 0.36, 0.17, and 0.24 for LG, MG, TA, and Sol, respectively). This indicates that truncating the stimulus duration did not affect the ability of the muscle to reach a maximal value. However, in the case of the steepness parameter, TA and Sol did exhibit significance differences while LG and MG did not (repeated measures ANOVA, stimulus duration as a within-subject factor, $p < 2.5 \times 10^{-4}, 1.0 \times 10^{-6}$,

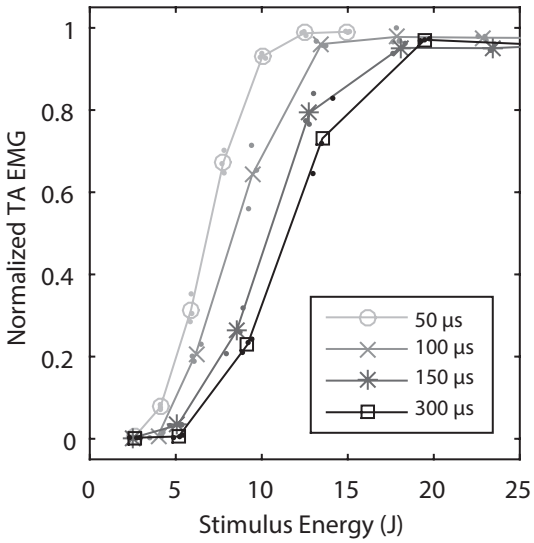

Figure 4.5: Recruitment Curves as a Function of Stimulus Duration
Stimuli with briefer durations produced a given tibialis anterior EMG response using less energy than stimuli with longer durations. For a given stimulus duration, stimulus energy was increased by increasing the capacitor discharge voltage. Markers indicate means of trials each bin (of 7 total bins), which are shown as small dots the same shade of gray as the corresponding line. Selected stimulus durations of 50, 100, 150, and 300 μs are shown with increasingly darker shades of gray.

0.11, and 0.16 for TA, Sol, LG, and MG, respectively). Generally, shorter durations resulted in a steeper curve, an example of which is visible when comparing the 50 and 300 μs curves for TA in 1 rat (Fig. 4.5). The finding of significance of the steepness parameter for TA and Sol compared to LG and MG may be the result of the coil being positioned to excite TA and Sol with a greater variation in effectiveness than LG and MG, although this was not explored in the present study. Finally, all of the muscles showed significant differences in the midpoint parameter as stimulus duration changed (repeated measures ANOVA, stimulus duration as a within-subject factor $p < 1.1 \times 10^{-2}, 1.3 \times 10^{-5}, 7.8 \times 10^{-7}$, and 2.5×10^{-3} for LG, MG, TA, and Sol, respectively). This parameter is the 50% criterion response level, with lower values indicating that less energy was necessary to evoke the same response. Generally, the midpoints of the curves for shorter values of duration were less than those of longer durations, implying that truncation reduced the energy needed for stimulation.

To more explicitly understand the effect of changing stimulus duration on the energy required to evoke a criterion response, we examined the stimulus energy required to evoke a criterion response as a function of the stimulus duration (Fig. 4.6A). The mean energy required to evoke a criterion response in TA decreased as stimulus duration decreased, from 10.7 J for a 300 μs duration stimulus to 7.1 J for a 50 μs duration, a reduction of 33%. We found this reduction to be significant in all muscles (t-test, $p < 1.7 \times 10^{-2}, 1.3 \times 10^{-3}, 1.5 \times 10^{-3}$, and 2.2×10^{-2} for LG, MG, TA, and Sol, respectively). To more clearly illustrate this reduction in energy, and remove the potential confound of inter-rat variability leading to different criterion response energies, criterion response energy in each experiment was normalized with respect to the energy required to evoke a criterion response with a 300 μs duration stimulus in that experiment (Fig. 4.6B). Jointly, these results indicate that continuing current flow through the coil after neural activation occurs results in increased energy consumption without increased neural activation.

Thermal Responses of Useful Stimuli

As the ultimate goal of this work was to reduce the temperature rise in the coil using truncated magnetic stimulation in the PNS, we used an infrared camera and a

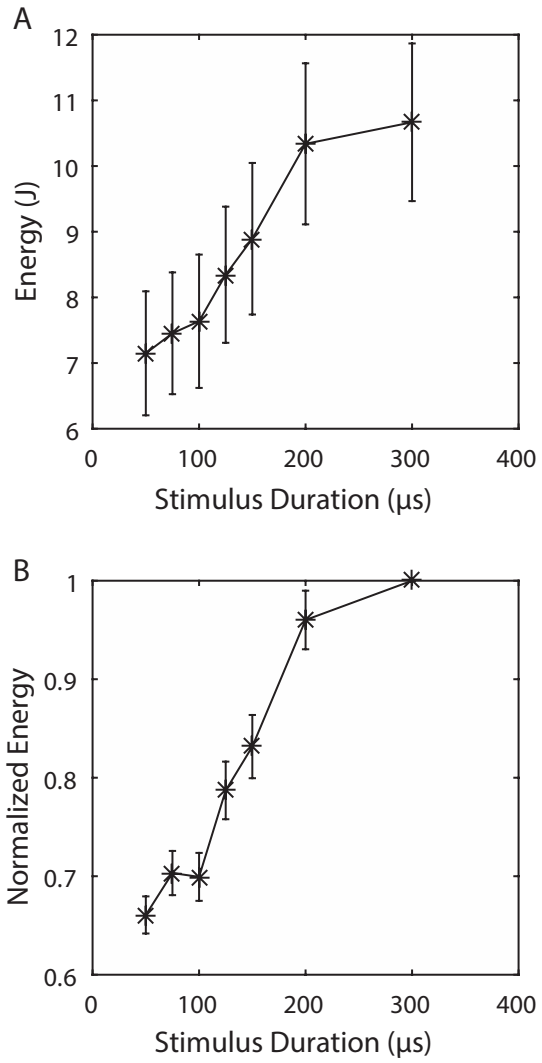

Figure 4.6: Strength Duration Curves Using Truncated Current Waveforms Strength-duration curves for tibialis anterior indicate that shorter duration pulses yield 20% criterion responses at lower (A) absolute and (B) normalized energies than longer duration pulses. Stars indicate the binned means of all trials with similar energies, while the standard error of the mean is indicated by the error bars.

thermistor in separate experiments to record the temperature of the new coil during stimulation. For various duration stimuli that evoke a 20% criterion response, the peak coil temperature rose as stimulus duration increased, from a 1.7 °C rise when stimulating with 50 μs pulses, to over 2.9 °C when stimulating with 300 μs pulses (Fig. 4.7A). The coil has a thermal time constant of about 50 s in air when a vacuum is placed in close proximity (Fig. 4.7B). When the coil was submerged in water to approximate the conditions of being implanted within tissue, the temperature rise was limited to about 0.4 °C for the 300 μs duration stimulus and about 0.2 °C for the 50 μs duration stimulus. The thermal time constant was under these conditions was about 55 s (Fig. 4.7C). Thus, current waveform truncation is an effective technique to decrease the heat developed in the coil during magnetic stimulation of the PNS.

Discussion

The results described herein support the hypothesis that truncating the current flowing through a magnetic stimulating coil can effectively evoke neuromuscular responses with reduced energy consumption compared with non-truncated stimuli. Moreover, the heat developed in the coils is also reduced with stimulus truncation. This may enable the future use of such a coil in a clinical application. In 6 animals, truncation of the current waveform reduced the required energy from 10.7 ± 5.1 J to 7.1 ± 4 J (Mean ± SD), and reduced peak coil temperature from 0.4 °C to 0.2 °C.

Pulse Trains Using Truncated Current Waveforms

Although this paper describes the development, use, and neuromuscular responses evoked with single stimulating pulses having 10 or more seconds between stimuli, a clinically relevant neuroprosthetic device will likely require the episodic use of pulse trains, with multiple pulses per second. The stimulation circuitry described herein is capable of generating such pulse trains, with the maximum stimulation frequency dictated by the capacitor charging time. For example, with the stimulation system described herein, a stimulus with 300 μs duration developing 10.7 J could be produced at 1 Hz, while a stimulus with 50 μs duration developing 7.1 J could be produced at 2 Hz. Alternatively, a pulse train containing 3 pulses at 10 Hz, each with 7.1 J of energy, could be generated once every 3 s indefinitely. All of these stimulation rates are

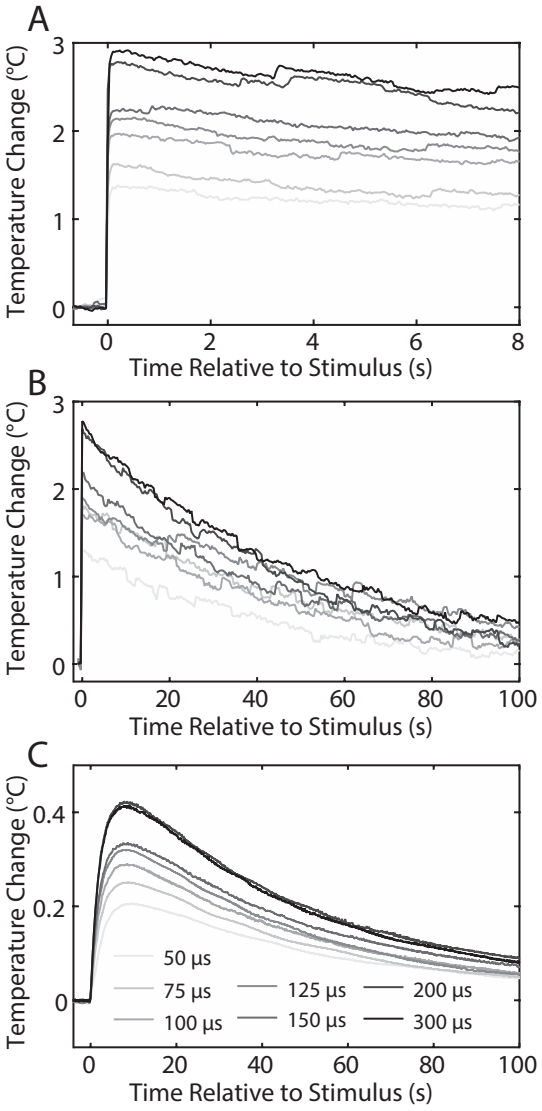

Figure 4.7: Coil Temperature Rise After Stimulation
Coil temperature rise and decay after stimulation. For stimuli of different durations that all produce the same 20% criterion response, stimuli with shorter durations produce a smaller rise in coil temperature compared to stimuli with longer durations. Measurements were taken in air with a thermal camera (A) and (B) or with a thermistor in a deionized water bath (C). Lines become darker for stimuli with longer durations.

ultimately limited by the power supply, which can be built to provide higher charging currents and shorter interpulse durations. However, none of these stimulation patterns address the heat developed in the coil.

Ultimately, the limiting factor for magnetic stimulation in the PNS is not the stimulation electronics but the risk of thermal damage to the nerve and tissue. Based on the a maximum safe heat increase of 2 °C [28], 10 stimuli could be produced in rapid succession, with each stimulus raising the coil temperature by 0.2 °C, while still remaining within safe thermal limits. Due to the relatively long heat dissipation time constant, sustained periodic stimulation is limited to about once every 5.8 s assuming a 55 s thermal time constant. In order to stimulate at 1 Hz, the thermal time constant would need to be about 6.5 s, substantially lower than the 55 s we reported here. However, in an implanted application, the reduction in thermal time constant as a result of blood perfusion may allow for a stimulation rate 25% faster than once per 5.8 s [29].

Applications for Magnetic Stimulation

While faster rates of stimulation may be possible with a more powerful supply, the heating of the coil must be considered when deciding how such a system will be used. Based on the typical minimum stimulation rate of 12 to 15 Hz for useful neuromuscular activation [5], the magnetic stimulation system will likely not be capable of safely providing such stimuli without the coil reaching unsafe temperatures in an implanted application. However, there may be value in using the device in the autonomic nervous system or the central nervous system. For example, several reports have shown that 1 Hz stimulation of the left vagus nerve reduces the incidence of epileptic partial-onset seizures [30, 31, 32]. Additionally, 1 Hz stimulation of the brain has been shown to produce a wide variety of effects capable of impacting disorders such as mania, schizophrenia, tics, depression, and epileptic seizures [33].

Micromagnetic Stimulation of the Central Nervous System

Recent studies have used stimulating coils with features in the sub-millimeter range to achieve useful neural responses in the central nervous system (CNS) with energies in the 1 mJ range [8, 9, 10, 11]. In the present study, the smaller of the

two coils had an outer diameter of 9.7 mm and we were able to evoke useful neural responses with stimulating energies in the 7 J range. However, there are several differences in methods and experimental preparation between the CNS studies and the present study that may explain the 5 order of magnitude difference in energy for effective stimulation. The first, and perhaps most important, difference is that using submillimeter-scale coils provides a much higher electric field gradient along the length of neural tissue compared to millimeter-scale coils, which is important in evoking neural responses [34]. However, despite the higher electric field gradient, the effective volume of excitation surrounding the submillimeter-coil is greatly reduced compared to mm-scale coils. Importantly, there is a substantive difference between the minimum distance from the stimulating coil to neural tissue. For example, the micro-scale coils used in CNS studies are placed in neural tissue, with as little as 5 μm separating the stimulating coil from cell bodies [11]. In contrast, the mm-scale coils described herein are separated by the insulating film, perineurium, and epineurium (estimated to be between 200 to 400 μm) [12, 22]. Next, stimulating in the CNS, whether *in vivo* or *in vitro*, likely yields the advantage of either "end effect" or bent nerve stimulation, both of which have been shown to reduce the energy required to evoke a neural response [14, 26, 35], whereas stimulating along a straight, unbroken nerve such as in the present study does not provide this same advantage. Additionally, neural excitation typically occurs with lower stimulus energy at the initial segment or first node of Ranvier, as is possible in the central nervous system, rather than further along the length of an axon as is the case in the present study [36, 37]. Finally, the metrics of neural activation in these studies were qualitatively different: In the studies on micromagnetic stimulation of the CNS, direct recordings of neuronal populations were used, which allowed for detection of individual action potentials, whereas in the present study, the population-level metric of EMG response was used, which by necessity requires many motor fibers to be activated to detect a neuromuscular response.

Concluding Remarks

We have demonstrated that magnetic stimulation of the peripheral nervous system was possible using a truncated current waveform. Using such a truncated current waveform reduced the energy required to evoke a useful neuromuscular response from 10.7 ± 5.1 J to 7.1 ± 4 J (Mean ± SD), and more importantly, reduced the instantaneous temperature rise of the coil for a single effective stimulus from 0.4 °C to 0.2 °C.

References

[1] A. Barker, *et al.*, "Magnetic stimulation of the human brain and peripheral nervous system: an introduction and the results of an initial clinical evaluation," *Neurosurgery*, vol. 20, pp. 100–109, Jan. 1987.

[2] P. M. Rossini, *et al.*, "Non-invasive electrical and magnetic stimulation of the brain, spinal cord and roots: basic principles and procedures for routine clinical application. Report of an IFCN committee.," *Electroencephalogr. Cinical Neurophysiol.*, vol. 91, pp. 79–92, Aug. 1994.

[3] M. S. George, *et al.*, "Transcranial magnetic stimulation: applications in neuropsychiatry.," *Arch. Gen. Psychiatry*, vol. 56, pp. 300–11, Apr. 1999.

[4] T. Burt, *et al.*, "Neuropsychiatric applications of transcranial magnetic stimulation: a meta analysis," *Int. J. Neuropsychopharmacol.*, vol. 5, pp. 73–103, Mar. 2002.

[5] P. H. Peckham and J. S. Knutson, "Functional electrical stimulation for neuromuscular applications.," *Annu. Rev. Biomed. Eng.*, vol. 7, pp. 327–360, Jan. 2005.

[6] A. Branner, *et al.*, "Selective stimulation of cat sciatic nerve using an array of varying-length microelectrodes," *J. Neurophysiol.*, vol. 85, pp. 1585–1594, Dec. 2001.

[7] F. J. Rodridguez, *et al.*, "Polyimide cuff electrodes for peripheral nerve stimulation," *J. Neurosci.*, vol. 98, pp. 105–118, Jun. 2000.

[8] G. Bonmassar, *et al.*, "Microscopic magnetic stimulation of neural tissue," *Nat. Commun.*, vol. 3:921, pp. 1–10, Jan. 2012.

[9] H.-J. Park, *et al.*, "Activation of the central nervous system induced by micro-magnetic stimulation," *Nat. Commun.*, vol. 4:2463, pp. 1–9, Sep. 2013.

[10] S. W. Lee and S. I. Fried, "Suppression of subthalamic nucleus activity by micromagnetic stimulation," *IEEE Trans. Neural Syst. Rehabil. Eng.*, vol. 23, pp. 116–127, Jan. 2015.

[11] S. W. Lee, *et al.*, "Implantable microcoils for intracortical magnetic stimulation," *Science Advances*, vol. 2, pp. e1600889–e1600889, Dec. 2016.

[12] Z. B. Kagan, *et al.*, "In vivo magnetic stimulation of rat sciatic nerve with centimeter- and millimeter-scale solenoid coils," *IEEE Transactions on Neural Systems and Rehabilitation Engineering*, vol. 24, pp. 1138–1147, Nov. 2016.

[13] M. Yamaguchi and S. Yamada, "Electromagnetic mechanism of magnetic nerve stimulation," *J. Appl. Phys.*, vol. 66, pp. 1459–1465, Aug. 1989.

[14] S. S. Nagarajan, *et al.*, "Mapping location of excitation during magnetic stimulation: effects of coil position.," *Ann. Biomed. Eng.*, vol. 25, pp. 112–125, Jan. 1997.

[15] A. Barker, "An introduction to the basic principles of magnetic nerve stimulation," *J. Clin. Neurophysiol.*, vol. 8, pp. 26–37, Jan. 1991.

[16] R. Jalinous, "Technical and practical aspects of magnetic nerve stimulation," *J. Clin. Neurophysiol.*, vol. 8, pp. 10–25, Jan. 1991.

[17] A. V. Peterchev, *et al.*, "A transcranial magnetic stimulator inducing near-rectangular pulses with controllable pulse width (cTMS)," *IEEE Trans. Biomed. Eng.*, vol. 55, pp. 257–266, Jan. 2008.

[18] A. V. Peterchev, *et al.*, "Repetitive transcranial magnetic stimulator with controllable pulse parameters (cTMS)," *2010 Annu. Int. Conf. IEEE Eng. Med. Biol. Soc. EMBC'10*, vol. 036016, pp. 2922–2926, Aug. 2010.

[19] A. V. Peterchev, "Circuit topology comparison and design analysis for controllable pulse parameter transcranial magnetic stimulators," *2011 5th Int. IEEE/EMBS Conf. Neural Eng. NER 2011*, pp. 646–649, Apr. 2011.

[20] A. V. Peterchev, *et al.*, "Controllable pulse parameter transcranial magnetic stimulator with enhanced circuit topology and pulse shaping.," *J. Neural Eng.*, vol. 11, p. 056023, Sep. 2014.

[21] E. Corthout, *et al.*, "Transcranial magnetic stimulation: Which part of the current waveform causes the stimulation?," *Exp. Brain Res.*, vol. 141, pp. 128–132, Nov. 2001.

[22] A. Ramrakhyani, *et al.*, "A um-scale computational model of magnetic neural stimulation in multifascicular peripheral nerves," *IEEE Trans. Biomed. Eng.*, vol. 9294, pp. 1–1, Dec. 2015.

[23] K.-H. Hsu, *et al.*, "Analysis of efficiency of magnetic stimulation.," *IEEE Trans. Biomed. Eng.*, vol. 50, pp. 1276–1285, Nov. 2003.

[24] Z. B. Kagan, *et al.*, "Magnetic stimulation of mammalian peripheral nerves in vivo: An alternative to functional electrical stimulation," *Conf. Proc. IEEE Eng. Med. Biol. Soc.*, pp. 2573–2576, Aug. 2014.

[25] H. A. C. Wark, *et al.*, "Selective activation of the muscles of micturition using intrafascicular stimulation of the pudendal nerve," *IEEE J. Emerg. Sel. Top. Circuits Syst.*, vol. 1, pp. 631–636, Dec. 2011.

[26] A. Rotem and E. Moses, "Magnetic stimulation of curved nerves.," *IEEE Trans. Biomed. Eng.*, vol. 53, pp. 414–420, Mar. 2006.

[27] E. Basham, *et al.*, "Magnetic Stimulation of Neural Tissue: Techniques and System Design," in *Implant. Neural Prostheses 1* (E. Greenbaum and D. Zhou, eds.), Biological and Medical Physics, Biomedical Engineering, pp. 293–351, New York, NY: Springer US, 2009.

[28] P. A. Bottomley, "Turning Up the Heat on MRI," *J Am Coll Radiol*, vol. 5, pp. 853–855, Jul. 2008.

[29] M. C. Kolios, *et al.*, "Blood flow cooling and ultrasonic lesion formation.," *Med. Phys.*, vol. 23, pp. 1287–1298, Jul. 1996.

[30] A. Handforth, *et al.*, "Vagus nerve stimulation therapy for seizures.," *J. Neurosurg. Anesthesiol.*, vol. 20, pp. 29–35, Jul. 1998.

[31] E. Ben-Menachem, "Vagus-nerve stimulation for the treatment of epilepsy," *Lancet Neurol.*, vol. 1, pp. 477–482, Dec. 2002.

[32] S. C. Schachter and C. B. Saper, "Vagus nerve stimulation," *Epilepsia*, vol. 39, pp. 677–686, Jul. 1998.

[33] E. M. Wassermann and S. H. Lisanby, "Therapeutic application of repetitive transcranial magnetic stimulation: a review.," *Clin. Neurophysiol.*, vol. 112, pp. 1367–77, Aug. 2001.

[34] F. Rattay, "Analysis of models for external stimulation of axons," *IEEE Trans. Biomed. Eng.*, vol. 33, pp. 974–977, Oct. 1986.

[35] M. Abdeen and M. Stuchly, "Modeling of magnetic field stimulation of bent neurons," *IEEE Trans. Biomed. Eng.*, vol. 41, pp. 8–11, Nov. 1994.

[36] C. C. McIntyre and W. M. Grill, "Excitation of central nervous system neurons by nonuniform electric fields.," *Biophys. J.*, vol. 76, pp. 878–888, Feb. 1999.

[37] C. C. McIntyre and W. M. Grill, "Extracellular stimulation of central neurons: influence of stimulus waveform and frequency on neuronal output.," *J. Neurophysiol.*, vol. 88, pp. 1592–1604, Oct. 2002.

CHAPTER 5

CONCLUSION

Previous to this work, magnetic stimulation of the peripheral nervous system (PNS) typically required energies unsafe for use in an implanted application due to the resulting temperature rise in the stimulating coil. Several advances to magnetic stimulation are presented in this dissertation. The results of these advances, shown in an *in vivo* rat sciatic nerve model, include improved stimulation efficacy using smaller coils that are appropriately sized for implantation. Stimulation with these smaller coils requires less energy than has been previously reported, allowing for new use cases of magnetic stimulation. Although some parameters related to stimulation efficacy, such as coil geometry, circuit capacitance, and stimulus duration, were improved, others such as safe maximum stimulation frequency still pose issues for future work.

Summary of Major Research Findings

In Chapter 2, we developed and validated a multiresolution, μm-scale computational model of magnetic stimulation in multifascicular peripheral nerves. The model used a range of resolutions to accurately describe the effects of tissue heterogeneities down to the 1 μm scale while using larger resolutions to conserve computational resources for more homogeneous tissues. The impedance method was used to determine the induced electric fields resulting from current flowing through the stimulating coil. Results from simulating the electric fields were used to estimate the transmembrane currents and determine whether a stimulus was sufficient to evoke a neural response using the NEURON simulation environments [1]. Four different coil designs were simulated and subsequently used in *in vivo* experiments. For every coil, the new heterogenous nerve model more accurately predicted the stimulus energy required to evoke a neural response compared to a simpler homogeneous model.

In Chapter 3, we studied 9 coils in the cm- to mm-scale range in an effort to reduce the energy required to evoke neuromuscular responses in the PNS. In particular, our goal was to translate the recent performance of micro-scale coils used in the CNS, which required on the order of 1 mJ of energy to evoke a neural response [2, 3], to the PNS. We developed a robust *in vivo* rat sciatic nerve preparation that permitted coils to be abutted against the nerve to further reduce the energy requirements. We demonstrated that whole nerve electrical stimulation and magnetic stimulation evoked the same neuromuscular responses with a dynamic range of approximately half of a logarithmic decade. Furthermore, the neuromuscular responses to magnetic stimulation were consistent across animals, indicating that desired response levels can be reliably evoked. We also demonstrated the effects of separating the coil and nerve as well as reducing the stimulus duration by changing the capacitance, which led to increased and decrease energies to evoke a given response, respectively. While the goal of translating the 1 mJ energy consumption from the CNS to the PNS was not achieved, we did reduce the energy needed to evoke useful neuromuscular responses in the PNS from about 50 J [4, 5] to 20 J [6].

In Chapter 4, we implemented a new stimulation circuit architecture that can truncate stimulating current waveforms in the coil, thus conserving charge in the capacitor that would otherwise heat the coil unnecessarily. The primary difference between this new circuit architecture and magnetic stimulation circuitry used previously is the replacement of the thyristor with an insulated gate bipolar transistor (IGBT). Both the thyristor and IGBT are electronically controlled switches, but once a thyristor begins conducting, it can not stop conducting until the current flowing through it drops to near zero. In contrast, an IGBT will conduct only while it is positively biased. Consequently, current flow can be immediately halted if the positive bias is removed. A new coil design was also used in this study that combined aspects of smaller mm-scale coils and larger cm-scale coils to improve on the best coil from Chapter 3. We found that when the current in the coil was truncated to 50 μs from an untruncated duration of 300 μs, the energy required to evoke a useful neuromuscular response decreased from 10.7 J to 7.1 J. Furthermore, we observed that the rise in coil temperature as a result of stimulation decreased from 1.5 °C to

0.5 °C in air, and from about 0.4 °C to about 0.2 °C in water. This indicates that an implanted coil could be used to stimulate 10 times within a 1 s period before a 2 °C safety limit was exceeded.

Limitations of Results

Although the research reported in Chapter 2 provided an accurate frequency-based, biophysical model of magnetic stimulation in multifascicular peripheral nerves, several notable assumptions and simplifications were made that may limit the applicability of the model as it relates to specific applications, particularly neuromuscular stimulation. First, an image of a cross sectional slice of a sciatic nerve of an adult rat [7] was extruded to build the high-resolution computational neural model. Thus, this model was incapable of accounting for changes in morphology, such as the nerve separating into smaller nerves or subtle fascicular reorganization as the nerve approaches its target organ, proximal or distal from the site of the cross section. Furthermore, the original image did not distinguish between sensory, motor, and sympathetic axons, which means that assumptions must be made regarding their distribution in space, even if their numerical distribution was known [8]. This poses an issue in this research because the metric of activation was EMG response, and while there is a relationship between motor axon activation and EMG response, we assumed that the motor fibers were randomly placed within fascicles, which is not the case [9]. More recent work [9] maps these morphological changes in more detail and labels axons by type, and should be used in future versions of the simulation platform. In the next step of the model, a multiresolution field simulator was implemented using the impedance method to solve the electric field distribution in the nerve. The electric field distribution was solved only once for a coil using a normalized peak time-derivative of current, which was then scaled to specific transmembrane currents. As a result, it was not readily practical to simulate temporally offset stimuli, because the electric field is solved in the frequency domain.

The work presented in Chapter 3 successfully reduced the energy required to evoke a neuromuscular response by stimulating a peripheral nerve from about 50 J to 20 J. However, there were a number of aspects of the study that did not replicate

the use case of an implanted device. The most egregious example of this in the preparation we developed was the creation of a boundary layer between the air and the tissue near the coil. Due to the differences in conductivity between adjacent media, the flow of induced current was impeded by the boundary layer. This issue would not be completely removed if the coil was implanted due to inhomogeneities across different types of tissue, but the effect of an air layer boundary would be greatly diminished. Although it is not an explicit limitation of the study, the result of the thermal measurement of the stimulating coil in response to stimulation has direct consequences for using this stimulation system in an implanted application. Specifically, the temperature rise of even 1 °C coupled with a thermal constant on the order of 1 minute indicates that the frequency of stimulation is limited to a rate well below 1 Hz when using the best coil from this study. Similarly, during the experiments, the interpulse interval was limited to a minimum of 10 s so the coil could return to room temperature and the energy storage capacitor could recharge. Another limitation of the study was during the investigation on pulse duration, which was evaluated by changing the capacitance of the energy storage capacitor. Ideally, pulse duration would have been investigated independently from capacitance, as changing the capacitance also changes the kinetics of the current in the coil and the total energy contained in each stimulus. This limitation ultimately became part of the motivation for the work presented in Chapter 4, which focused on adjusting the stimulus duration without changing the capacitance. Furthermore, we were limited in our use of only 5 capacitance values spanning about 1 order of magnitude. While this range provided stimulus durations similar to those used in previous literature [4], the effects of using capacitance values outside this range may only be extrapolated.

The results described in Chapter 4 showed that truncating the current waveform in the stimulating coil reduced the energy required to evoke a useful neuromuscular response by 33% from 10.7 J to 7.1 J. Despite this improvement, the state of the art of magnetic stimulation of the PNS is still limited in its possible applications compared to electrical stimulation due to the heating of the stimulating coil. Although efforts were made to approximate the effect of coil heating in an implanted application by measuring coil temperature in a water bath, this is a relatively basic experiment.

Specifically, it does not account for the cooling effects of biological tissues and moving fluids moving heat away from the coil which may substantially reduce the heating effect and permit faster stimulation rates. Another flaw with this study is the current conduction limit of the IGBT of 1600 A. If this limit is exceeded, the device will immediately stop conducting to prevent damage to the device. This limitation prevented the best coil from the previous study from being investigated using higher stimulus energies, as the 1600 A limit was reached using an initial capacitor discharge voltage of 260 V.

Finally, there was a broad limitation across all of these studies that warrants attention: the use of air core solenoid coils made of copper wire. Other coil geometries have been investigated that may produce stronger or more precise electric fields for a given stimulus energy, such as figure-8 coils or coils with even more complicated geometries [10]. While some of the work discussed in this dissertation applies to all coil design, such as the truncation effect of reducing energy, much of the work only pertains to the specific coil used in that particular experiment, or is otherwise incomparable when considering other coil designs that are not simple round solenoids. The use of copper exclusively is also worth mentioning: We cannot compare many of the results presented here with coils made from a different material, as resistivity and thermal conductivity play a critial role in determining current flow and coil heating and cooling. For example, a coil made from a material with a lower resistivity than copper would produce larger currents for a given capacitor voltage, which would induce stronger electric fields and thus more easily evoke neural responses than a copper coil. Jalinous described such a coil made of silver, and noted that the reduction in resistivity comes at the expense of a similarly reduced thermal capacity, indicating that a silver coil would be heated more than a copper coil for the same energy [11].

Future Work

While we improved the state of the art of magnetic stimulation of the peripheral nervous system by building a simulation platform that provides accurate coil performance predictions, reducing coil sizes without compromising performance, and reducing energy requirements to evoke useful neuromuscular responses by truncating

the current waveform, there are clear paths to follow that would improve all of these and pave the way for a new type of neurostimulation device. We are also looking towards identifying specific applications for this reduced energy peripheral nerve magnetic stimulator, with targets in the autonomic nervous system such as the vagus nerve for treating a host of disorders [12].

As alluded to in the previous section, updating the peripheral nerve model to include morphological changes as a function of space and identification of axon types will improve the accuracy of the simulation. Notably, it may shed light on optimal coil positioning which could impact muscular selectivity (i.e., the ability to evoke only the desired muscle activity by stimulating the corresponding motor fibers in order to develop complex movements.) We will use the updated simulating platform to help identify new coil geometries as we continue to work towards smaller, more effective coils. Furthermore, we can use several of these smaller coils in conjunction with independently controlled stimulators to provide neural excitation to very localized volumes of neural tissue, again possibly realizing lower energy stimulation or selective muscle activation. As a first step in developing new coils, we are investigating the effect of rotating a figure-of-8 coil on stimulation efficacy using the simulating platform and *in vivo* rat sciatic nerve preparation.

Another natural next step in this work is to investigate the feasibility of a chronically implanted coil. Fortunately, there is already substantial literature on the design requirements for a chronically implantable electrical neurostimulator, which will ease the development of an implanted stimulating coil. This background work could help address issues such as a percutaneous connector system complexity, encapsulation of the stimulating coil with a biocompatible material, and device lifetime testing. Additionally, new problems such as thermal control of the implanted coil will need to be solved.

References

[1] N. Carnevale and M. Hines, *The NEURON Book*. Cambridge, UK: Cambridge University Press, 2006.

[2] G. Bonmassar, *et al.*, "Microscopic magnetic stimulation of neural tissue," *Nat. Commun.*, vol. 3:921, pp. 1–10, Jan. 2012.

[3] H.-J. Park, *et al.*, "Activation of the central nervous system induced by micro-magnetic stimulation," *Nat. Commun.*, vol. 4:2463, pp. 1–9, Sep. 2013.

[4] M. Yamaguchi and S. Yamada, "Electromagnetic mechanism of magnetic nerve stimulation," *J. Appl. Phys.*, vol. 66, pp. 1459–1465, Aug. 1989.

[5] S. S. Nagarajan, *et al.*, "Mapping location of excitation during magnetic stimulation: effects of coil position.," *Ann. Biomed. Eng.*, vol. 25, pp. 112–125, Jan. 1997.

[6] Z. B. Kagan, *et al.*, "In vivo magnetic stimulation of rat sciatic nerve with centimeter- and millimeter-scale solenoid coils," *IEEE Transactions on Neural Systems and Rehabilitation Engineering*, vol. 24, pp. 1138–1147, Nov. 2016.

[7] M. B. Christensen and P. A. Tresco, "Differences exist in the left and right sciatic nerves of naïve rats and cats," *Anat. Rec.*, vol. 298, no. 8, pp. 1492–1501, 2015.

[8] H. Schmalbruch, "Fiber composition of the rat sciatic nerve," *Anat. Rec.*, vol. 215, pp. 71–81, May 1986.

[9] J. Badia, *et al.*, "Topographical distribution of motor fascicles in the sciatic-tibial nerve of the rat.," *Muscle Nerve*, vol. 42, pp. 192–201, Aug. 2010.

[10] Z. Deng, *et al.*, "Electric field depth–focality tradeoff in transcranial magnetic stimulation: simulation comparison of 50 coil designs," *Brain Stimul.*, vol. 6, pp. 1–13, Jan. 2013.

[11] R. Jalinous, "Technical and practical aspects of magnetic nerve stimulation," *J. Clin. Neurophysiol.*, vol. 8, pp. 10–25, Jan. 1991.

[12] E. M. Wassermann and S. H. Lisanby, "Therapeutic application of repetitive transcranial magnetic stimulation: a review.," *Clin. Neurophysiol.*, vol. 112, pp. 1367–77, Aug. 2001.